**Experimental Response and Analysis Model of an
Innovative Pile-To-Pile Mechanical Connector**

by

Ramon O. Rosales-Espinoza

A thesis submitted in partial fulfillment of the requirements for the degree of

Master of Science

in

Structural Engineering

Department of Civil and Environmental Engineering
University of Alberta

ABSTRACT

Pile-to-pile mechanical connections are used when the depth of the soil layers with sufficient bearing strength exceeds the standard pile length and extensions are needed to reach the deep stable soil. Mechanical connectors permit a safe transmission of forces while meeting strength and serviceability requirements. Common types of connectors consist of an assembly of sleeve-type external couplers, bolts, pins, and other mechanical interlock devices that ensure the transmission of compressive, tensile, torsional and bending stresses between leading and extension pile segments. While welded connections allow for a relatively simple structural design, mechanical connections are advantageous over welded connections because they lead to shorter installation times and significant cost reductions since specialized workmanship and inspection activities are not required.

The current designs of mechanical connections seem to be effective to sustain installation torque and service loads, but systematic studies or in-depth research data has not been made available. It is not known how piling companies test or design their proprietary connectors. This indicates a need for developing a pile-to-pile mechanical connector designed following rational guidelines from limit states design and provide experimental evidence for its mechanical performance. In this way, pile-to-pile connections can be designed in a safe and economic manner.

In this study, the experimental response under compressive forces of a type of mechanical connector is presented in terms of strength, deformations, and failure mode. The tests revealed that the type of connector used can safely transmit forces from pile to pile. Using the results from the compressive tests, an analysis model was developed using the Finite Element Analysis (FEA) method. The model was used to study the interaction of the components in the connection under an axial compressive load and present a tool that helps developing a more efficient design of

mechanical connections. The results from the FE model show its capability of effectively reproducing the response of an actual mechanical connection under axial compressive loading conditions.

A parametric study was conducted to address the influence of the thickness of the external coupler, and the diameter of the pins in the overall behaviour of the connection under axial compressive load. The location of the connector in full-length piles was also changed to determine its influence on the system under compressive and lateral loads. The results were able to demonstrate how the stiffness of the connection can be compromised if the thickness of the coupler or the diameter of the pins are reduced. The reduction of the stiffness of the full-length piles was found to occur when the connection is located where the highest moments are caused in the assembly. Further analyses can be developed from the FE model presented in this study and implementations to the design can be applied to achieve the safest and most economic design of mechanical connections.

Keywords – Piles, mechanical connection, design, experiment, FEA, model.

DEDICATION

To:

God,

My two giants,

My two young great brothers,

My three angels,

My old man,

My love,

Me.

"Try not to become a man of success, but rather try to become a man of value."

Albert Einstein

ACKNOWLEDGEMENTS

I want to thank the contributions of Dr. Ali Imanpour and Dr. Lijun Deng for serving as my committee members. Invaluable thanks to professors Dr. Robert Driver, Dr. Samer Adeeb, Dr. Mustafa Gül, and Dr. Yong Li, for the invaluable gift of restlessly sharing their knowledge.

I would like to express my sincere gratitude to my supervisor, Dr. Carlos A. Cruz Noguez, for seeing in me what I sometimes could not. For challenging me, for pushing me to find my new limits, and for becoming an important guide in my life as an engineer.

My thanks also go to my fellow graduate students. Because this time of sharing not only engineering matters, but sharing our lives, made us become friends. And that is the most important part. That is what we will always remember.

Countless thanks to my family. My parents Ramón and Carmen, my two giants. If I can see a horizon far away and dream with a better tomorrow, is because you taught me how to do it. My brothers Adrián and Edgar, for you to never stop dreaming and never stop smiling while chasing those dreams. To Papá Lupe, my master builder. Because your hands made more than you think. They made our family. We are here because of you.

I cannot say how much I thank you Val, my friend, my always, my love, my forever. For making me remember who I am and who I have always been. For making me understand how it is to be immensely happy. For making me discover what is it like to be deeply in love. For being.

Thanks to God my father. Because He gave me His star and it shines whenever I most need it.

TABLE OF CONTENTS

LIST OF TABLES

LIST OF FIGURES

xiii

CHAPTER 1.   INTRODUCTION

1.1 Problem Statement

Piles are foundation systems used to transfer superstructure loads to a deep, stable soil stratum that may be located under water or below weak compressible soil. Even though the main purpose of the piles is to transfer the compressive loads from the superstructure, they may also be required to resist lateral and overturning loads caused by wind, seismic events, waves in coastal constructions, and uplifting loads from combinations of vertical and horizontal loads.

Piles were initially fabricated out of timber as shown in constructions built by the Romans (100 BC to AD 400) and by the Hang Dynasty in China (200 BC to AD 200). The installation of these piles was done by hammering them into the soil, and their strength was limited by the capacity of the girth of the natural timber to sustain the installation process. Before the 19th century, timber was the only material used thanks to its convenient light weight, high strength, durability, and ease of cutting and handling. Later, reinforced-concrete and steel arose as alternatives to replace timber due to their higher strength-to-weight ratio.

Reinforced-concrete is used either as precast, prestressed or cast-in-situ piles, facilitating dimensioning the pile as required by the soil conditions. Concrete offers a durable and economic solution for load transfer.

Steel piles have the advantage of their ease of fabrication and handling, and higher strength-to-weight ratio compared to concrete. Steel piles can be fabricated from H, W, or tube sections. Problems of corrosion when used in marine structures and extremely acid or alkaline soils have been solved by a wide range of effective coating protection systems, helping the steel piles become an effective foundation system under any condition (Tomlinson and Woodward 1995).

Extension shafts are needed when the depth of the soil layers with sufficient bearing strength exceed the original length of the pile brought to the site. The original length of the piles is determined by fabrication and transportation specifications, which have to be met to facilitate the overall construction process. Due to the almost unavoidable (and frequent) need of adding

extensions to piles already installed in the soil, pile-to-pile connections have been an important area of research and industrial development.

When tube sections are used, one of the earliest methods of assemblage between the lead shaft and the extensions was to weld a short steel section to the piles at the junction level. These sections were fabricated with larger diameters than the piles to act as sleeves and guaranty the transfer of load from the extension to the lead pile. However, high installation times, and the high cost of weld-related workmanship and inspection activities, caused the welded connections to become highly ineffective and expensive when extensions were required.

As a result, mechanical connections started to be developed by the piling industry. Common designs include but are not exclusive to sleeve-type piles that are welded to the extension on the shop and then bolted on site to the pile initially drilled into the soil. Several factors are taken into account when selecting the most convenient features in the mechanical connection. These characteristics include the thickness of the coupler, the size of the weld used between the coupler and the extension, the number of holes in the connector, the diameter of these holes and pins, the internal diameter of the coupler to determine the existing gap between this and the piles, and more.

Although many different designs exist, very few studies have been conducted to investigate the performance of pile-to-pile mechanical connectors under compressive, tensile, or torque loading conditions. Test data is scarce or nonexistent, since typically designs are protected by patents or by confidentiality agreements to maintain a commercial advantage.

Manufacturer information regarding connector performance indicates under service conditions or the ultimate limit state is scarce. Although current designs of mechanical connections seem to be effective to sustain installation torque and service loads, systematic studies or in-depth research data has not been made available and improvements to the designs have not been effectively addressed. It is not known how piling companies test or design their proprietary connectors.

The preceding discussion indicates the need for developing a pile-to-pile mechanical connector designed according to rational guidelines from limit states design and provide experimental evidence for its mechanical performance. In this way, pile-to-pile connections can be designed in a safe and economic manner.

1.2 Objective and Scope

In this study, the design of a mechanical connection is performed and then fabricated to be tested under axial compressive load to better understand its behaviour in ultimate conditions. The system consists of a sleeve-type external coupler with drilled holes and pins. Holes are drilled in the external coupler, which is welded to the extension pile in the shop (minimizing on-site welding costs). The lead pile already installed in the soil, has the same set of holes as the coupler. When the extension pile (with the coupler welded at the bottom) is brought to the field to be installed at the top of the lead pile, pins or bolts are placed through the common holes and secured with a tack weld.

The proposal of a mechanical connection will be designed under axial compressive load conditions. The failure mode as per the limit states design criteria will be determined and the maximum capacity calculated before the experimental tests are conducted.

The experimental response of the connector under compressive forces will be investigated and the results discussed in terms of strength, deformations, and failure mode.

A Finite Element (FE) method will be developed and validated with the results from the experimental tests. The model will be used to study the interaction of the components in the connection under an axial compressive load and present a tool that helps developing a more efficient design of mechanical connections. A parametric study will be conducted to address the influence of some selected features in the overall behaviour of the connection.

The specific aims pursued to achieve the research objective are:

- To design a standard type of mechanical connection used in steel helical piles as per the Limit States Design and testing considerations.
- To conduct an investigation of the performance of the mechanical connection under axial compressive load.
- To retrieve the response of the mechanical connection in terms of load-displacement of the assembly, deformations and strains of the coupler from the experimental tests.
- To identify the most critical areas in the connection and determine the failure mode as per the observations made after the tests.

- To develop a realistic 3D FE model of the tested mechanical connection, validating the model with the results from the experimental tests in terms of load-displacement response, deformations, and strains.
- To perform a series of parametric analyses on selected features of the mechanical connection that present room for improvement.

The scope of the study does not consider forces other than compression, such as torsion, shear, tension or a combination. Also, only one type of connector will be tested. However, a parametric analysis was implemented in a different type of connection accounting for different values of the thickness of coupler, the diameter of pins and the location of the connection in full-length piles.

The stiffness of the soil surrounding the piles was not taken into consideration in the design calculations, FE, and testing.

1.3 Thesis Outline

This document is organized into 7 chapters including the Introduction. Chapter 2 covers the relevant available literature on piles design and installation, and some of the research done in mechanical connections.

In Chapter 3, the design of the proposed mechanical connection is presented. The limit states that were considered to predict the capacity of the assembly are included in this chapter.

In Chapter 4, the test program is described. The details of the specimens, including geometry and material properties, the equipment used for testing, the instrumentation used in the specimens, and the loading procedure are presented. The results achieved from the tests in terms of load-displacement response, deformations, and strains tracked during the application of the load are included.

Chapter 5 presents the description of a FE model developed to accurately predict the behaviour of the mechanical connection under an axial compressive load. The material and geometric properties are reproduced as per the tested specimens. The boundary conditions and the loading scenario are replicated as per the test conditions and followed procedures during the test. The analysis of the

results obtained by the FE model are also presented in this chapter. The load-displacement response, the strains, and the stress in the connection are included within the set of results.

Chapter 6 presents a parametric analysis in which the thickness of the external coupler, the diameter of the pins, and the location of the connection in full-length piles were changed to investigate their influence in the connector and pile system responses.

The conclusions achieved through this study are summarized in Chapter 7 and recommendations for further research on this topic are provided.

CHAPTER 2.   BACKGROUND AND LITERATURE REVIEW

2.1 Introduction

One of the objectives of this research program is to evaluate the behaviour of pile-to-pile mechanical connections used under axial compressive load conditions. Comprehensive background information is needed to be able to identify the gap in the current knowledge and the shortcomings of current design methods.

2.2 Pile Foundations

Piles are foundation systems working as columnar elements with the function of transferring the load from the superstructure through a weak soil or water, onto stiffer soils or rock beds. The piles require to sustain torque loads during installation, compressive loads applied by the superstructure and the self-weight of the pile, and uplifting tensile loads when winds or waves exert overturning forces to the top structure (Tomlinson and Woodward 1995).

According to the British Standard Code of Practice for Foundations (BS 8004: 1986), there are three different categories of piles:

- Large displacement piles.
- Small displacement piles.
- Replacement piles.

Large displacement piles can be solid or hollow with a closed end. They are driven or jacked into the ground while displacing the soil. Small displacement piles are also driven or jacked into the ground but they have a relatively small cross-section area and an open end. Examples of these piles are rolled steel I- or H-sections. Finally, replacement piles are installed after boring a hole using drilling machinery. Concrete, steel, or timber piles may be used to transfer the loads from the superstructure to the supporting soil (Tomlinson and Woodward 1995).

The type of pile-to-pile mechanical connector developed and investigated in this study is to be used in steel piles with hollow circular sections.

The structural design of a pile must consider the sum of two components: shaft friction and base resistance. A pile in which the shaft-frictional component predominates is known as a friction pile, while a pile bearing on rock or some other hard incompressible material is known as an end-bearing pile (Tomlinson and Woodward 1995).

When the strength and deformation characteristics from the soil are available, the ultimate end-bearing resistance (q_o) of a pile can be determined from the following expression obtained from Vesic (1977):

(2 - 1)
$$q_0 = cN_c^* + q_v N_q^*$$

where c represents the strength intercept-cohesion of the assumed straight-line Mohr envelope, N_c^* and N_q^* are dimensionless bearing-capacity factors, and q_v is the effective vertical stress in the ground at the foundation level. The bearing capacity factor N_c^* can be determined using Eq. 2 - 2, and N_q^* can be determined using Table 2 - 1 or Fig. 2 - 1.

(2 - 2)
$$N_c^* = (N_q^* - 1)\cot\phi$$

where ϕ is the angle of shearing resistance.

Table 2 - 1. Experimental values of Nq* in sand
(Tomlinson and Woodward 1995)

SAND COMPACTNESS	RELATIVE DENSITY (%)	N_q*	
		DRIVEN PILES	BORED PILES
Very dense	>80	60–200	40–80
Dense	60–80	40–80	20–40
Medium	40–60	25–60	10–30
Loose	<40	20–30	5–15

When the soil data is available, the ultimate friction resistance can be determined using the following expression:

(2 - 3)
$$f_s = N_s q_v$$

where N_s represents a dimensionless bearing capacity factor used when the pile is located in normally consolidated clays and can be determined from:

$$ (2\text{ - }4) \qquad N_s = \frac{sin\phi' cos\phi'}{1 + sin^2\phi'} $$

where ϕ' represents the angle of shearing resistance of remolded clay in drained conditions. This information is obtained from field tests.
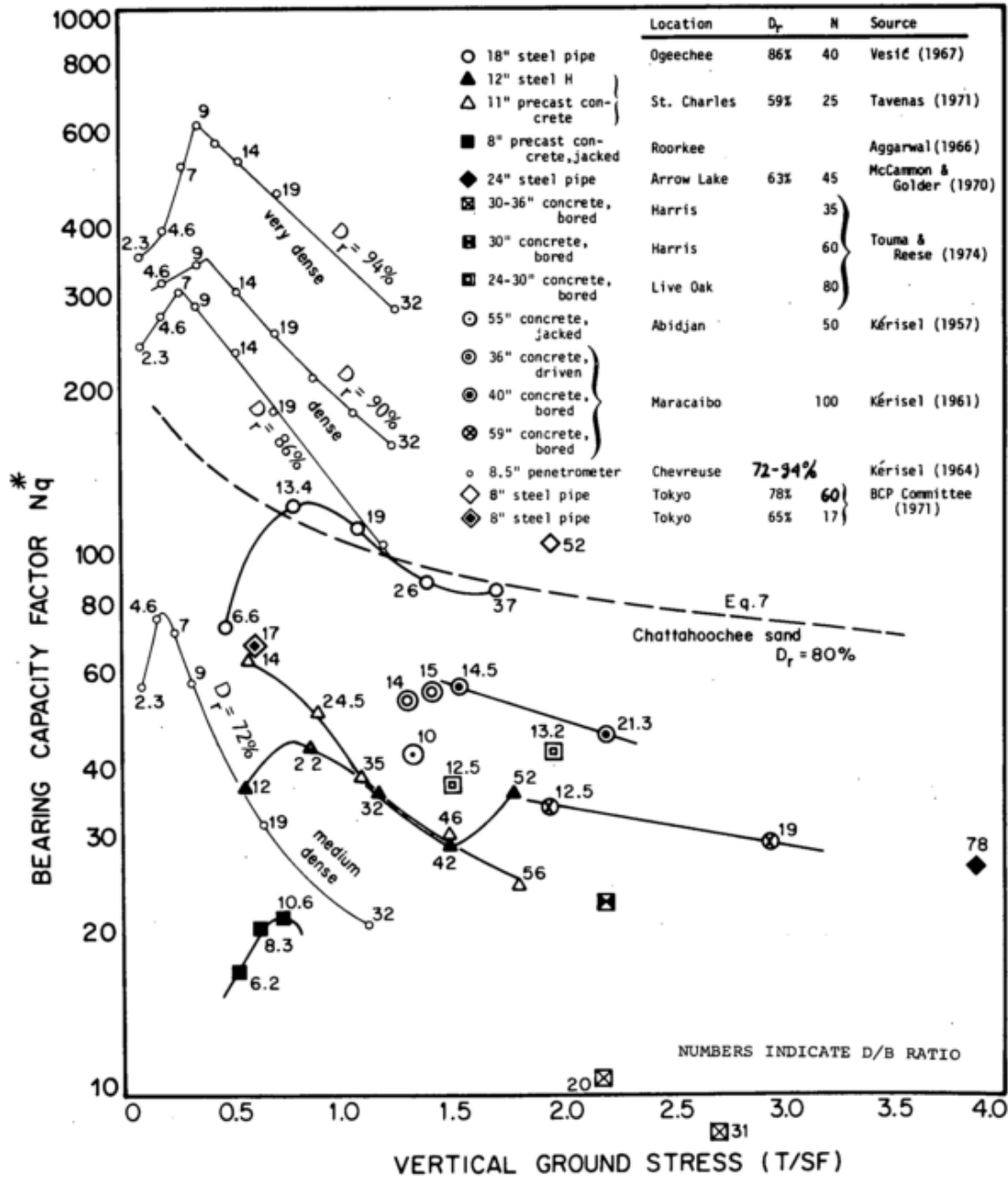
Figure 2 - 1. Experimental values of N_q^* in sand from different investigations.
Source: (Tomlinson and Woodward 1995)

When the piles are driven in over-consolidated clays, the following expression to determine the friction capacity can be used:

(2 - 5) $$f_s = \alpha s_u$$

where α can be taken as 0.45 and s_u is the undrained shear strength of the soil.

For piles in sand, the friction capacity is related to a relative density and is determined using Fig. 2 - 2 as a guide.
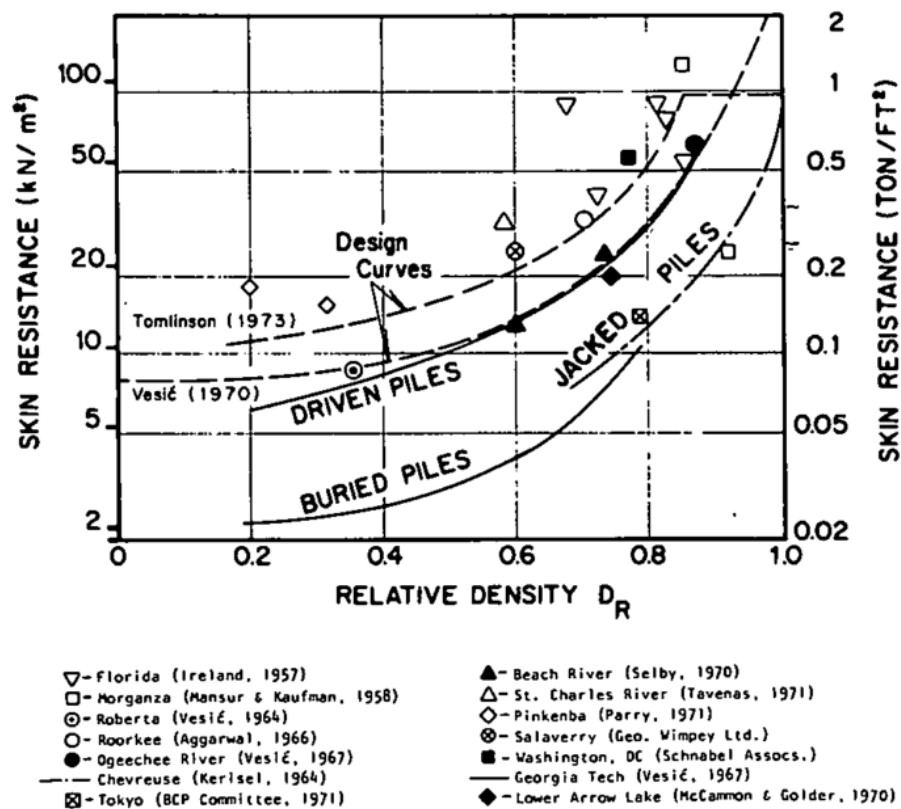
Figure 2 - 2. Variation of skin resistance of piles in sand with relative density.
Source: (Vesic 1977)

The preferable way of determining the bear and shaft friction resistances is by conducting field tests. By doing so, the exact geotechnical information can be used to determine the most convenient method to use in calculating the capacity of the pile (Vesic 1977).

9

2.3 Mechanical Connections (Couplings)

The strong soil or the bed rock that has to be reached by a pile is sometimes deeper than the originally provided length of the pile. When this happens, extension shafts have to be added to the lead pile by welding or by using mechanical connections (Fig. 2 - 3). The original pile segment is called the lead pile and the added segment is called the extension pile. A welded connection can be conducted by using pile splices welded to both lead pile and extension piles. However, welded connections are expensive in terms of time and costs due to the time consuming process and the high costs for the execution, inspection, and approval processes. As a result, mechanical connections have been developed by the industry.

A number of designs of mechanical connections have been performed by the pile industry since the piles started to being used as foundation systems. The patents of these designs have been published in several countries and they have allowed the development of new and more effective designs based on previous observations.

(a)   (b)
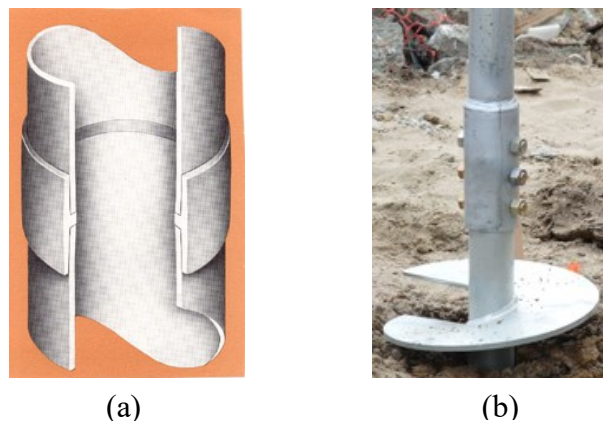
Figure 2 - 3. (a) Welded pile splice, (b) mechanical connection
Sources: (a) www.pilebuck.com, (b) www.foundationsupportworks.com

2.3.1 Jointing Devices for Concrete Piles

Published in 1967, this document presents the use of steel collar-type connections to interlock two sections of a concrete pile and form a single unit with an increased length. Even though it is not

used in steel helical piles, it starts showing the evidence that the transmission of loads had to be accomplished by an effective connection system. Steel sleeves with triangular-shaped slots were designed to create an interlocking device which could provide the load transmission from one section of the pile to the other one (Nilsson and Börje 1967). Figure 2 - 4 shows the sketch of the proposed connection in concrete piles.
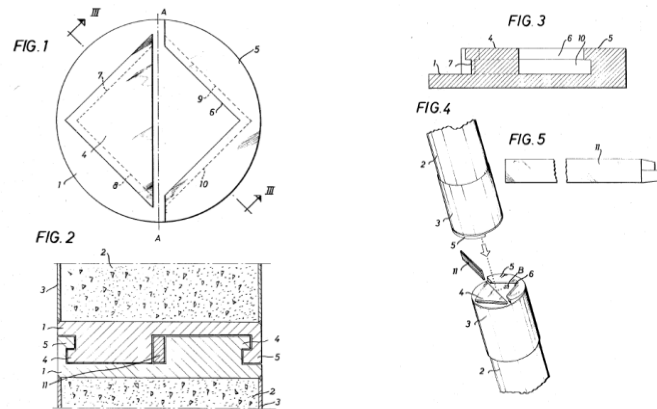
Figure 2 - 4. Sketches of the device proposed by Nilsson and Börje.

2.3.2 Quick-Coupling Connector Group for Pipes, Piles, or the Like

Montanari and Sala (1988) presented this invention under the constant difficulty of installing piles longer than the commercially available or transportable length. Structural continuity had to be achieved by providing a connection that could permit the use of simple equipment for the installation of the piles and cannot accidentally loosen. However, it can be noted in Fig. 2 - 5 that the complexity of the connection would lead to difficulties in manufacturing the sleeve and ensure an effective connection between piles.

2.3.3 Apparatus for Use in Forming Piles

Bullivant (1998) presented simpler designs of mechanical connections. In these designs, the lead pile and the extension have a drilled hole, and a mechanism with coincident holes join them together and creates the transmission of the load. The torque, compression, and lifting capacity of the piles is considered in this design as the loads to be transmitted from one section of pile to the

other. As depicted in Fig. 2 - 6, the design proposed by Bullivant starts resembling the current designs for mechanical connections.
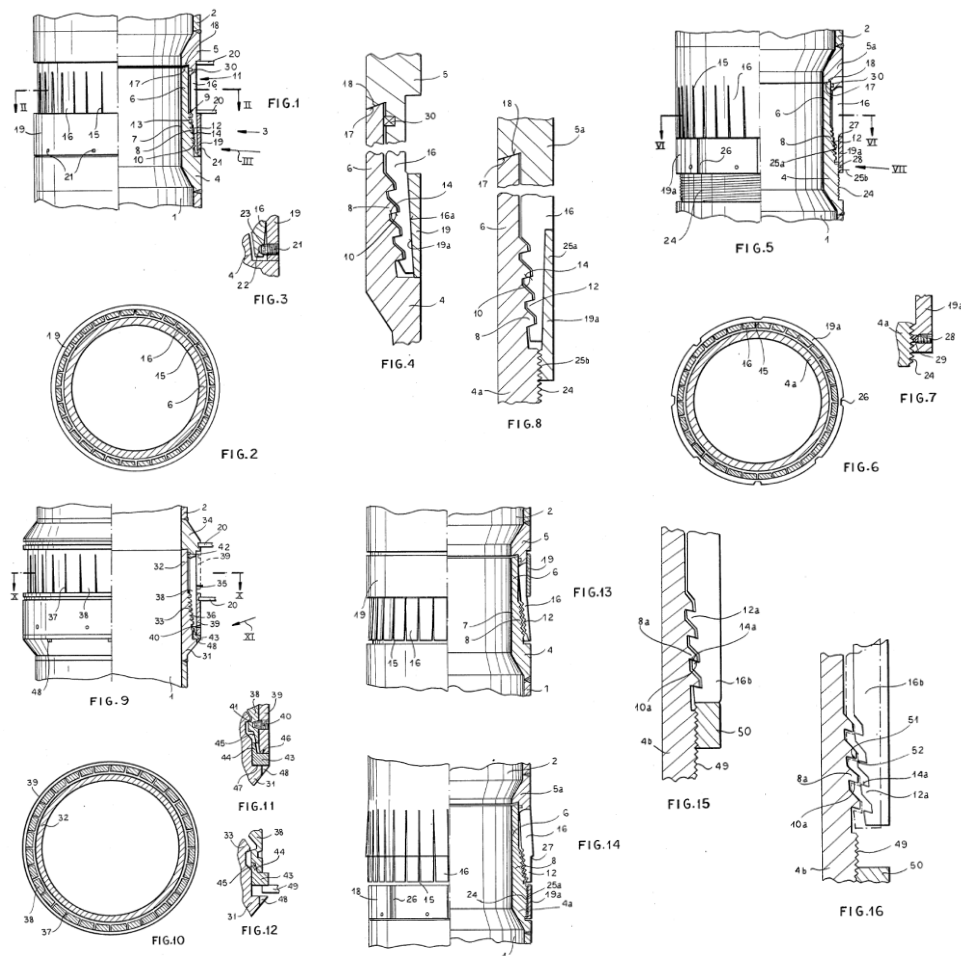
Figure 2 - 5. Sketches of the coupling proposed by Montanari and Sala.

2.3.4 Helix Pier Coupling System Used for Soil Stabilization

Rupiper (2003) presented a design of a mechanical connection as a solution to add extensions namely in steel helical piles. In this connection, the transfer of the load from the extensions to the lead pile is done by a sleeve-type piece welded to the lead pile and bolted to the extension. Both lead and extension piles will have a cut in the bottom of the shaft to work as a lead point when installing the pile into the ground surface. A cut in the upper end of the piles can be used with a

coupling to mate with the cut from the extension. The designs presented by Rupiper as shown in Fig. 2 - 7 are currently used with minimal modifications in the piling industry.
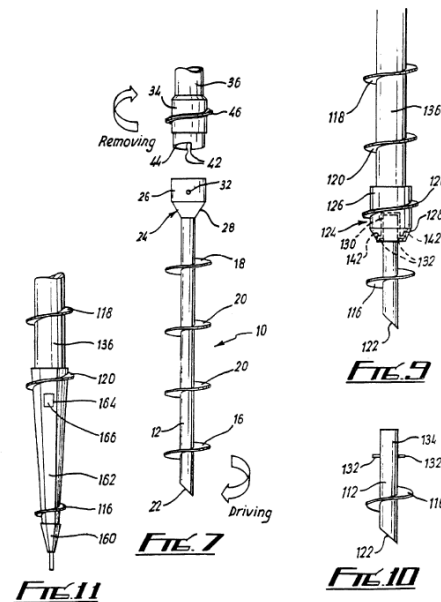
Figure 2 - 6. Sketch of the coupler proposed by Bullivant.

2.3.5 Modular Tubular Helical Piering System

Jones (2006) invented a modular system used to assemble helical piles with hollow squared cross-sections with connectors and helices. Removable flat pins are inserted through holes punched in the lead pile and in a sleeve-type coupler welded to the extension. The helices can also be added using bolts as needed in the shafts as shown in Fig. 2 - 8. This modular design represents an important reduction of weld work in the helices and in the connections. However, the efficacy of the pins used in helices compared to the welded ones is not part of the scope of the current research.
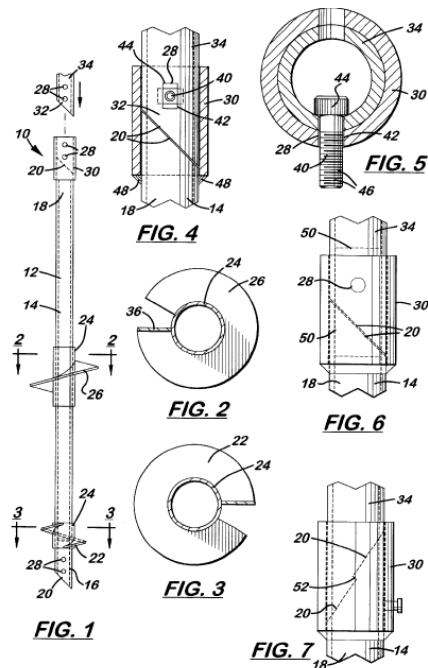
Figure 2 - 7. Sketches of the coupling method proposed by Rupiper.
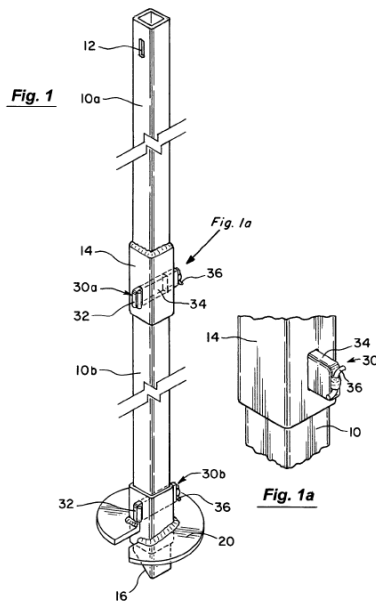
Figure 2 - 8. Sketches of the modular piles proposed by Jones.

2.4 Structural Research on Mechanical Connections

Even though it exists an extensive range of different designs of mechanical connections, very few research has been published regarding their structural design. The competitive nature of the market in the pile design industry leads the companies to keep key information confidential.

One of the few documents revealing some information about the design of a connection dates from 1979 and it was published by F.L. Hettinger, from Vetco Offshore Inc. The connection presented was used in offshore piles and it ranged in size from 30 inches to 72 inches in external diameter. The connector was modeled using the finite element method and tested under tensile, pressure, bending, functional, and installation tests. The objective of conducting all the analyses was to ensure that the stress levels were lower in the connector than in the piles. Moreover, to guarantee that the fatigue life of the connector should be longer than the one of the piles. All the results were validated using experimental tests conducted by the same company and by contractors using that connection (Hettinger 1979).

Even though the design methods are not presented by Hettinger, the methodology followed to test and approve the design of the mechanical connection is of high relevance for the current research. By developing a finite element model validated with experimental results, Vetco Offshore Inc. was able to ensure the effectiveness of the design of their mechanical connection.

The process of analyzing a connector by conducting experimental tests and finite element models must be preceded by the hand calculations of the ultimate capacity that could be achieved by the system under axial compressive loads.

As explained before, the external coupler is welded to the extension in the shop and then bolted to the lead pile on site. The capacity of the weld is not within the scope of the current project, but the bolted connection between the lead pile and the coupler is included.

This bolted connection is analyzed under the ultimate states design method, which is used to check the performance of a structure against conditions concerning safety. The final objective of these checks is to ensure that the maximum strength of a structure is greater than the loads that will be applied to it with a reasonable margin against failure (Kulak and Grondin 2011).

The ultimate limit state criterion is illustrated in Fig. 2 - 9. It shows a hypothetical frequency of distribution curves for the effect of loads (Si) on a structural element and its strength, or resistance (R). Where the two curves overlap, the shaded area indicates the effect of the loads is greater than the resistance of the element, and it will fail (Kulak and Grondin 2011).
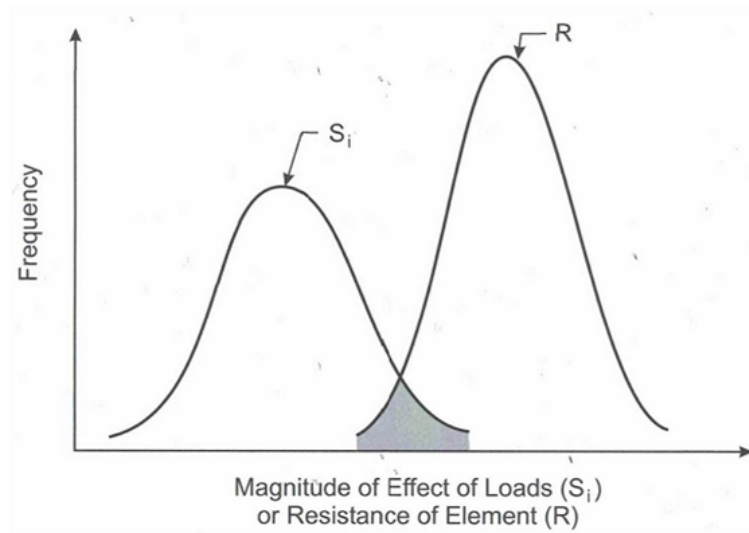
Figure 2 - 9. Frequency distribution curves.

The basic equation to check the ultimate state condition is mentioned by Kulak and Grondin (20101) and is as follows:

(2 - 6)
$$\varphi R \geq \alpha_i S_i$$

where φ is the resistance factor, R is the nominal resistance of an element, α_i is the load factor, and S_i is the load effect under specified loads.

The resistance factor (φ) is applied to the nominal member strength to take into account the fact that the actual strength of a member may be less than anticipated because of a series of variabilities. The nominal resistance (R) is the strength calculated using the specified material properties, nominal dimensions and equations describing the theoretical behaviour of a member.

The factor α_i is used to account for the variability of loading and the probability of having loads from various sources acting simultaneously on the structure. The load effects (S_i) are the resulting

from the application of the specified loads in the structure (dead load, earthquake, live load, snow load, and wind load) (Kulak and Grondin 2011).

In the specific case of mechanical connections, the approach as per the limit states design method is not well defined. The pile systems work under compression, but the junction of the coupler with the lead pile is isolated to be analyzed as a bolted connection. The failure modes under which a connection can fail are determined as: global compressive resistance, bearing resistance, *block shear, end tear-out*, shear resistance of the bolts, and strength of the weld.

2.4.1 Global Compressive Resistance

The global compressive resistance (C_y) can be calculated for short columns as the product of the cross-sectional area, A, and the yield stress level, (σ_y) (i.e., $C_y = A\sigma_y$) (Kulak and Grondin 2011).

For longer columns, the maximum load depends on the length of the member and its bending stiffness (EI) due to stability conditions that might cause failure before yielding takes place in the cross-section (Kulak and Grondin 2011).

CSA S16-09 (2010) provides an equation that can be used for both long and short columns taking into account a slenderness parameter defined by the following expression:

(2 - 7)
$$\lambda = \frac{KL}{r}\sqrt{\frac{F_y}{\pi^2 E}}$$

where r is the radius of gyration of the cross-section and L is the length of the member.

The slenderness ratio in this expression is defined by L/r. The effective length factor is K and it is determined by the boundary conditions of the column as shown in Fig. 2 - 10.

The global compressive resistance of a member is given by the following expression in CSA S16 (2010):

(2 - 8)
$$C_r = \varphi A F_y(1 + \lambda^{2n})^{-1/n}$$

The parameter n in Eq. (2 - 8) is defined by the procedure followed during the fabrication of the member. A value of 1.34 is used for hot-rolled or fabricated shapes and Class C HSS. And a value of 2.24 is used for WWF with oxy-flame-cut flanges and Class H HSS.

Buckled shape of column is shown by dashed line	(a)	(b)	(c)	(b)	(e)	(f)
Theoretical K value	0.5	0.7	1.0	1.0	2.0	2.0
Recommended design value when ideal conditions are approximated	0.65	0.80	1.2	1.0	2.10	2.0

End condition code		
	Rotation fixed and translation fixed
	Rotation free and translation fixed
	Rotation fixed and translation free
	Rotation free and translation free

Figure 2 - 10. Effective length factors with idealized end conditions
Source: (Duan and Chen 1999)

2.4.2 Bearing Resistance

Bearing resistance is the capacity of the material adjacent to the bolt to sustain the load applied. The failure associated to this resistance consists on excessive deformation in the holes of the plates and they should be limited by the designer. Several methods were found to determine the bearing resistance of a bolted connection.

2.4.2.1 Bearing Equation by Kulak and Grondin (2011)

An equation to calculate the bearing resistance is presented by Kulak and Grondin (2011). They established the bearing resistance of one bolt as the capacity of the plate adjacent to the bolt and is defined by the following expression:

(2 - 9)
$$B_r = \varphi t n e F_u \qquad \text{for: } e < 3d$$

where φ is the resistance factor, t is the thickness of the piles, n is the number of pins, e is the distance from the center of the hole to the edge of the plate, and F_u is the ultimate strength of the material.

This equation was derived under the assumption that $e < 3d$, where d is the diameter of the holes. When this is not the case, a different expression is given by CSA S16 and explained in the following section.

2.4.2.2 Bearing Equation in CSA S16-09

The current equation describing the bearing resistance of the material in a mechanical connection used in CSA S16-09 (2010) is determined by the assumption that $e \geq 3d$. This assumption was done based in several tests showing that the bearing stress is in function of the ratio e/d up to a value of about 3, being d the diameter of the bolts. Beyond this limit, the failure mode could change from one where the material shears out beyond the bolt to one where large hole deformations occur (Kulak and Grondin 2011). The expression to calculate the bearing resistance when this condition is met is the following:

(2 - 10) $$B_r = 3\varphi t d n F_u \qquad \text{for: } e \geq 3d$$

where φ is the resistance factor, t is the thickness of the piles, n is the number of pins, d is the diameter of the pins, and F_u is the ultimate strength of the material.

2.4.2.3 Bearing Equation by Rogers and Hancock (2000)

Rogers and Hancock suggested a method that contains a gradated bearing coefficient dependent on d/t. Where d is the diameter of the bolt and t is the thickness of the plate. The expression they proposed to calculate the nominal bearing capacity (V_b) is the following:

(2 - 11) $$V_b = C t d F_u$$

where t and d are the thickness of the plate and the diameter of the bolts, respectively. The bearing coefficient (C) is calculated as per Table 2 - 2, which was proposed by Rogers and Hancock (2000) as well.

Table 2 - 2. Proposed factor C for bearing resistance

d/t	C
d/t ≤ 10	3.0
10 < d/t < 22	4.0 – 0.1 d/t
d/t ≥ 22	1.8

2.4.3 Block Shear in CSA S16-09

When a tensile load is applied to a bolted connection, shear stress can also take place in the planes parallel to the load as shown in Fig. 2 - 11 (Kulak and Grondin 2011). When this occurs, a block of material could detach from the rest of the element in the connection causing a *block shear* failure mode.
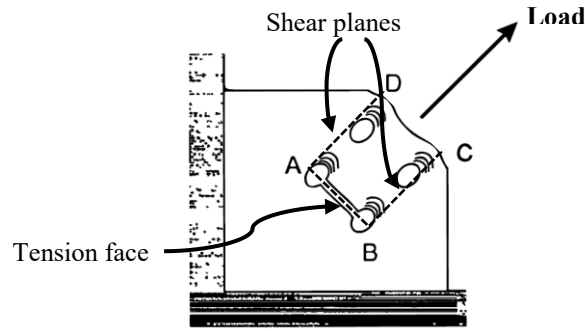
Figure 2 - 11. Block shear failure due to tensile load.

CSA S16-09 (2010) defines the shear strength of the material as per the von Mises criterion, giving a value for it of $0.6F_y$. When *block shear* occurs, it has been found that the average of the yield strength and ultimate strength gives better results when is taken as the stress in the shear planes (Kulak and Grondin 2011). According to this, the block shear capacity of a bolted connection is defined as:

(2 - 12)
$$T_r = \varphi_u \left[U_t A_n F_u + 0.6 A_{gv} \frac{(F_y + F_u)}{2} \right]$$

where A_{gv} is the gross area taken along the potential shear planes, A_n is the net area in tension, and the constant U_t is a symmetry factor (taken as 0.9 for this study as in coped beams with one bolt line).

20

2.4.4 *End Tear-Out*

Failure by *end tear-out* can occur in connections with a single bolt line (Fig. 2 - 12) or with two or more bolt lines origin individual patterns of material tear-out (Fig. 2 - 13).
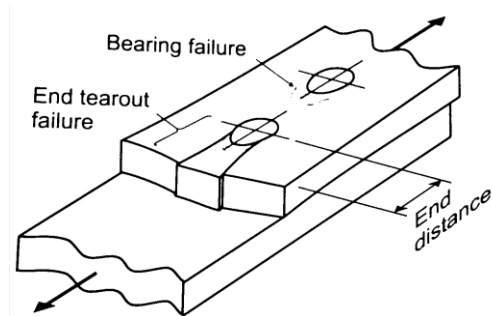
Figure 2 - 12. End tear-out failure in a connection of single line of bolts.
Source: (Kulak and Grondin 2011).
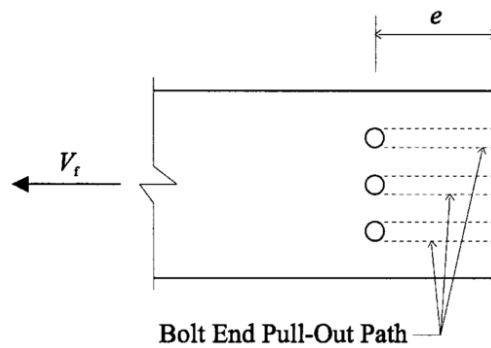
Figure 2 - 13. End tear-out in a connection of three lines of bolts.
Source: (Rogers and Hancock 2000).

The failure of a connection by *end tear-out* can be calculated based on the block shear calculations with a tension area taken as zero, and the gross shear area taken as twice the end distance multiplied by the thickness of the plate (Kulak and Grondin 2011). Also by multiplying the ultimate strength of the material by a specified cross-sectional net area (Rogers and Hancock 2000). Or by taking the resistance of the connection under shear stress (CSA S16).

2.4.4.1 *End Tear-Out* by Kulak and Grondin

The calculations for *end tear-out* failure can be obtained from the expression used for *block shear* defined in Eq. (2 - 12). However, the inexistence of a net tensile area causes it to be taken as zero, while the gross shear area is taken as twice the end distance times the plate thickness (Kulak and Grondin 2011). The formulation of this expression is as follows:

(2 - 13)
$$T_r = \varphi_u \left[2 \text{ x } 0.6 A_{gv} \frac{(F_y + F_u)}{2} \right]$$

where the variables are the same as the ones in *block shear*. The only remaining part is the shear capacity of the material, neglecting the tensile capacity.

2.4.4.2 *End Tear-Out* by Rogers and Hancock

One of the expressions recommended by Rogers and Hancock (2000) is the equation provided by the Australian/New Zealand (1996) and U.S. (1997) codes to determine the *end tear-out* capacity of a bolted connection as follows:

(2 - 14)
$$V_f = teF_u$$

where e is the distance from center of hole to edge of pile and t is the thickness of the pile.

The second recommended equation appeared in CSA S16 (1994). This expression represents the *end tear-out* capacity per bolt and it is determined as follows:

(2 - 15)
$$V_f = A_n F_u$$

With the variation that the net cross-sectional area (A_n) for each bolt is defined as:

(2 - 16)
$$A_n = 0.60 \text{ x } 2t \left(e - \frac{d_h}{2} \right)$$

where d_h is the diameter of the bolt hole.

2.4.4.3 *End Tear-Out* in CSA S16-01 (2007)

According to Clause 13.11, the resistance of a connection under shear stress would be the lesser of the two following equations:

(2 - 17) $T_r = 0.60\varphi A_{gv} F_y$

(2 - 18) $T_r = 0.60\varphi A_{nv} F_u$

where the difference is in the areas taken into account, being A_{gv} the gross shear area, and A_{nv} the clear distance from the bolt to the edge of the plate.

2.4.5 Shear Resistance of Bolts (Kulak and Grondin 2011)

The failure of the bolts occurs if their shear strength is exceeded at the interface of the two piles. The shear strength of the high-strength bolts is approximately 0.60 times the tensile strength of the bolt material as per an extensive set of experimental data (Kulak and Grondin 2011). The expression given to calculate the shear resistance of the bolts is as follows:

(2 - 19) $V_r = 0.60\ \varphi_b n m A_b F_u$

where φ_b is the safety factor, n is the number of bolts in the connection, m is the number of shear planes, A_b is the cross-sectional area of one bolt, and F_u is the ultimate strength of the material of the bolts.

2.4.6 Strength of the Weld

There are a few number of cases in which the unit resistance of the weld is the same as the calculated resistance of the base metal. The fillet welds and the plug welds are within these cases and they are shown in Fig. 2 - 14 (Kulak and Grondin 2011).

The fillet welds may be oriented longitudinally to the applied load, transversely to it, or at any angle in between these two. Depending on this angle of inclination, the ductility and strength of the weld will vary and its load-deformation response to the application of the load will be as shown in Fig. 2 - 15 (Kulak and Grondin 2011).

(c) Fillet weld   (d) Plug weld
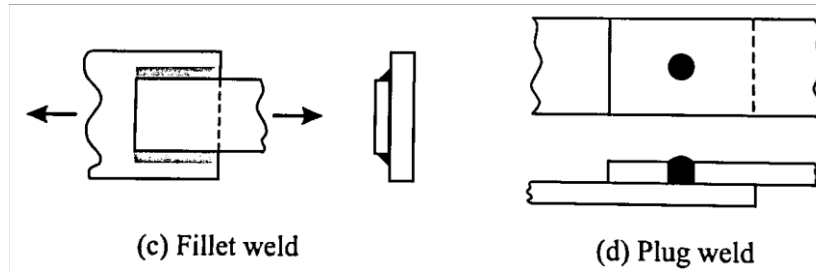
Figure 2 - 14. Fillet weld and plug weld.
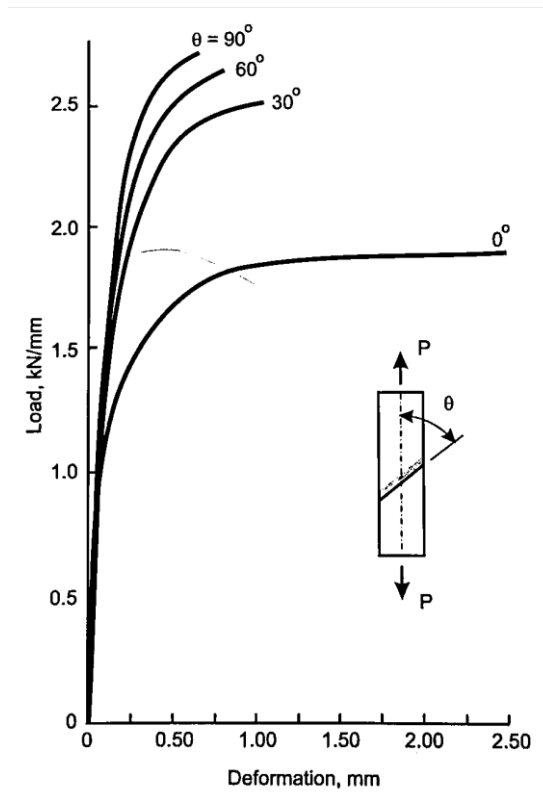
Figure 2 - 15. Load – Deformation response of fillet welds.

The strength of fillet welds and plug welds was calculated as the resistance of the base metal. For plug welds, this calculation was conducted as per the following expression:

(2 - 20) $$V_r = 0.67\varphi_w A_m F_u$$

where A_m is the area of the fusion face, which is the area of the metal in contact with the weld, F_u is the ultimate strength of the base metal, and φ_w is the safety factor. The numerical modifier 0.67 relates the shear strength of the weld to the specified electrode tensile strength (Kulak and Grondin 2011).

For fillet welds, the strength is determined also by the angle of the axis of the weld with respect to the line of action of the load applied as presented by Eq. (2 - 21) (Kulak and Grondin 2011).

(2 - 21) $$V_r = 0.67\varphi_w A_w X_u (1.0 + 0.5\ sin^{1.5}\theta)M_w$$

where A_w is the effective throat area of the weld as shown in Fig. 2 - 16, X_u is the ultimate tensile strength of the electrode, θ is the angle between the axis of the weld and the load vector, and M_w is a strength reduction factor for welded joints with welds in two or more directions (taken as 1.0 in this study).
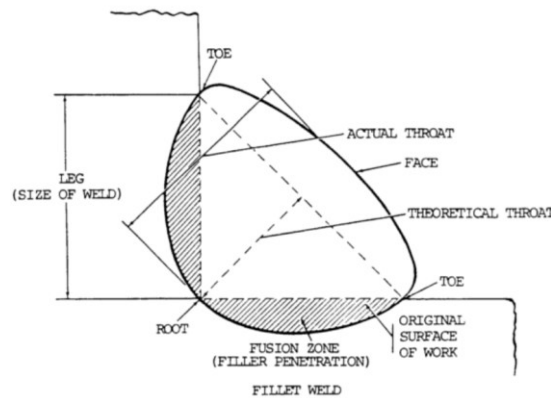
Figure 2 - 16. Terminology of fillet welds (Kulak and Grondin 2011).

The electrode ultimate tensile strength (X_u) is very similar to that of the base metal. Some values for matching electrodes with base metals from CSA G40.21 are presented in Table 2 - 3 from Kulak and Grondin (2011).

Table 2 - 3. Matching electrodes for CSA G40.21 steels

Matching electrode Ultimate tensile Strength (MPa)	G40.21 Grades (MPa)						
	260	300	350	380	400	480	700
430	X	X					
490	X	X	X	X			
550					X		
620						X	
820							X

CHAPTER 3.   DESIGN OF MECHANICAL CONNECTION

3.1 Introduction

A full-scale test program was designed and conducted to investigate the behaviour of the mechanical connection under axial compressive load. Three identical specimens were fabricated by Almita Piling Inc. and tested at the University of Alberta.

The design of the mechanical connection was performed in accordance with CSA S16 (2014) "Design of Steel Structures" and it included specific requirements established by the fabricator and by the contractor. It was also dependent on the loading limitations from the testing equipment, which can only apply a maximum of 6000 kN of compressive load.

The design proposal was based in the exact dimensions of a standard mechanical coupler. However, special considerations made by the author that differed from the actual features of a pile-to-pile mechanical connector were implemented. These special considerations were suggested based on the outputs required for this study.

The general objective of the experimental program was to investigate the behaviour of the mechanical connection under axial compressive load. This objective was reached by obtaining and analyzing the vertical load-vertical displacement response of the mechanical connection, the deformations of the components involved, and the strain response associated to the applied load.

3.2 Proposed Connector

The connector design consists of a short length of pile with larger diameter than both the lead and extension piles, with a number of holes drilled through it. This is called external coupler. The external coupler is welded in the shop to the extension pile once the holes are drilled on it. When the extension pile and the attached external coupler are positioned on top of the lead pile, high strength steel pins are installed through matching holes in the external coupler and the leading pile. Tack welds are provided to secure the connection and to prevent the pins from slipping out.

3.3 Material Properties

3.3.1 Pile Shafts

The steel material used in the external coupler must have the same properties than the steel used in the piles fabricated and installed by the contractor. The material used for the piles in this study was Grade 3 steel according to ASTM A252. This steel grade has a yield strength of 310 MPa and an ultimate strength of 455 MPa (ASTM Standard 2002).

Three dogbone specimens were cut from a pile used as mechanical connector in the longitudinal direction in order to obtain coupons as flat as possible. The sides of the coupons were flattened to allow for a better grip. A transition zone was left between the flat and curved zones of the specimens. The dimensions of the coupons are shown in Fig. 3 - 1. The cross-section zones are shown in Fig. 3 - 2.
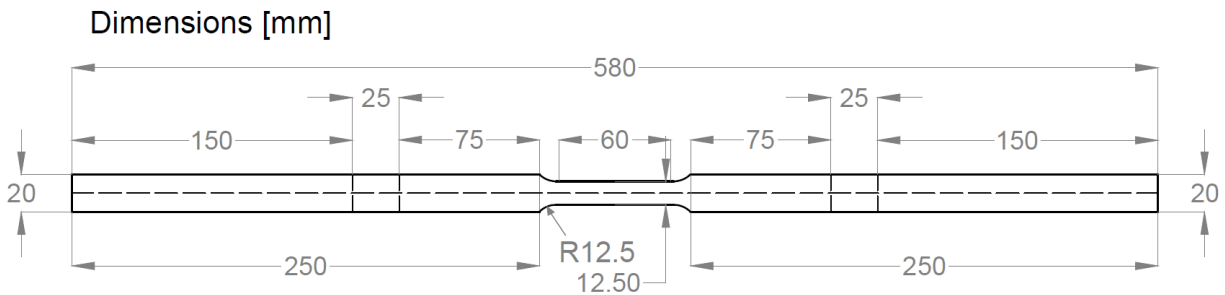
Figure 3 - 1. Dimensions of coupons for standard tensile test.
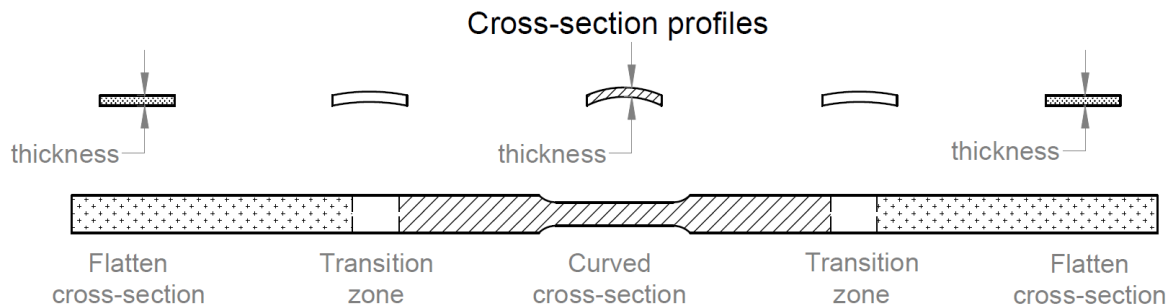
Figure 3 - 2. Cross-section transitions along the coupons.

The three coupons were tested in accordance to ASTM E8/E8M standard (ASTM Standard 2009). The engineering stress-strain curve was obtained dividing the tensile load applied to the coupon by the initially measured cross-sectional area. In order to remove the effect of the strain rate in the test, the load was paused during the test and static points were obtained. These static points are sudden drops in the load capacity and they defined the static yield and ultimate stress of the material under static conditions. After the short pauses, the loading was resumed and the complete curves were plotted as shown in Fig. 3 - 3.
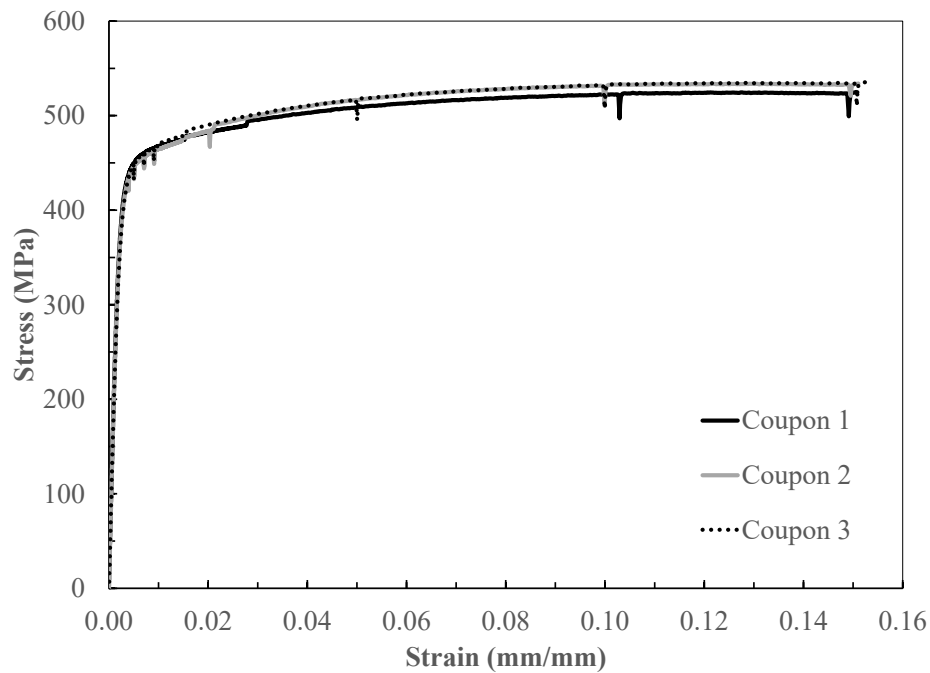
Figure 3 - 3. Stress-strain curves from tensile coupon tests with static load points.

The results from the coupon tests are summarized in Table 3 - 1. It is seen that all the three coupons present a higher yield and ultimate stress than the specified as Grade 3 in ASTM A252, recalling that the values in the norm are 310 MPa and 455 MPa for yield and ultimate stress, respectively.

Table 3 - 1. Coupon tests results

Specimen ID	Yield Stress (MPa)	Ultimate Stress (MPa)	Elastic Modulus (MPa)
1	441	499	204,814
2	422	521	182,530
3	438	510	224,662

3.3.2 Pins

The material used to produce the pins was determined by the norm ASTM A193 as Grade B7, which has a yielding strength of 720 MPa and an ultimate strength of 860 MPa (ASTM Standard 2012). Coupons tests of the material used for the pins were conducted by the fabricator and both the yielding and ultimate strengths and strains were documented in Material Test Reports (MTR). The reported values were provided and no more tests were conducted by the author since the shear resistance of the pins is very high compared to the compressive resistance of the piles. The values from the MTR provided by the fabricator are shown in Table 3 - 2.

Table 3 - 2. Stress and strain values from MTR provided

	Stress (MPa)	Strain (mm/mm)
Yielding	979	0.0049
Ultimate	1069	0.1900

3.4 Preliminary Design

A standard complete assembly of a mechanical connection is composed of the extension pile, fillet weld, plug welds (when needed), the external coupler, the pins, and the lead pile. The overall diameter of the pile shafts was chosen to match typical piles installed in the field by Almita Piling Inc., and the location of the holes were determined to match the drilling equipment available from the company.

The extension pile and the external coupler are welded in the shop by a fillet weld. Four plug welds were included to improve the transfer of loads from the extension pile to the external coupler.

The external coupler is attached to the lead pile by two high-strength steel pins. The schematic of the mechanical connection is shown in Fig. 3 - 4.
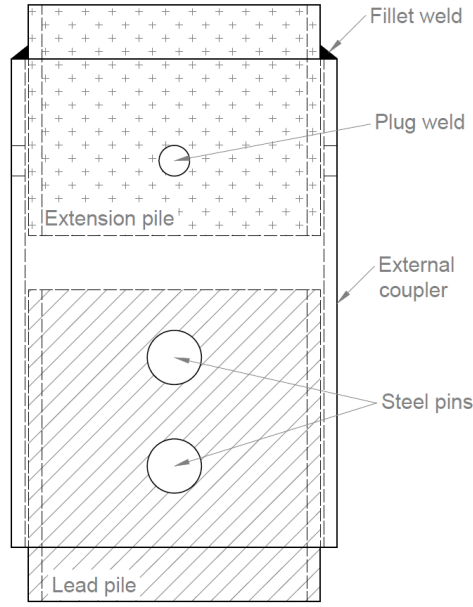
Figure 3 - 4. Components in a standard mechanical connection.

3.4.1 Maximum Capacity Based on the Gross Cross-Section Area

A proposed mechanical connection was initially designed based on the compressive strength of gross cross-section area of the assembly as per Eq. $(3 - 1)$. This equation is used assuming that global or local buckling will not occur in the assembly and that ideal conditions for the existence of a distributed stress through the full cross-section are met (Kulak and Grondin 2011).

(3 - 1)
$$C_r = \varphi A_g F_y$$

where the safety factor (φ) is taken as 1.0 since the actual resistance of the pile is to be investigated, A_g is the gross cross-section area of each component, and F_y is the yielding strength of the pile shafts obtained through coupon tests.

An external coupler with an outside diameter of 12" (304.80 mm) is commonly used for piles with an outside diameter of 10 3/4" (273.05 mm) by the contractor. Based on these dimensions, the maximum gross section capacities are shown in Table $3 - 3$ as per Eq. (3 - 1). It can be seen that the maximum strength is provided by the external coupler and it does not exceed the maximum capacity of the actuators, 6000 kN.

Table 3 - 3. Gross section resistances of piles and coupler in connection

Component	φ	F_y [MPa]	A_g [mm²]	C_r [kN]
Coupler	1	422	11,654	**4,918**
Lead pile shaft	1	422	10,388	**4,384**
Extension pile shaft	1	422	10,388	**4,384**

The minimum pitch is determined by Clause 22.3.1 in CSA S16 (CSA Standard S16-09 2010) as 2.7 times the diameter of the bolts, which for this case results in 128.59 mm. However, the installation machinery used for these piles has a smaller pitch, 101.6 mm. Considering a pitch of 101.6 mm, the final dimensions of the connection are defined and presented in Fig. 3 - 5.

3.4.2 Local Buckling

After determining the gross area compressive capacity of the proposed cross-sections, local buckling provisions by CSA S16 (CSA Standard S16-09 2010) were checked. Local buckling effect on a circular hollow thin-wall cross-section will not occur if the following expression is met:

(3 - 2)
$$\frac{D}{t} \leq \frac{23\ 000}{F_y}$$

where D is the outside diameter of the cross-section and t is the wall thickness. The thickness for the piles and coupler used in the mechanical connection is 0.5 inches (12.7 mm). The local buckling checks for the components used in the assembly are presented in Table 3 - 4.
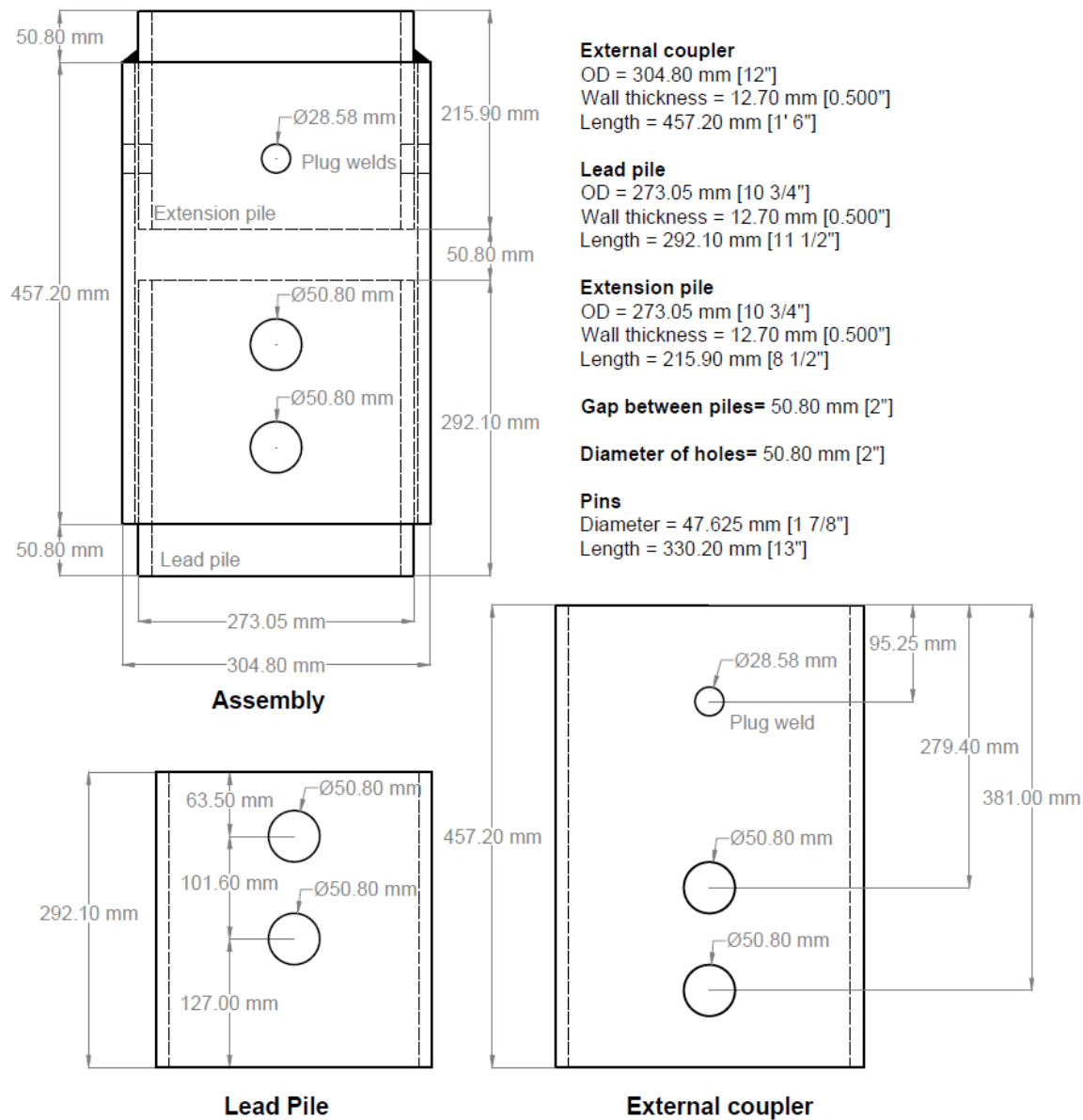
Figure 3 - 5. Final dimensions of the components in mechanical connection.

Table 3 - 4. Determination of the occurrence of local buckling in coupler and piles

Components	D [mm]	t [mm]	Fy [MPa]	$\dfrac{D}{t}$	$\dfrac{23\,000}{F_y}$	$\dfrac{D}{t} \leq \dfrac{23\,000}{F_y}$
Coupler	304.80	12.7	422	24.0	54.5	No local buckling
Lead and extension piles	273.05	12.7	422	21.5	54.5	No local buckling

33

It is seen that no local buckling will occur in neither the external coupler nor the piles used in the assembly.

A gap of 50.8 mm was left between the extension pile and the lead pile. This gap does not correspond to the gap left in real conditions, which is 12.7 mm. This change was intended to neglect the contact between the piles as a source of axial load capacity in the assembly.

3.5 Limit States Design

The connection was checked to determine the a) global compressive resistance of the assembly, b) bearing resistance of the holes, c) *block shear,* d) *end tear-out*, e) shear resistance of the bolts, and f) weld resistance.

3.5.1 Global Compressive Resistance

Due to the complexity in the interaction of the components involved in the mechanical connection, the use of Eq. (2 - 8) presented in Chapter 2 or closed-form solutions to determine the global buckling of a member with different cross-sections under axial compressive load, such as the Bifurcation Analysis and Energy Methods (e.g. Ryleigh's Method) is complex and out of the scope of this study. It is expected that the experimental data and the analysis model obtained in this study will enable for the accurate assessment of global buckling strength. This is an important design aspect when the connection is considered as part of a full pile, warranting a separate study. It is likely that an accurate estimate of this strength be possible only through finite-element analysis in a practical manner.

To provide an estimate of what the global buckling strength would be if the connection was a short column, with constant cross section, and rigid, Eq. (2 - 8) is evaluated in Table 3-5 and showed once again in this section as Eq. (3 - 4), preceded by the slenderness parameter (Eq. (3 - 3)). As expected, it is seen that for such a short connector, the capacity is very close to that obtained based on the gross section capacity as the connection experiences inelastic buckling.

(3 - 3)

$$\lambda = \frac{KL}{r}\sqrt{\frac{F_y}{\pi^2 E}}$$

The effective length factor is K and it is determined by the boundary conditions of the column as shown in Fig. 3 - 6. A conservative value of K is the one corresponding to pinned-pinned boundary conditions.

Figure 3 - 6. Effective length factors with idealized end conditions
Source: (Duan and Chen 1999)

(3 - 4)

$$C_r = \varphi A F_y (1 + \lambda^{2n})^{-1/n}$$

In this study, the section used is a hollow circular cross-section Class C (cold-formed non-stress-relieved) element and its value for n is 1.34 (Kulak and Grondin 2011). The resistance factor (φ) is used as 1.0 to obtain the unfactored strength of the piles. The net cross-sectional area (A_n) was considered for the external coupler and the extension pile accounting for the area reduction due to the presence of the holes. The gross cross-sectional area (A_g) was considered for the extension pile.

Table 3 - 5. Calculation of global compressive resistance of coupler and piles

Component	L [mm]	K	r [mm]	λ	A_n [mm²]	n	C_r [kN]
Coupler	457	1.0	30.45	0.2195	10,364	1.34	**4,318**

3.5.2 Bearing Resistance

Several procedures are currently used to calculate the bearing resistance of the holes in steel bolted connections. Since there is no specific method to use in mechanical connections in hollow structural members as the piles, three of the current methods were considered as explained in Chapter 2.

3.5.2.1 Bearing Equation by Kulak and Grondin (2011)

The equation for bearing resistance presented by Kulak and Grondin (2011) in Chapter 2 is brought for reference once again as follows:

(3 - 5) $$B_r = \varphi t n e F_u \qquad \text{for: } e < 3d$$

where t is the thickness of the piles, n is the number of pins, e is the distance from the center of the hole to the edge of the plate, and F_u is the ultimate strength of the material obtained in the coupons tests. The values of e are different for the external coupler and the lead pile, and are shown in Fig. 3 - 7. Calculated as per Eq. (3 - 5), the bearing resistance of the piles connected by two pins is presented in Table 3 - 6.

It can be seen that the capacity of the assembly is governed by the lead pile with an ultimate strength of 1932 kN because of a shorter distance e. However, the bearing capacity obtained for the lead pile is very conservative under the fact that it has been cut and e is extremely short when compared to a full length pile.
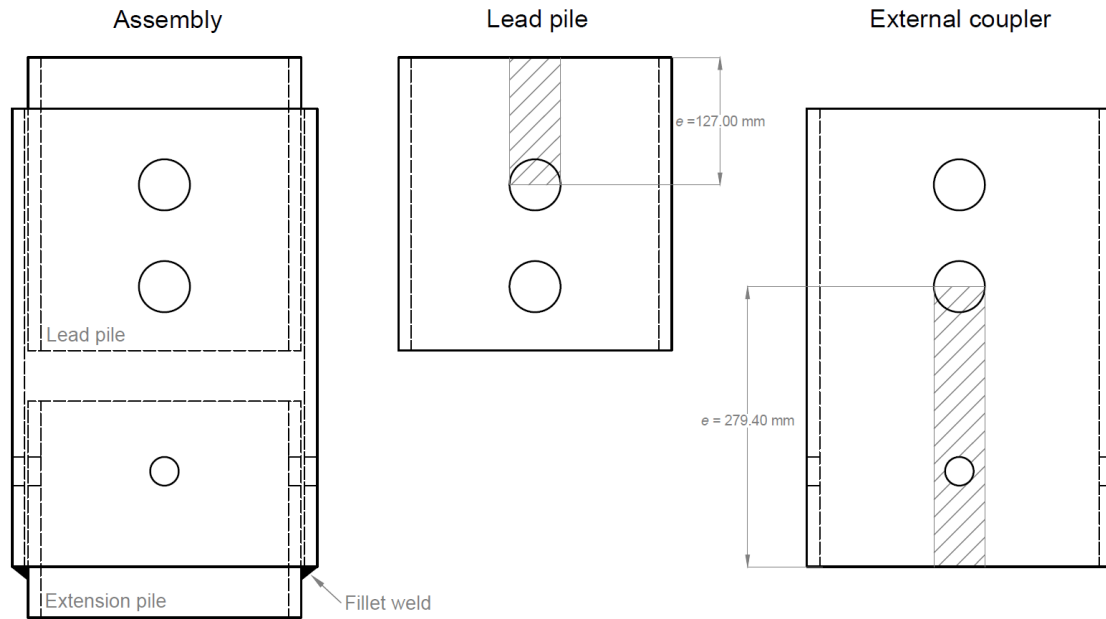
Figure 3 - 7. Values for *e* in the lead pile and the external coupler.

Table 3 - 6. Bearing resistance of coupler and lead pile as per Kulak and Grondin (2011)

Component	Distance to close end	t [mm]	n	e [mm]	Fu [MPa]	B_r [kN]
Coupler	279.40	12.70	2	279	599	**8,502**
Lead pile	127.00	12.70	2	127	599	**3,865**

3.5.2.2 Bearing Equation in CSA S16-09

The current equation describing the bearing resistance of the material in a mechanical connection used in CSA S16-09 (2010) is determined by the assumption that $e \geq 3d$. The expression to calculate the bearing resistance when this condition is met is the following:

(3 - 6) $$B_r = 3\varphi t d n F_u \qquad \text{for: } e \geq 3d$$

In this case, F_u is the ultimate strength of the material obtained in the coupons tests and the resistance factor (φ) was used as 1.0.

As per Eq. (3 - 6), the bearing capacity of the mechanical connection is presented in Table 3 - 7.

Table 3 - 7. Bearing resistance of coupler and lead pile as per CSA S16

Component	t [mm]	n	d [mm]	Fu [MPa]	B_r [kN]
Coupler	12.70	2	47.63	599	**4,348**
Lead pile	12.70	2	47.63	599	**4,348**

Both ultimate strengths of the coupler and the pile are equal. This capacity is an upper limit set for the strength of the external coupler, where the hole is far away from the edge. But the strength of the lead pile is non-conservative because e is smaller than $3d$ and the correct expression given by Kulak and Grondin should be used instead.

3.5.2.3 Bearing Equation by Rogers and Hancock (2000)

As explained in Chapter 2, Rogers and Hancock suggested a method that contains a gradated bearing coefficient (C) dependent on d/t as shown in Eq. (3 - 7):

(3 - 7)
$$V_b = CtdF_u$$

The nominal value for F_u was not used in this study, but the actual value obtained from the coupon tests was used instead. The bearing coefficient (C) is calculated as per Table 3 - 8 copied from Chapter 2 for reference purposes:

Table 3 - 8. Proposed factor C for bearing resistance

d/t	C
d/t ≤ 10	3.0
10 < d/t < 22	4.0 – 0.1 d/t
d/t ≥ 22	1.8

The bearing strength calculated with the method proposed by Rogers and Hancock (2000) is presented in Table 3 - 9.

Table 3 - 9. Bearing capacity as per Rogers and Hancock (2000)

Component	t [mm]	d [mm]	C	F_u [MPa]	V_b (1 bolt) [kN]	n	V_b (n bolts) [kN]
Coupler	12.70	47.63	3	599	1,087	2	**4,348**
Lead pile	12.70	47.63	3	599	1,087	2	**4,348**

In these calculations, both external coupler and lead pile have the same bearing capacity. It is also the same capacity as the one calculated with Eq. (3 - 6), because the value for the bearing coefficient (C) from Rogers and Hancock corresponds to the constant value of 3 imposed in the equation from CSA S16. If the diameter of the bolts and the thickness of the piles were such that the lowest value for C was used, the resultant bearing capacity would be significantly reduced.

3.5.3 Block Shear in CSA S16-09

The expression for *block shear* failure as explained in Chapter 2 is presented once again for reference purposes as Eq. (3 - 8).

(3 - 8)
$$T_r = \varphi_u \left[U_t A_n F_u + 0.6 A_{gv} \frac{(F_y + F_u)}{2} \right]$$

where A_{gv} is the gross area taken along the potential shear planes, A_n is the net area in tension, and the constant U_t is a symmetry factor (taken as 0.9 for this study as in coped beams with one bolt line). The safety factor (φ_u) is taken as 1.0 to obtain the unfactored capacity of the connection. The block shear patterns under a compressive axial load are shown in Fig. 3 - 8 and the results are shown in Table 3 - 10.
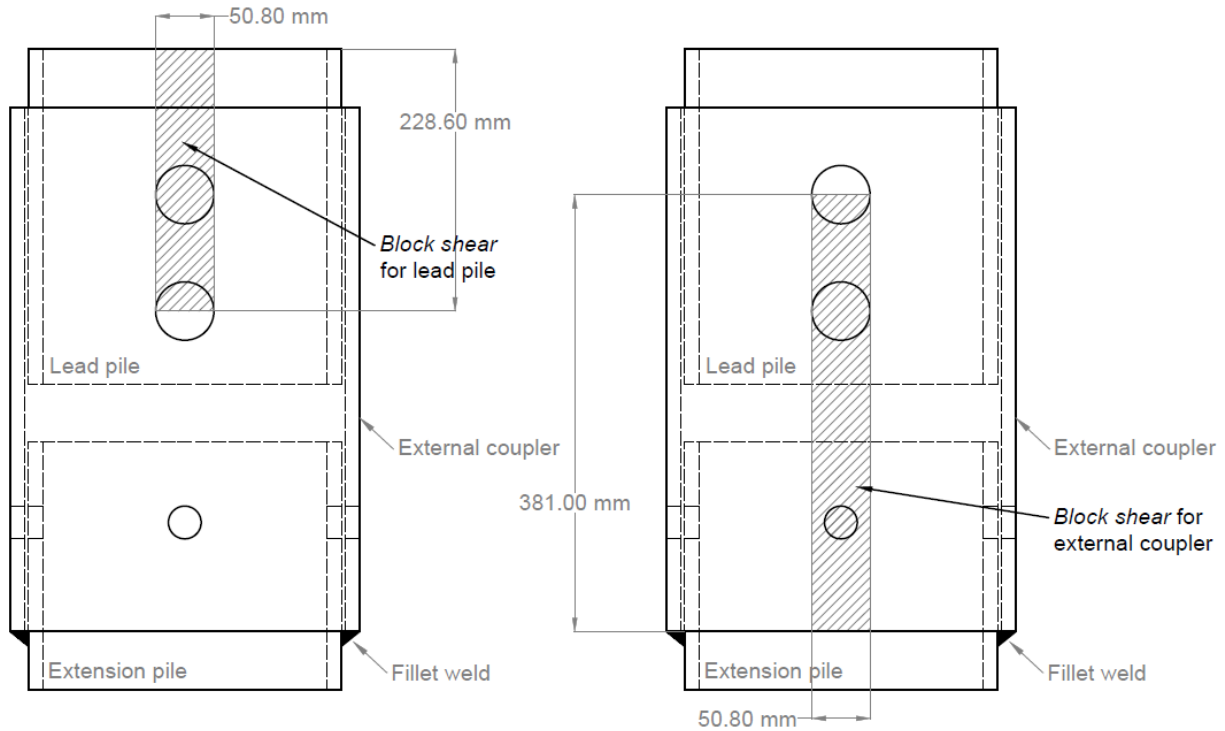
Figure 3 - 8. Block shear patterns for elements in mechanical connection.

Table 3 - 10. Block shear capacity of lead pile and external coupler

Component	U_t	F_y [MPa]	F_u [MPa]	A_n [mm²]	A_{gv} [mm²]	T_r [kN]
Coupler	0.90	422	599	645	9,677	**6,624**
Lead Pile	0.90	422	599	645	5,806	**4,253**

High capacities were obtained for the external coupler due to the long path to be developed in the shear planes for block shear to occur. Furthermore, the presence of the extension pile hinders the propagation of a possible crack in this component.

For the lead pile, this particular block shear could occur if the gap between the piles was shorter than the length of the shear planes that could develop in the lead pile. However, the lead pile governs the design of *block-shear* capacity.

3.5.4 *End Tear-Out*

Failure by *end tear-out* can govern the capacity of the end bolts in a bolted connection as explained in Chapter 2. The three references presented were used in this section and the results are presented for each one of them. In order to be able to compare the *end tear-out* resistance of the connection, the results presented in this section should be multiplied by 2 when the resistance of the material between the holes is calculated. This takes into account the presence of the second bolt which provides more resistance to the connection. This is not followed in the design process of a bolted connection but it has to be done for the sake of effective comparison between the different failure modes.

3.5.4.1 *End Tear-Out* by Kulak and Grondin (2011)

As explained in Literature Revie, the calculations for *end tear-out* failure can be obtained from the expression used for *block shear* defined in Eq. (3 - 8) with some modifications. The formulation of this expression is as follows:

(3 - 9)
$$T_r = \varphi_u \left[2 \; x \; 0.6 A_{gv} \frac{(F_y + F_u)}{2} \right]$$

where the variables are the same as the ones in block shear. The only remaining part is the shear capacity of the material, neglecting the tensile capacity.

Substituting the values in Eq. (3 - 9), the *end-tear out* occurring in both sides of the piles as shown in Fig. 3 - 9 was calculated and the results are presented in Table 3 - 11.
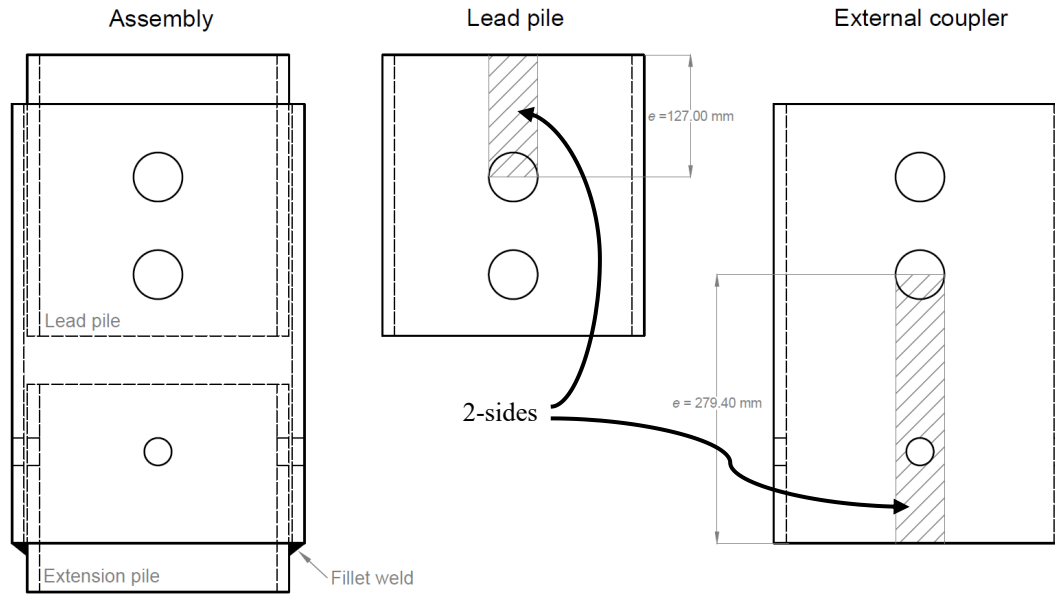
Figure 3 - 9. Areas where end tear-out developed in each component.

Table 3 - 11. End tear-out capacities of components in mechanical connection

Component	U_t	F_y [MPa]	F_u [MPa]	A_{gv} [mm²]	T_r [kN]
Coupler	0.90	422	599	3,548	**8,695**
Lead Pile	0.90	422	599	1,613	**3,952**

High tear-out strengths are obtained in the external coupler due to the large lengths between the holes and the end of the pile. As in block shear, the *end tear-out* of the lead pile would occur if the gap between this and the extension was shorter than the distance from the hole to the end of the pile.

End tear-out failure can occur also between the holes, as shown in Fig. 3 - 10. The calculation for the failure in this area reduces significantly the capacity of the assembly as shown in Table 3 - 12.
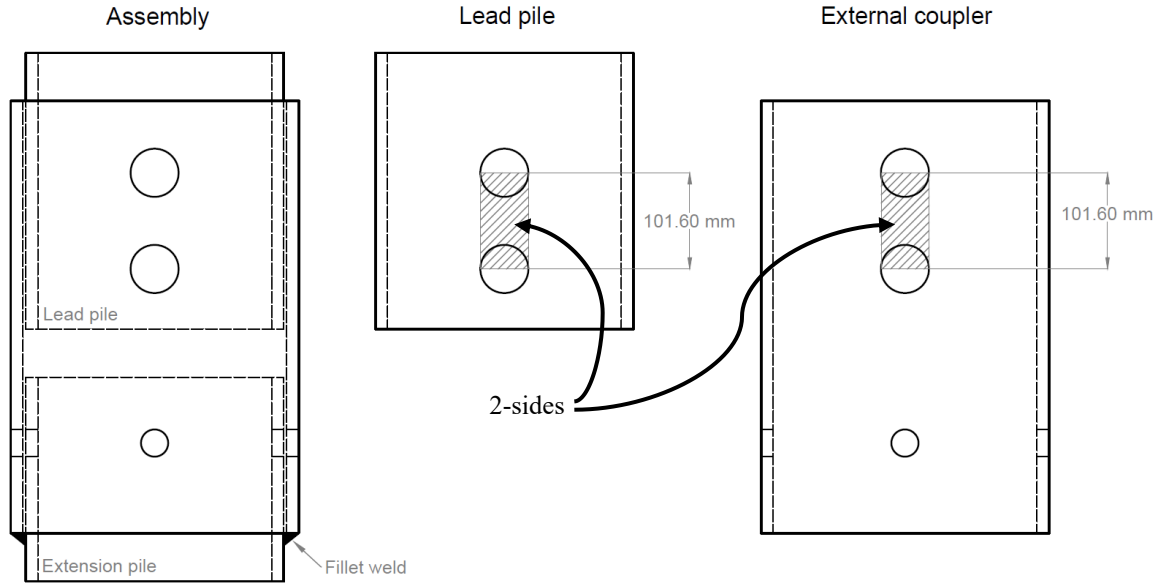
Figure 3 - 10. Areas between holes under end tear-out.

Table 3 - 12. End tear-out capacities taking the shear area between the holes.

Component	U_t	F_y [MPa]	F_u [MPa]	A_{gv} [mm²]	T_r [kN]	$2\,T_r$ [kN]
Coupler	0.90	422	599	1,290	3,162	6,324
Lead Pile				1,290	3,162	6,324

3.5.4.2 *End Tear-Out* by Rogers and Hancock (2000)

The three expressions given by Roger and Hancock (2000) as presented in Chapter 2 for *end tear-out* are the following:

(3 - 10)
$$V_f = teF_u$$

(3 - 11)
$$V_f = A_n F_u$$

(3 - 12)
$$A_n = 0.60 \; x \; 2t \left(e - \frac{d_h}{2} \right)$$

43

Both methods were used to calculate the *end tear-out* in two zones: from the holes to the end of the pile, and between the holes. The results are presented in Table 3 - 13.

Table 3 - 13. End tear-out capacities in two different locations of components

	Aus/NZ (1996) and U.S. (1997)					CSA S 136 (1994)		
From hole to end of plate								
Component	t	e	F_u	V_f		d_h	A_n	V_f
	[mm]	[mm]	[MPa]	**[kN]**		[mm]	[mm²]	**[kN]**
Coupler	12.7	279.4	599	**8,502**		50.8	3,871	**9,275**
Lead pile	12.7	127.0	599	**3,865**		50.8	1,548	**3,710**

	Aus/NZ (1996) and U.S. (1997)					CSA S 136 (1994)			
From hole to hole									
Component	t	e	F_u	V_f	$2V_f$	d_h	A_n	V_f	$2\,V_f$
	[mm]	[mm]	[MPa]	**[kN]**	**[kN]**	[mm]	[mm²]	**[kN]**	**[kN]**
Coupler	12.7	101.6	599	**3,092**	**6,184**	50.8	1,161	**2,782**	**4,344**
Lead Pile	12.7	101.6	599	**3,092**	**6,184**	50.8	1,161	**2,782**	**4,344**

High values of tear-out strength were obtained following the codes from Australia and USA compared to the results given by the Canadian code. The main contributor to these differences is that CSA S16 accounts for a reduced area by deducting half of the holes and by multiplying by the factor 0.60, whereas Australian and American codes take the full *e* length to determine the strength of the connection and do not present any reduction factor.

3.5.4.3 *End Tear-Out* in CSA S16-01 (2007)

As presented in Chapter 2, according to Clause 13.11, the resistance of a connection under shear stress would be the lesser of the two following equations:

(3 - 13)
$$T_r = 0.60\varphi A_{gv}F_y$$

(3 - 14)
$$T_r = 0.60\varphi A_{nv}F_u$$

where the difference is in the areas taken into account, being A_{gv} the gross shear area, and A_{nv} the clear distance from the bolt to the edge of the plate. Both areas are illustrated according to the zones being calculated following this procedure in Fig. 3 - 11 and Fig. 3 - 12. The results are presented by zones as follows:

44

Case 1: End tear-out capacities from end of pile to closest hole (Table 3 - 14).

Case 2: End tear-out capacities from hole to hole (Table 3 - 15).

In case 2, where the gross shear areas between the holes were considered as per Eq. (3 - 13), a strength reduction of 63% was observed in the external coupler and a 20% strength reduction was observed in the lead pile when compared to case 1.

When the net shear areas between the holes were considered as per Eq. (3 - 14) (case 2), a strength reduction of 70% was observed in the external coupler compared to case 1. In the lead pile, a 25% strength reduction occurred from case 1 to case 2.

These results reflect that the governing failure will be given by the material between the holes rather than the material from the hole to the edge of the pile.

Table 3 - 14. End tear-out capacities of lead pile and external coupler as per CSA S16 from end of pile to closest hole (Case 1)

Component	Eq. (3 - 13) $T_r = 0.60\varphi A_{gv}F_y$					Eq. (3 - 14) $T_r = 0.60\varphi A_{nv}F_u$				
	t	e	A_{gv}	F_y	T_r	d_h	$e_2 = e - d_h/2$	A_{nv}	F_u	T_r
	[mm]	[mm]	[mm2]	[MPa]	[kN]	[mm]	[mm]	[mm2]	[MPa]	[kN]
Coupler	12.70	279.40	7,097	422	**7,188**	50.80	254.00	6,452	599	**9,275**
Lead pile	12.70	127.00	3,226	422	**3,267**	50.80	101.60	2,581	599	**3,710**
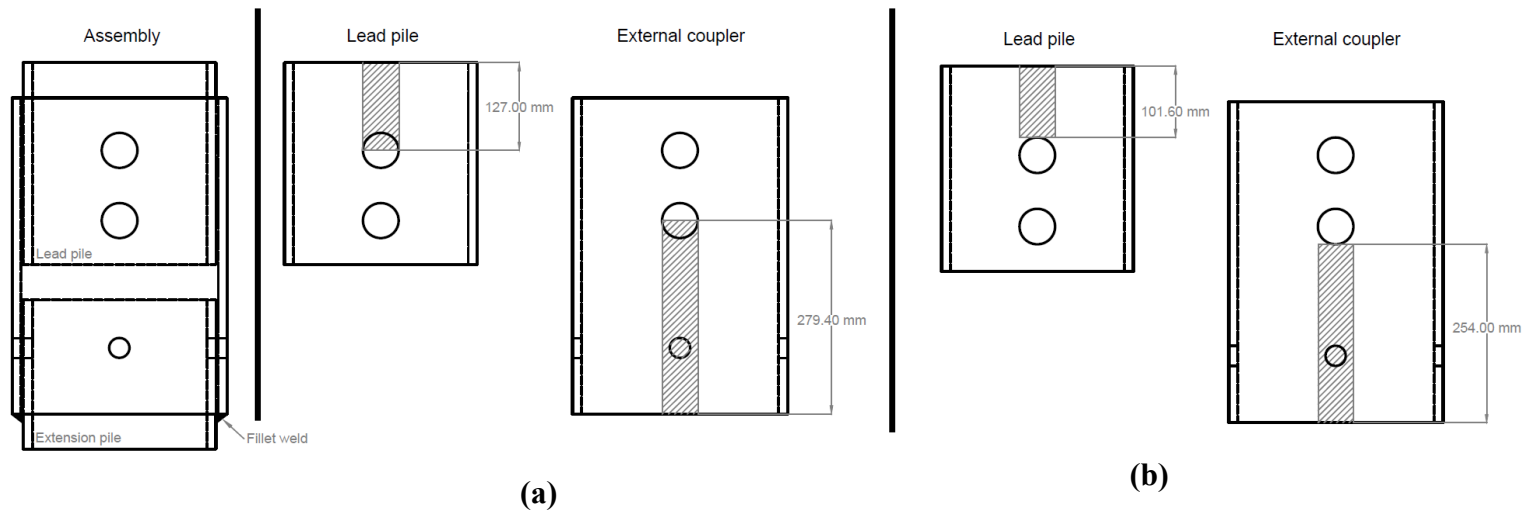
Figure 3 - 11. Location of end tear-out zones from end of pile to closest hole as per (a) Eq. (3 - 13) and (b) Eq. (3 - 14).

Table 3 - 15. End tear-out capacities of lead pile and external coupler as per CSA S16 from hole to hole (Case 2)

	Eq. (3 - 13) $T_r = 0.60\varphi A_{gv}F_y$						Eq. (3 - 14) $T_r = 0.60\varphi A_{nv}F_u$					
Component	t	e	A_{gv}	F_y	T_r	$2\,T_r$	d_h	$e_2 = e - d_h/2$	A_{nv}	F_u	T_r	$2\,T_r$
	[mm]	[mm]	[mm2]	[MPa]	[kN]	[kN]	[mm]	[mm]	[mm2]	[MPa]	[kN]	[kN]
Coupler	12.7	101.6	2,581	422	**2,614**	**5,228**	50.8	76.2	1,935	599	**2,782**	**5,564**
Lead pile	12.7	101.6	2,581	422	**2,614**	**5,228**	50.8	76.2	1,935	599	**2,782**	**5,564**

(a) **(b)**
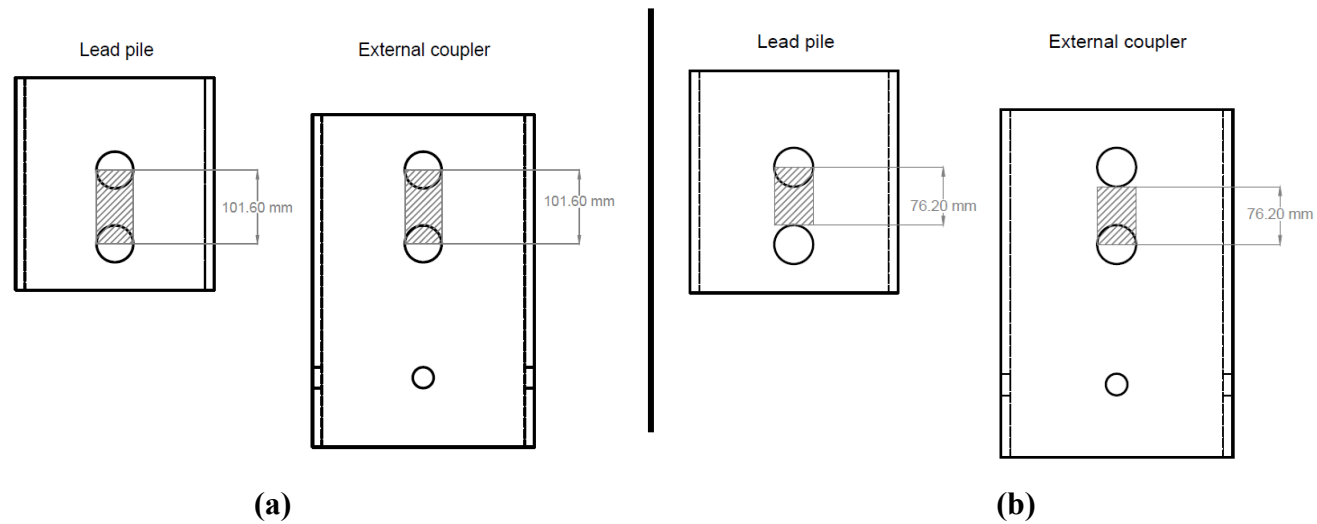
Figure 3 - 12. Location of end tear-out zones from hole to hole as per (a) Eq. (3 - 13) and (b) Eq. (3 - 14).

3.5.5 Shear Resistance of Bolts (Kulak and Grondin 2011)

The expression given to calculate the shear resistance of the bolts is as follows:

$$(3 - 15) \qquad\qquad V_r = 0.60 \; \varphi_b n m A_b F_u$$

where the safety factor φ_b is defined as 1.0 for this study, n is the number of bolts in the connection, m is the number of shear planes, A_b is the cross-sectional area of one bolt, and F_u is the ultimate strength of the bolts given in the MTR.

The calculation of the shear strength of the bolts is presented in Table 3 - 16.

Table 3 - 16. Shear strength of the bolts in the mechanical connection

Component	φ_b	m	n	A_b [mm]	F_u [MPa]	V_r [kN]
Pins	1.0	2	2	2,285	1,069	**4,570**

The high yield and ultimate strengths of the material provided a high shear strength to the pins. However, this capacity is similar to the capacity of the piles in some limit states previously analyzed and the assumption that the pins will not fail in shear cannot yet be taken.

3.5.6 Strength of the Weld

The strength of fillet welds and plug welds was calculated as the resistance of the base metal. For plug welds, this calculation was conducted as per the following expression from Chapter 2:

$$(3 - 16) \qquad\qquad V_r = 0.67 \varphi_w A_m F_u$$

where A_m is the area of the fusion face, which is the area of the metal in contact with the weld, F_u is the ultimate strength of the base metal, and φ_w is the safety factor with a value of 1.0 to determine if the actual weld strength used in the assembly is suitable for the applied load. The numerical modifier 0.67 relates the shear strength of the weld to the specified electrode tensile strength (Kulak and Grondin 2011).

For fillet welds, Eq. (3 - 17) was used as explained in Chapter 2.

(3 - 17)
$$V_r = 0.67\varphi_w A_w X_u (1.0 + 0.5\ sin^{1.5}\theta)M_w$$

The strength reduction factor for welded joints (M_w) was taken as 1.0 in this study. The calculation of the capacities of the fillet weld and the 4 plug welds used in the assembly are shown in Table 3 - 17 with the following terminology added:

B: fusion face of fillet weld.

d_o: external diameter of extension pile.

d_w: diameter of the plug weld.

n_p: number of plug welds.

It can be seen that the capacity of the fillet weld compromises the integrity of the assembly by being similar or lower to several failure modes explained before in this sections. Hence, the adequacy of the four plug welds to contribute to the total resistance of the weld.

Table 3 - 17. Calculation of weld capacities

Weld	φ_w	B	d_o	$A_w =$ $0.707*B*d_o$	X_u	θ	M_w	V_{rF}
		[mm]	[mm]	[mm²]	[MPa]	[deg]		[kN]
Fillet	1.0	12.70	273.05	7702.21	550	90	1.00	4,257

		φ_w	d_w	$A_m =$ $(\pi d_w^2)/4$	F_u	n_p		V_{rP}
			[mm]	[mm²]	[MPa]			[kN]
Plug		1.0	28.58	641.30	599	4		1,029

					V_{rF}	V_{rP}		V_{rT}
Total					[kN]	[kN]		**[kN]**
					4,257	1,029		**5,287**

3.6 Summary of Limit States Design

The results of each one of the limit states calculated to design mechanical connections are presented in Table 3 - 19. This table presents the values obtained, the equations used, important observations about the applicability of each expression, and the governing mode as per each author.

Setting an upper limit defined by the capacity of the gross cross-section of the piles and coupler was the starting point to define this range of results. From this, it was found that local buckling was not likely to occur and that the calculation of the limit states used for bolted connections was the next step.

The global compressive resistance of the mechanical connection was complex by involving bolted curved plates under compression, bolts that are not snug tight, and gaps between piles, concluding that closed-form solutions were not suitable for the case. However, a piece of pile with the dimensions of the mechanical coupler with no connection involved was analyzed and its capacity obtained. The global compressive resistance was calculated for the sake of knowing the capacity of a continuous short pile, but all the assumptions taken discard it from becoming the governing failure mode.

The bearing resistance expressions used by different authors led to a series of results changing whether calculating the external coupler or the lead pile, and the holes near to the edges of the piles or the holes far away from them. In general, the lead pile presented lower capacities than the external coupler, with the strength of 3856 kN given by Kulak and Grondin as the most critical one.

The capacities of *block shear* and *end tear-out* capacities were the most important ones by giving the first applicable approach and governing failure modes in the connection. The results diverged from a low strength of 2614 kN given by CSA S16 to a strength of 3162 kN given by the Australian and US codes. Both results were obtained from the calculations of the *end tear-out* between the holes of the lead pile and external coupler, becoming these zones the governing areas of the assembly. *Block shear* strengths of the components in the assembly were higher than *end tear-out*. Hence, they will not govern.

For the sake of comparison between the modes related to the failure of the plates, *end tear-out* resistance was multiplied by two when the material between the holes was analyzed. This was done to effectively present a comparison between all the failure modes accounting for the presence of the two bolts. However, the prediction is that cracks will develop from one hole to the other one due to the load applied by one single bolt. The distance between the edge of the pile and the hole closest to it is long enough to discard the development of cracks in that zone.

The shear resistance of the bolts and the weld were higher than the governing failure modes calculated for the shafts. A failure of the pins or the weld are not expected to occur during the application of the load.

Summarizing, the governing limit state expected to occur is the *end tear-out* of the material between the holes in both the external coupler and the lead pile under an axial compressive load of 2614 kN.

Table 3 - 18. Limit states calculation for mechanical connection

Limit State	Method	Zone	Component	Ultimate Capacity [kN]	Equation	Observations
Global Compressive Resistance	CSA S16	N/A	External coupler	4,318	$C_r = \varphi A F_y (1 + \lambda^{2n})^{-1/n}$	**Not applicable** - The coupler does not work as a continuous short pile, but as a bolted connection. - The presence of pins as load transmission system is not being analyzed. The capacity of the assembly should be analyzed as bolted connection.
Bearing Resistance	Kulak & Grondin	N/A	External coupler	8,502	$B_r = \varphi t n e F_u$	**External Coupler: Not applicable** **Lead Pile: Does not govern** - This formula accounts for a minimum pitch of 2.7d, which is not met in the current design. - The small pitch in both lead pile and external coupler will lead to tear-out of the material in between the holes. Bearing resistance of one row of holes cannot be developed and should not be taken into account. - The ratio e/d in the external coupler is larger than 3 and the formula provided by CSA S16 should be used instead.
			Lead pile	3,865		
	CSA S16	N/A	External coupler	4,348	$B_r = 3\varphi t d n F_u$	**External Coupler: Does not govern** **Lead Pile: Not applicable** - This formula accounts for a minimum pitch of 2.7d, which is not met in the current design. - The small pitch will lead to tear-out of the material in between the holes. Bearing resistance of one row of holes cannot be developed and should not be taken into account. - The ratio e/d in the lead pile is lower than 3 and the formula given by Kulak & Grondin should be used instead.
			Lead Pile	4,348		

Table 3 - 19 (cont'd). Limit states calculation for mechanical connection

Limit State	Method	Zone	Component	Ultimate Capacity [kN]	Equation	Observations
Bearing Resistance (cont'd)	Rogers & Hancock	N/A	External coupler	4,348	$V_b = CtdF_u$	**External Coupler: Does not govern** **Lead Pile: Not applicable** - The ratio e/d in the lead pile is lower than 3 and the formula given by Kulak & Grondin should be used instead. - The small pitch in both lead pile and external coupler will lead to tear-out of the material in between the holes and bearing resistance of these holes cannot be developed.
			Lead pile	4,348		
Block Shear	CSA S16	N/A	External coupler	6,624	$T_r = \varphi_u \left[U_t A_n F_u + 0.6 A_{gv} \frac{(F_y + F_u)}{2} \right]$	**External Coupler: Does not govern** **Lead Pile: Governs** - Long distance exists between the holes and the end of the external coupler. - Extension pile interferes in the block shear path of the external coupler.
			Lead pile	4,253		

Table 3 - 19 (cont'd). Limit states calculation for mechanical connection

Limit State	Method	Zone	Component	Ultimate Capacity [kN]	Equation	Observations
End Tear-Out	Kulak & Grondin	Hole to end of pile	External coupler	8,695	$T_r = \varphi_u \left[2 \; x \; 0.6 A_{gv} \dfrac{(F_y + F_u)}{2} \right]$	**Coupler and pile: *End tear-out* of material between holes governs** - The distance from the holes to the end of the external coupler is extremely long. The zones between the holes will tend to tear-out first. - The extension pile hinders the tear-out path of the external coupler. - The distance from the holes to the edge of the lead pile is longer than the gap between the piles. This gap will close before reaching a full *tear-out* of the material at the end of the lead pile. - The *end tear-out* of the material between the holes was the load obtained in the tests, as will be presented in Chapter 4.
			Lead pile	3,952		
		Hole to hole	External coupler	3,162 x2 = 6,324		
			Lead pile	3,162 x2 = 6,324		
	Rogers & Hancock (AUS/NZ 1996, US 1997)	Hole to end of pile	External coupler	8,502	$V_f = te F_u$	**Coupler and pile: *End tear-out* of material between holes governs** - The distance from the holes to the end of the external coupler is extremely long. Zones between the holes will tend to tear-out first. - However, it has been seen that the shear flow in the shear areas is better represented by the average of ($F_y + F_u$) and not only by F_u. - Shear stress is considered to be 0.60 the normal stress, which is not taken into account in this expression. - This expression presents a non-conservative approach to the *end tear-out* capacity of the piles by accounting for F_u.
			Lead pile	3,865		
		Hole to hole	External coupler	3,092 x2 = 6,184		
			Lead pile	3,092 x2 = 6,184		

Table 3 - 19 (cont'd). Limit states calculation for mechanical connection

Limit State	Method	Zone	Component	Ultimate Capacity [kN]	Equation	Observations
End Tear-Out (cont'd)	Rogers & Hancock (CSA S136)	Hole to end of pile	External coupler	9,275	$V_f = A_n F_u$ $A_n = 0.60 \; x \; 2t \left(e - \dfrac{d_h}{2} \right)$	**Coupler and pile: _End tear-out_ of material between holes governs** - The distance from the holes to the end of the external coupler is extremely long. Zones between the holes will tend to tear-out first. - A non-conservative approach to the _end tear-out_ capacity of the piles is obtained when accounting for F_u.
			Lead pile	3,710		
		Hole to hole	External coupler	2,782 x2 = 4,344		
			Lead pile	2,782 x2 = 4,344		
	CSA S16 (Gross shear area)	Near hole to free edge	External coupler	7,188	$T_r = 0.60 \varphi A_{gv} F_y$	**Coupler and pile: _End tear-out_ of material between holes governs** - The shear flow in the shear areas is better represented by the average of $(F_y + F_u)$ and not only by F_y. - The distance from the holes to the end of the external coupler is extremely long. Zones between the holes will tend to tear-out first. - This was the lowest value obtained for _end-tear out_ strength and the governing mode predicted to occur.
			Lead pile	3,267		
		Hole to hole	External coupler	2,614 x2 = 5,228		
			Lead pile	2,614 x2 = 5,228		
	CSA S16 (Net shear area)	Near hole to free edge	External coupler	9,275	$T_r = 0.60 \varphi A_{nv} F_u$	**Coupler and pile: _End tear-out_ of material between holes governs** - A non-conservative approach to the _end tear-out_ capacity of the piles is obtained when accounting for F_u. - The distance from the holes to the end of the external coupler is extremely long. Zones between the holes will tend to tear-out first.
			Lead pile	3,710		
		Hole to hole	External coupler	2,782 x2 = 5,564		
			Lead pile	2,782 x2 = 5,564		

Table 3 - 19 (cont'd). Limit states calculation for mechanical connection

Limit State	Method	Zone	Component	Ultimate Capacity [kN]	Equation	Observations
Shear Resistance of Bolts	Kulak & Grondin	N/A	Bolts	4,570	$V_r = 0.60\ \varphi_b nmA_b F_u$	**Not governing failure mode** - The material used for bolts is made of higher resistance than the piles in order to avoid shear failure. The bolts capacity is higher than the ultimate strength of the connection obtained in the test, as expected. This check must be conducted every time to ensure the higher capacity of the bolts.
Weld capacity	Kulak and Grondin 2011	N/A	Fillet weld + Plug welds	5,287	$V_{r,F} = 0.67\varphi_w A_w X_u (1.0 + 0.5\ sin^{1.5}\theta)M_w$ $V_{r,P} = 0.67\varphi_w A_m F_u$	**Not governing failure mode** - The capacity of the fillet weld plus the four plug welds added was calculated to avoid weld failure in the assembly. The overall capacity of the welds together is higher than the rest of the possible failure modes to occur.

CHAPTER 4.   EXPERIMENTAL PROGRAM

4.1 Introduction

The objective of the full-scale test program was to investigate the behaviour of the mechanical connection under axial compressive loads. Based on the design presented in Chapter 3 of this document, three identical specimens were fabricated by Almita Piling Inc. and tested at the University of Alberta.

4.2 Test Setup

The axial load was applied through an MTS 6000 actuator, which has a maximum compressive capacity of 6000 kN. On the head of the actuator a load cell retrieved the applied load. The displacement measured at the head of the MTS was recorded.

The mechanical connection was instrumented with a Digital Image Correlation (DIC) system. It is composed by a series of cameras that follow a pattern of dots which are painted on the surface of the test specimen. By measuring the relative displacement of the dots, the DIC is capable of determining the displacements and the strains of that area.

Figure 4 - 1 shows the painting process followed in the external coupler. The mill scale was removed from the areas of interest, then these areas were painted in white, and finally the black dots were sprayed on them.

Figure 4 - 1. Painting process for each specimen.

When the piles are installed in the field, the lead pile is the first element being drilled into the soil. The mechanical coupler is welded to the bottom of the "extension pile" in the shop. Then, the extension pile is positioned on top of the lead pile, with the connector resting on the top of it. The coupler and lead pile are connected by pins and the drilling process continues. Figure 4 - 2 (a) shows the position of the components of the assembly in the field.

To facilitate the use of the DIC, it was decided to test each specimen in an upside-down position. Therefore, the lead pile was on the top of the assembly. Figure 4 - 2 (b) show how the assembly was positioned for the tests. Figure 4 - 3 shows the complete test set-up including the circular plates of the MTS 6000 and the camera system from the DIC.
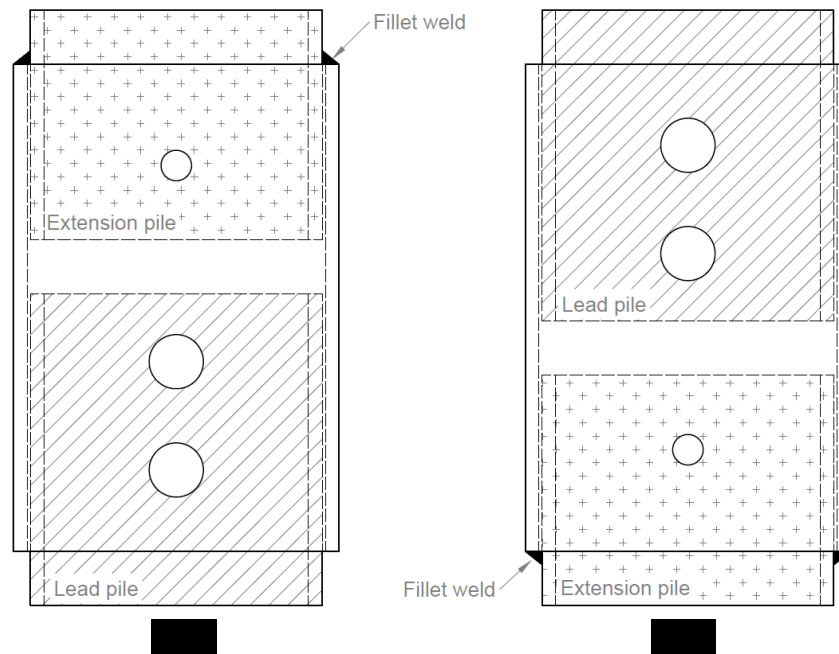
Figure 4 - 2. (a) Assembly position in real conditions. (b) Assembly position for tests.
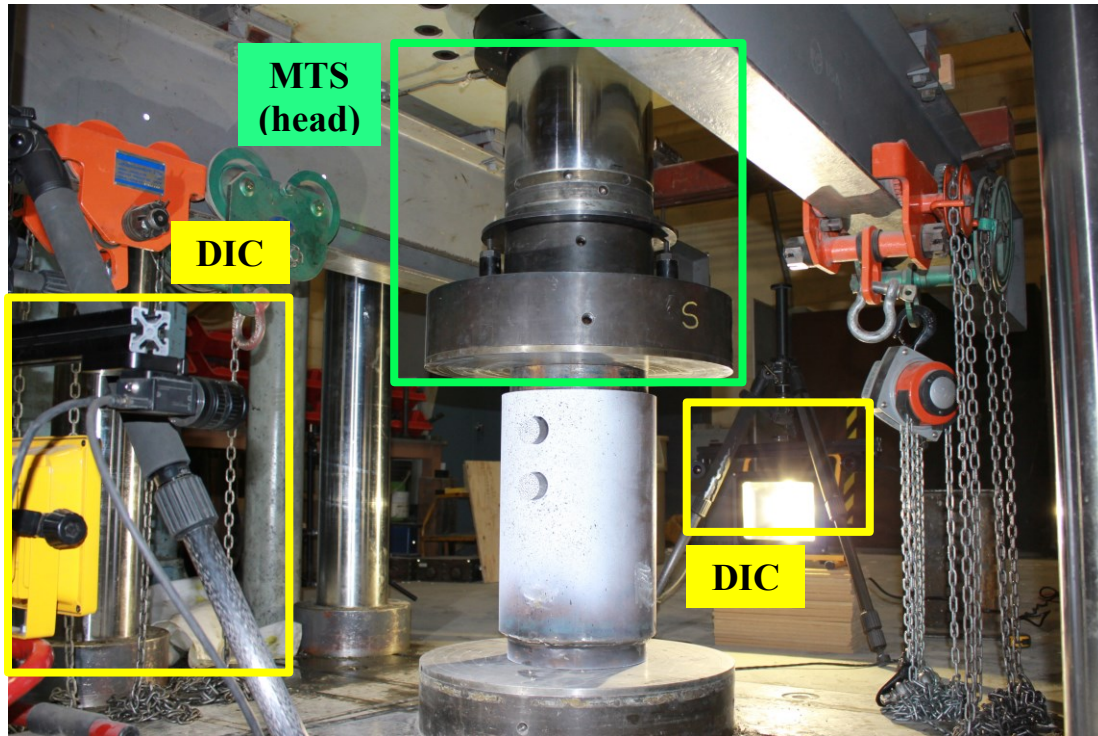
Figure 4 - 3. Experimental setup.

4.3 Test Procedure

The MTS actuator exerted a downward displacement at the top of the assembly. A load cell was used to retrieve the reaction vertical force, while the vertical displacement of the actuator head was recorded. The DIC was used to retrieve the deformations of the surface of the external coupler.

The experimental program started with the positioning of the specimens between the circular plates of the actuator. The cameras of the DIC system were set in position, adjusted, and calibrated. The head of the actuator was displaced until it established contact with the lead pile, located at the top of the assembly. When the plate from the actuator and the lead pile established contact, some reaction forces were detected. These were attributed to uneven settlement of the pins in the eight holes of the assembly.

The presence of the external coupler limited the observation of deformations in the lead pile. To examine the state of the leading pile, the first test was stopped at a downwards displacement of approximately 25.4 mm (1 inch). This corresponded to an approximate service deflection as indicated by the contractors. The actuator was removed from the assembly and observations were

made on the state of the lead pile. No cracks were detected in the inner surface of the lead pile, although significant deformations of the holes were apparent. After the observations, the load was applied once again. Unfortunately, the data from the second part of the loading process in specimen 1 was lost due to malfunction of the equipment.

For specimens 2 and 3, it was decided to apply the loads without interruptions up to a maximum displacement of approximately 50.8 mm (2 inches). This displacement level was sufficient to achieve the complete closure of the gap between the piles and was imposed to also investigate if the weld could sustain the applied load before the piles established contact. This would verify the assumption that weld strength is not the governing failure mode of the connection.

The rate of the applied displacement for specimen 1 was determined as 0.5 mm/min. Due to the excessive time taken to accomplish the desired displacement, specimens 2 and 3 were tested under a rate of 2 mm/min. Several static points were obtained in the three specimens by stopping the loading and resuming it once the drop of the load occurred. The load-displacement data for the three specimens was obtained from the MTS and the load-deformation tables and pictures were obtained from the DIC system.

4.4 Test Results

Three sets of results were retrieved from the experimental work: load-displacement response of the assembly, deformations, and strains of the external coupler holes. General specifications and after-test data for each one of the specimens are presented in Table 4 - 1. In all three specimens, the failure mode consisted of vertical cracks that spread from the top hole to the bottom hole in the lead pile.

Table 4 - 1. General results observed in the tests.

Specimen ID	Strain rate (mm/min)	Max. Displacement (mm)	Max. Load (kN)	Failure Mode
1	0.5	28*	2,700*	End tear-out
2	2.0	43	3,331	End tear-out
3	2.0	42	3,161	End tear-out

* Last recorded measurements (subsequent data lost due to malfunction)

60

4.4.1 General Observations After-Tests

4.4.1.1 Specimen 1 – Service load (2700 kN)

The first areas to show significant deformations were the holes in the lead pile (Fig. 4 - 4 (a)). The deformations occurred in the vertical direction and out-of-plane deformations of the holes (bulking effect) were observed in the zones in contact with the pins as it is marked in Fig. 4 - 4 (b). The external coupler presented also vertical deformations of the holes and the bulking effect of the material on the areas in contact with the pins. Horizontal radial deformations were observed in the external coupler as shown in Fig. 4 - 4 (c). The lead pile did not present these radial deformations due to the confinement effect provided by the external coupler.

4.4.1.2 Specimens 1, 2 and 3 – Failure load (Avg. 3246 kN)

Large deformation of the holes and bulking were observed. The failure mode was characterized by two cracks that appeared between the top and bottom holes of the lead pile, one in each side of the holes as depicted in Fig. 4 - 5 and Fig. 4 - 6. These cracks were caused by the concentrated loads exerted by the pins. The weld did not present any deformation or cracking at the failure load. The pins exhibited no perceptible damage nor deformation.
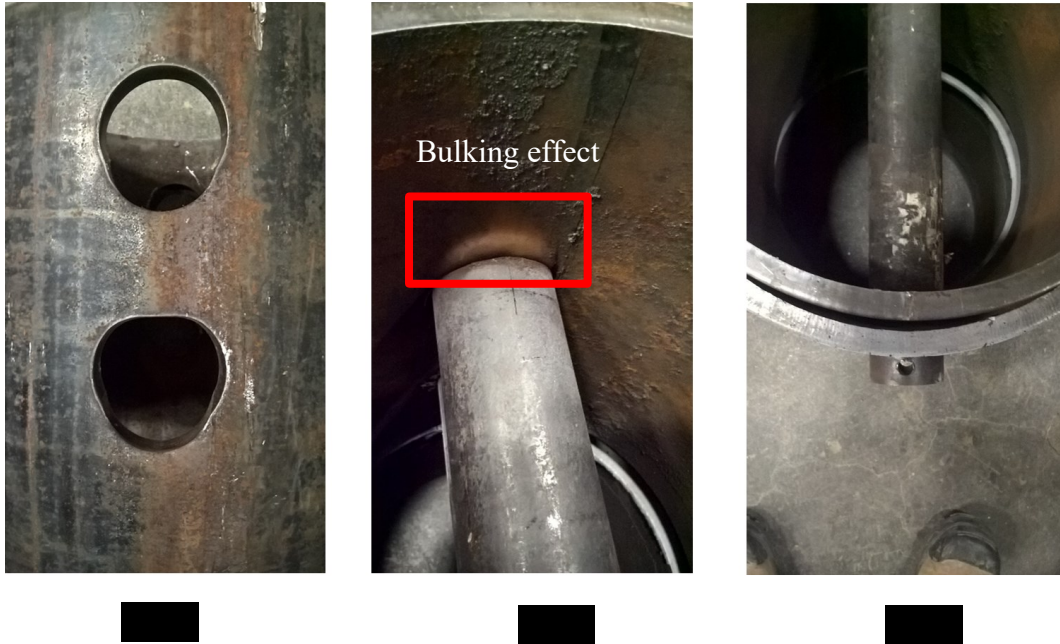
Figure 4 - 4. Deformations in Specimen 1.
a) Vertical ovalization of holes in the lead pile. b) Out-of-plane deformations of holes in lead pile. c) Deformation of cross-section of external coupler.
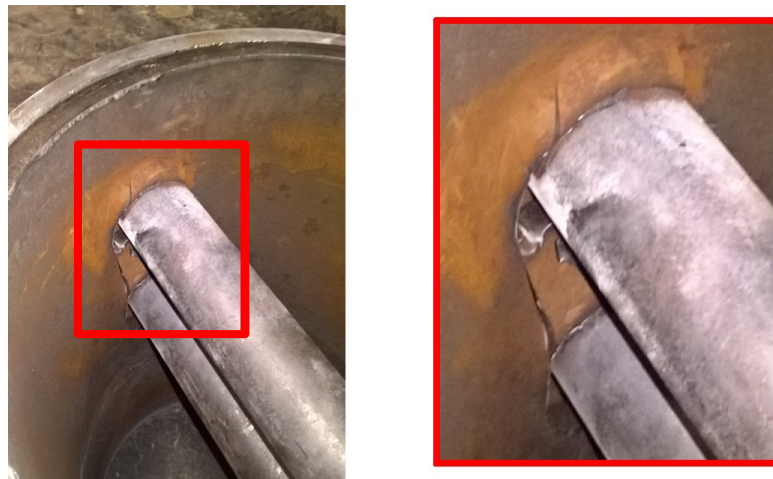
Figure 4 - 5. Specimen 2: Cracks between the two pins in the inner surface of the lead pile.
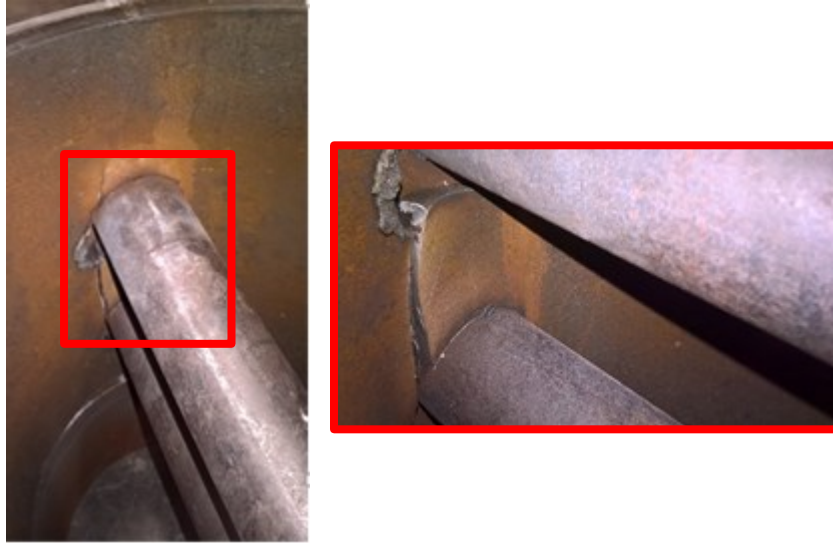
Figure 4 - 6. Specimen 3: Cracks between the two pins in the inner surface of the lead pile.

4.4.2 Load-Deformation Response

The load-deformation relationship of the assembly was obtained from the load cell located at the top of the MTS plate and it is shown in Figure 2-28 for the three tested specimens. Data from specimen 1 was recorded up to a displacement of 25.4 mm (1 inch), and was lost afterwards, while the data from specimens 2 and 3 was recorded up to a displacement of 50.8 mm (2 inches).

The load-displacement curves in Fig. 4 - 7 show that the three specimens present similar responses. The initial part of the curve shows a region in which reaction forces appear when the pins start to settle. This initial stabilization process occurs under very small loads in the range from 0 kN to approximately 100 kN and it is attributed to possible misalignment of the holes or out-of-plumbness of the piles at the beginning of the test, which produce uneven settlement of the pins.

After a load of approximately 100 kN, the load-carrying capacity of the three specimens started increasing steeply, with a nearly constant stiffness. This occurred when the pins were completely settled on the holes in the lead pile and the coupler. The elastic part of the load-displacement response extended up to a load of approximately 1200 kN.
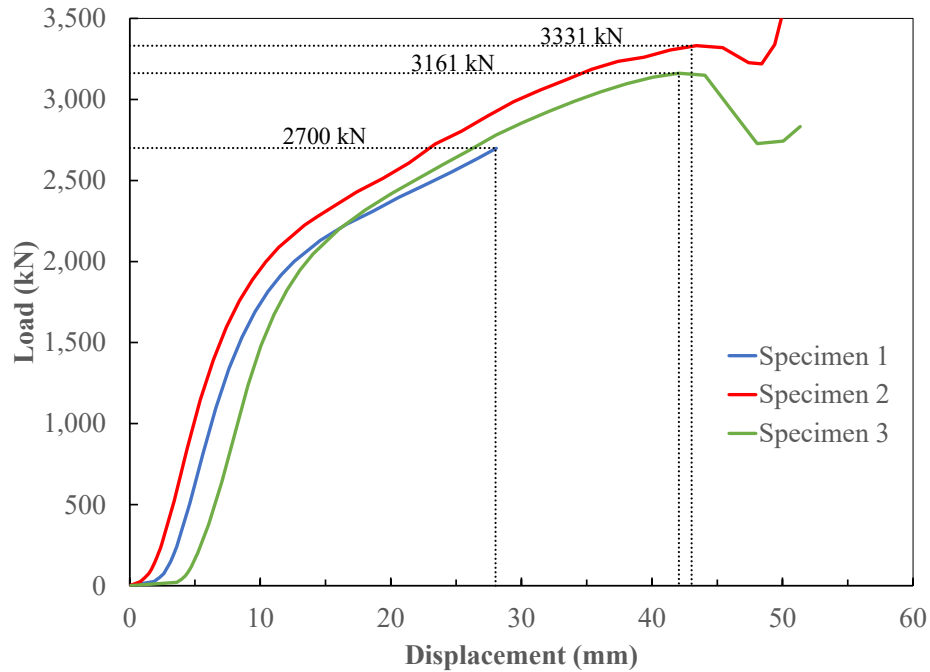
Figure 4 - 7. Load-displacement curves obtained from tests.

The plastic portion of the curve was characterized by noticeable deformation at the holes of the lead pile and the external coupler, and bulking of the material at the hole portions in contact with the pins. As the cracks formed there was a drop in the capacity of the assemblies. The maximum load reached by specimen 2 was 3331 kN and for specimen 3 it was 3161 kN. After the capacity drop, the lead and extension piles established contact and a sudden increment of the strength was observed. However, the contact between the two piles is not a reliable source of axial capacity for the mechanical connection, since minor imperfections or deformations of the coupler may cause that the two piles do not establish adequate contact. Because of this, the failure load in the experimental tests of the coupler is assumed to be the load associated with the development of cracks.

4.4.3 Deformation of the Holes (Ovalization)

The vertical deformation of the holes is termed ovalization. It was retrieved using the Digital Image Correlation (DIC). The software used for this purpose is able to capture the displacement of the black points sprayed on the white surface of the external coupler.

To determine the ovalization of each hole, the displacement of the material at the top of the hole and the vertical displacement of the pin were retrieved. The ovalization is obtained after deducting the absolute top displacement from the absolute displacement of the pin as stated in Eq. (4 - 1).

(4 - 1) $$Ovalization = |V_{pin}| - |V_{TH}|$$

where V_{pin} is the vertical displacement of the pin and V_{TH} is the displacement at the top of the hole. The areas where the displacements were retrieved are shown in Fig. 4 - 8 where an ovalization of 1.56 mm is used as an example.

The ovalization of the four holes in the external coupler was determined because the holes did not deformed equally. The deformed shape of the holes was different for the top and bottom holes of the piles as it is illustrated in Fig. 4 - 9.

To determine the different deformation in the four holes of the external coupler, the numbers 1 and 2 were assigned to the top holes located on opposite sides of the coupler and numbers 3 and 4 were assigned to the bottom holes as shown in Fig. 4 - 10. The load-ovalization relationship for the holes in each specimen is shown from Fig. 4 - 11 to Fig. 4 - 13. The deformations of the holes in the external coupler through the complete application of the load in the three specimens are presented in Table 4 - 2.
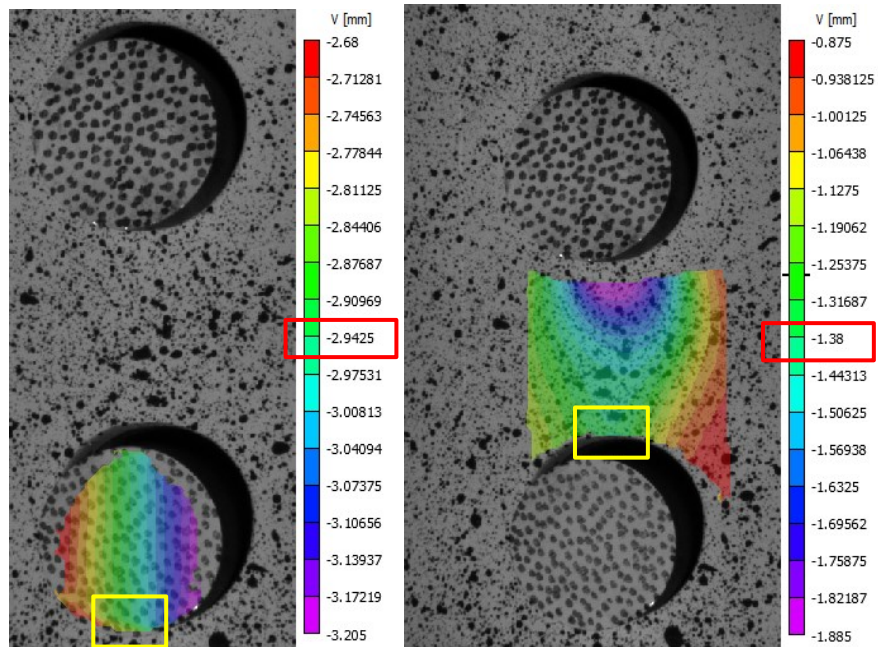
Figure 4 - 8. Measurement zones of holes deformations: pin (V_{pin}) and top of the hole (V_{TH}).

Figure 4 - 9. Deformed shape of the holes in the external coupler.
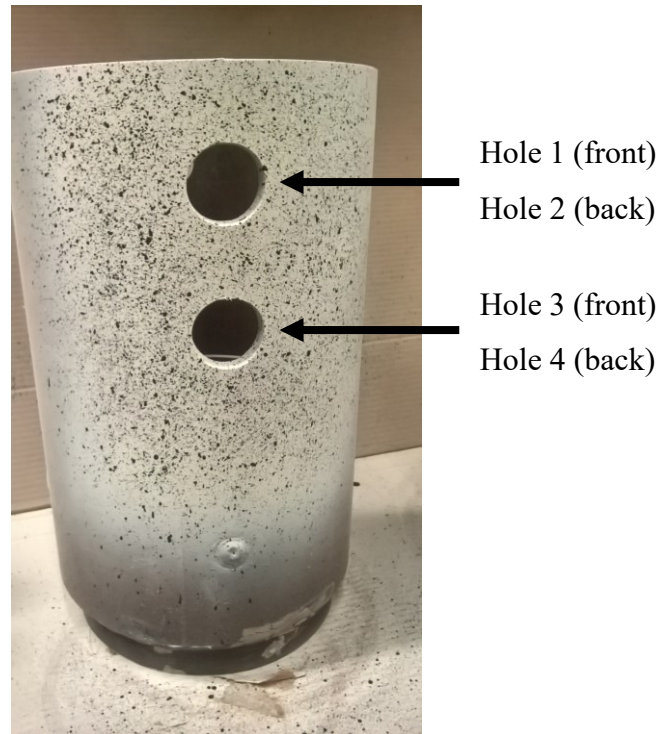
Figure 4 - 10. Numbering of holes in external coupler.
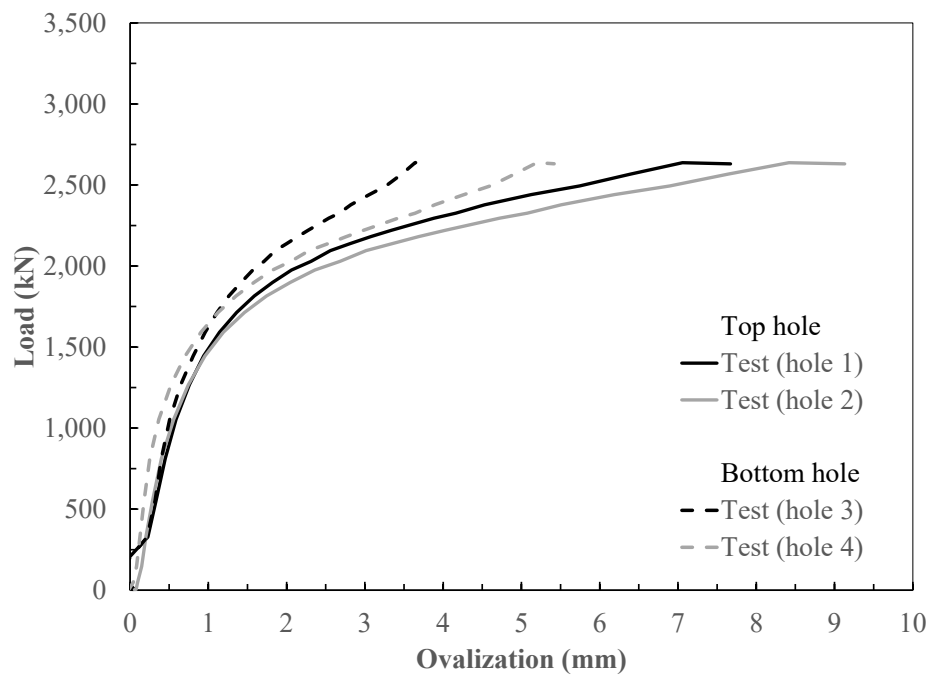
Figure 4 - 11. Load-ovalization relationship of specimen 1.
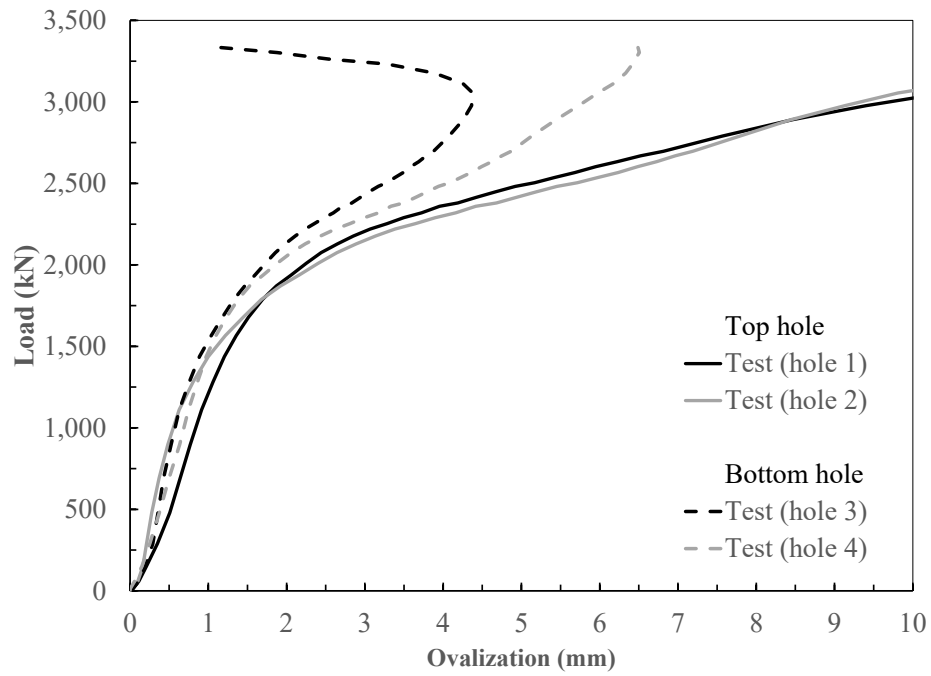
Figure 4 - 12. Load-ovalization relationship of specimen 2.
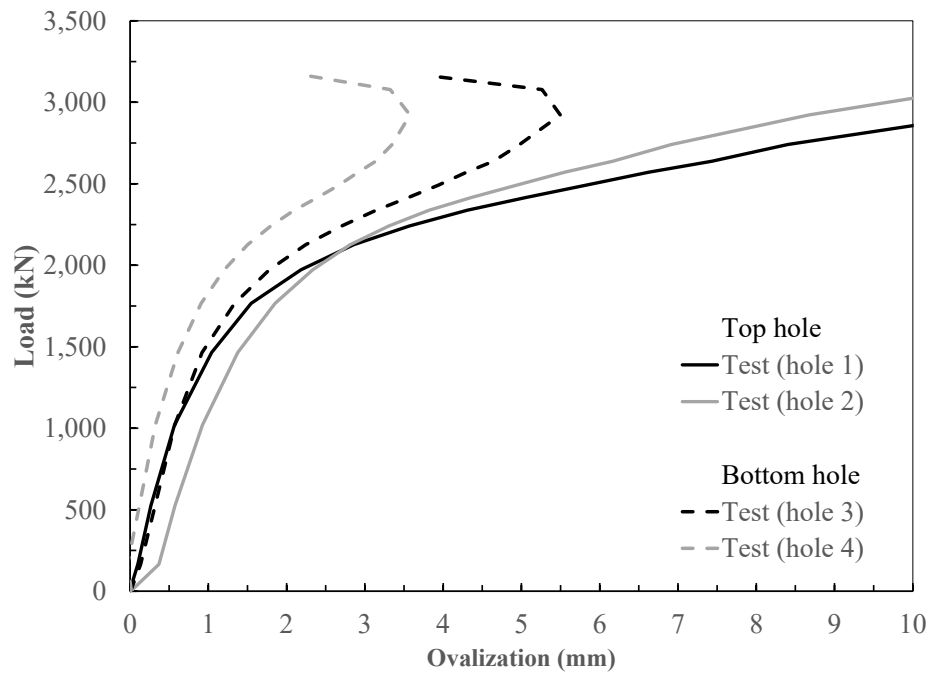
Figure 4 - 13. Load-ovalization relationship of specimen 3.

68

Table 4 - 2. Deformation of the holes in the external coupler of the three specimens.

Load (kN)	Specimen 1				Specimen 2				Specimen 3			
	Top holes		Bottom holes		Top holes		Bottom holes		Top holes		Bottom holes	
	H1	H2	H3	H4	H1	H2	H3	H4	H1	H2	H3	H4
300	0.19	0.19	0.21	0.13	0.36	0.22	0.29	0.26	0.17	0.46	0.21	0.03
600	0.35	0.31	0.34	0.19	0.59	0.33	0.40	0.46	0.31	0.62	0.36	0.15
900	0.49	0.45	0.43	0.29	0.77	0.49	0.53	0.64	0.49	0.84	0.51	0.27
1,200	0.70	0.68	0.60	0.48	0.99	0.72	0.70	0.81	0.70	1.08	0.68	0.43
1,500	1.01	1.04	0.86	0.77	1.29	1.12	0.97	1.04	1.12	1.45	0.97	0.65
1,800	1.53	1.67	1.22	1.29	1.72	1.73	1.36	1.41	1.66	1.92	1.40	0.95
2,100	2.61	3.08	1.89	2.34	2.54	2.77	1.92	2.15	2.75	2.74	2.18	1.46
2,400	4.77	5.77	2.92	4.04	4.33	4.83	2.90	3.59	4.98	4.31	3.51	2.36
2,700	-	-	-	-	6.83	7.20	3.88	4.87	8.13	6.71	4.90	3.31
3,000	-	-	-	-	9.75	9.37	4.38	5.82	12.27	9.65	5.50	3.51
3,161	-	-	-	-	12.28	11.12	4.01	6.30	16.75	12.95	3.84	2.28
3,331	-	-	-	-	16.99	14.62	1.16	6.49	-	-	-	-

The deformation of the holes in specimen 1 was retrieved up to a service load of 2700 kN. The non-symmetric loading pattern can be observed in Fig. 4 - 11 by looking at the deformation of holes 1 and 3 under loads below 250 kN. An extremely small ovalization is developing in these holes while the load is increasing. At this stage, the load is being taken completely by the holes 2 and 4 at one side of the assembly. Beyond 250 kN, similar deformations started occurring in both sides of the assembly.

The developing of plastic deformations is noticeable under a load of approximately 1200 kN, as it was observed in the load-displacement curves presented in Section 4.4.2. The stabilization caused different deformations in the initial stage of the loading, but once the full engagement was achieved, the deformations were very similar in the holes on opposite sides of the coupler. Due to this effective stabilization of the pins with the holes, the four holes tended to yield under the same load of approximately 1200 kN.

The ovalization of the holes in specimen 2 is presented in Fig. 4 - 12, where a maximum load of 3331 kN was observed. Similar behaviour to specimen 1 is observed up to a load of 2700 kN. However, when the ultimate strength of 3331 kN was reached, a drop from 4.01 mm to 1.16 mm was observed. This drop was due to the development of excessive plastic deformations in the material between the holes. The deformations of the top holes caused a downwards vertical displacement of the complete block of material, causing the reduction of the diameter of the bottom holes. This drop is only observed in hole 3, indicating that the deformations of the top holes in opposite sides of the external coupler developed under slightly different loads.

The ovalization of the holes in specimen 3 as shown in Fig. 4 - 13 is the most symmetric in this study under high loads. Under low loads it is very similar to specimens 1 and 2, developing yielding at around 1200 kN and the cracks above 3000 kN. However, it can be seen that both holes at the bottom present a drop in the ovalization at a load of 3161 kN. This indicates that the engagement of the pins with the piles was effective enough to develop symmetric deformations in the top holes on opposite sides of the external coupler.

Even a symmetric load pattern was observed in specimen 3, the engagement of the pins in the stabilization stage was not effective enough to develop a load as high as the one reached by specimen 2. The ultimate strength of specimen 3 was 3161 kN, while for specimen 2 was 3331 kN. The difference of 170 kN is assumed to exist due to a longest phase of stabilization in specimen 3.

4.4.4 Equivalent Plastic Strain

Plasticity can be defined as the ability of the material to accommodate high permanent strains until fracture appears, i.e., when the strain reaches the ultimate fracture strain (Kut 2010). Based on this definition and by tracing the strain values at the locations in the model in which cracking was observed during the experiments, an estimate of the load at which the ultimate fracture strain is reached can be made.

The coupons used for the standard tensile tests were rectangular, as specified in Section 3.2.1 and the strain components in the longitudinal and transversal directions are calculated as follows:

(4 - 2)
$$\varepsilon_1 = ln\left(\frac{b_1}{b_0}\right)$$

(4 - 3)
$$\varepsilon_2 = ln\left(\frac{g_1}{g_0}\right)$$

(4 - 4)
$$\varepsilon_3 = -(\varepsilon_1 + \varepsilon_2)$$

where the directions 1, 2, and 3, and the dimensions b_0, b_1, g_0, and g_1 correspond to the ones showed in Fig. 4 - 14.

Considering that the ductile fracture strain (ε_p) corresponds to the equivalent strain (ε_z) which is based on the von Mises criterion, it can be calculated following the expression:

(4 - 5)
$$\varepsilon_p = \varepsilon_z = \sqrt{\frac{2}{3}} \cdot \sqrt{\varepsilon_1^2 + \varepsilon_2^2 + \varepsilon_3^2}$$

And substituting Eq. (4 - 2), (4 - 3), and (4 - 4) into Eq. (4 - 5), the ductile fracture strain for rectangular cross-section coupons is determined by the following equation:

(4 - 6)
$$\varepsilon_p = \sqrt{\frac{2}{3}} \cdot \sqrt{\varepsilon_1^2 + \varepsilon_2^2 + [-(\varepsilon_1 + \varepsilon_2)]^2}$$

This expression to calculate the ultimate fracture strain was derived under the assumption that the specimens cross-section shape did not change after the deformation. However, it can be seen in Fig. 4 - 14 how the shape changes once the strain develops. This change in the shape of the specimens means a significant variance between the strains in the sides of the coupons and the center of it.

Even though the strains are different through the cross-section and the assumption that the cross-section shape did not change was made, Kut (2010) performed a series of FE analysis and determined that the dimensions b_0, b_1, g_0, and g_1 should be taken from the sides of the specimen. In these locations, the state of stress is closest to the uniaxial tension being applied to the coupons and the ultimate fracture strain of the material is more accurate.
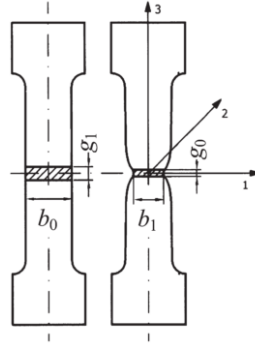
Figure 4 - 14. Strain vectors and dimensions in a typical rectangular cross-section coupon.

The initial dimensions were set as 200 mm for g_1 and 12.5 mm b_0. After the load was applied and the coupons cracked, the new values were set as g_0 and b_1. From the new dimensions, the strain in each direction was calculated and the ultimate fracture strain of the material used to build the mechanical connection determined.

The dimensions corresponding to each coupon are presented in Table 4 – 3. The calculations of ε_p using Eq. (4 - 2) to Eq. (4 - 6) are also shown. It can be seen that the three coupons present very similar results and the average of the three of them led to an ultimate fracture strain of 0.6353.

Table 4 - 3. Dimensions in coupons after strains and calculation of ε_p

Coupon ID	g_1 [mm]	b_0 [mm]	g_0 [mm]	b_1 [mm]	ε_1	ε_2	ε_3	ε_p
1			219.14	7.55	-0.5042	-0.0914	0.5956	0.6415
2	200	12.5	220.17	7.62	-0.4950	-0.0961	0.5910	0.6343
3			219.31	7.63	-0.4936	-0.0922	0.5858	0.6300
							$\varepsilon_{p,avg}$	0.6353

This value of 0.6353 for ε_p represents the strain of the steel under which the cracks will develop and the brittle failure of the material will occur.

The development of plasticity in the critical zones of the mechanical connection was tracked by monitoring the strains during the test of the specimens. The zones of the lead pile where the cracks were observed in specimens 2 and 3 were selected in the external coupler to retrieve the strain. They were named as Zone 1, 2, 3, and 4 as shown in Fig. 4 - 15. Letters a, and b were assigned to these four points to distinguish between opposite sides of the external coupler.
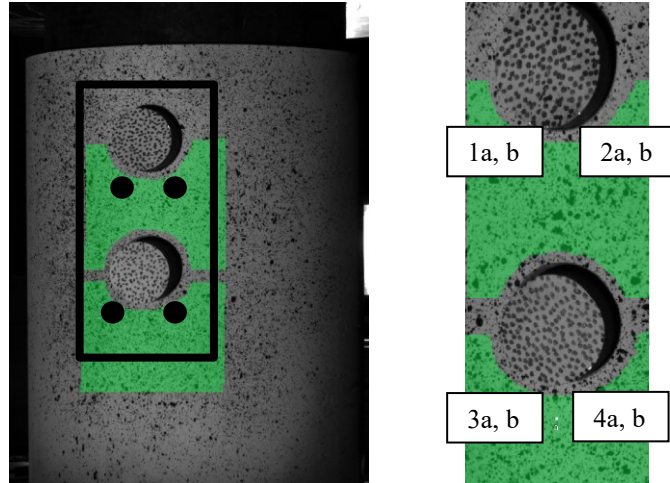
Figure 4 - 15. Identification of zones for retrieval of strains.

The strain retrieved in these zones was the von Mises strain, which was calculated by the DIC system based on the principal strains retrieved in the critical zones. The strains retrieved in these zones are shown in Fig. 4 - 16 to Fig. 4 - 18 and the data is shown in Tables 4 - 3 to 4 – 5, where the strain at the maximum load is highlighted for reference.
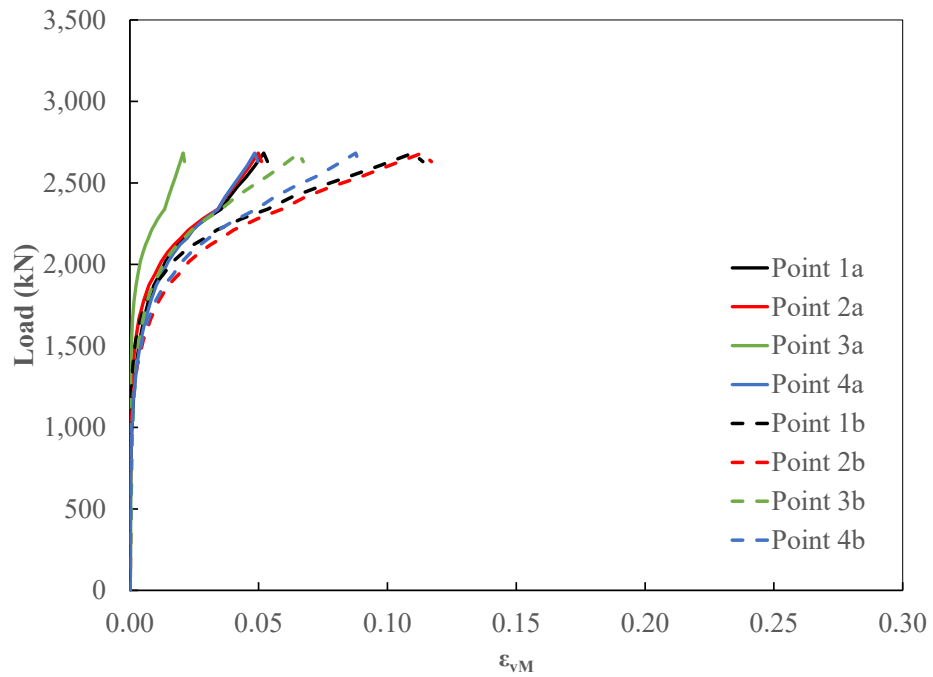
Figure 4 - 16. Load-von Mises Strain relationship of Specimen 1.
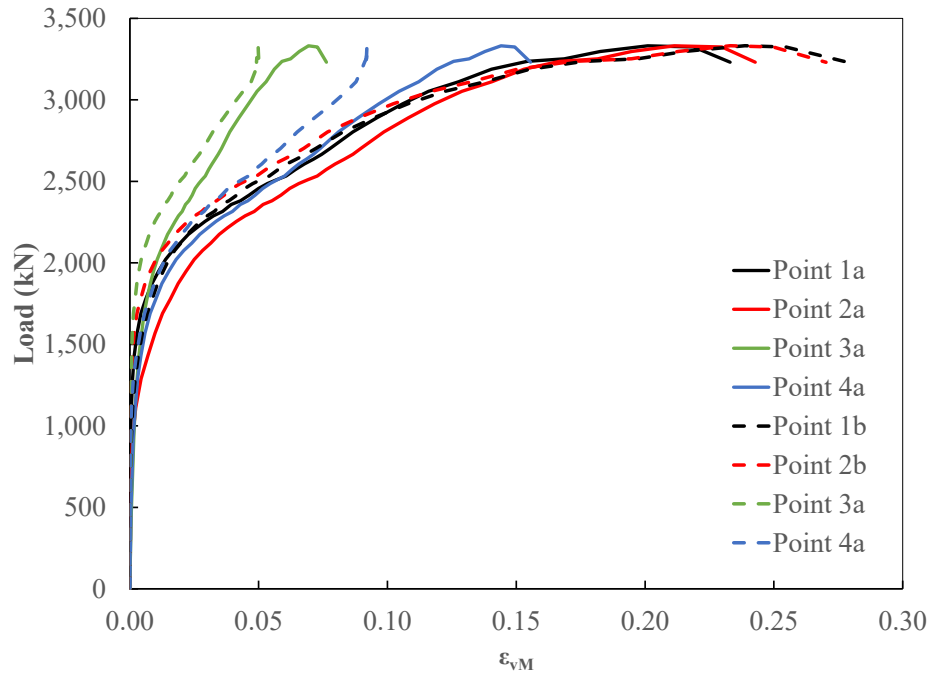
Figure 4 - 17. Load-von Mises Strain relationship of Specimen 2.
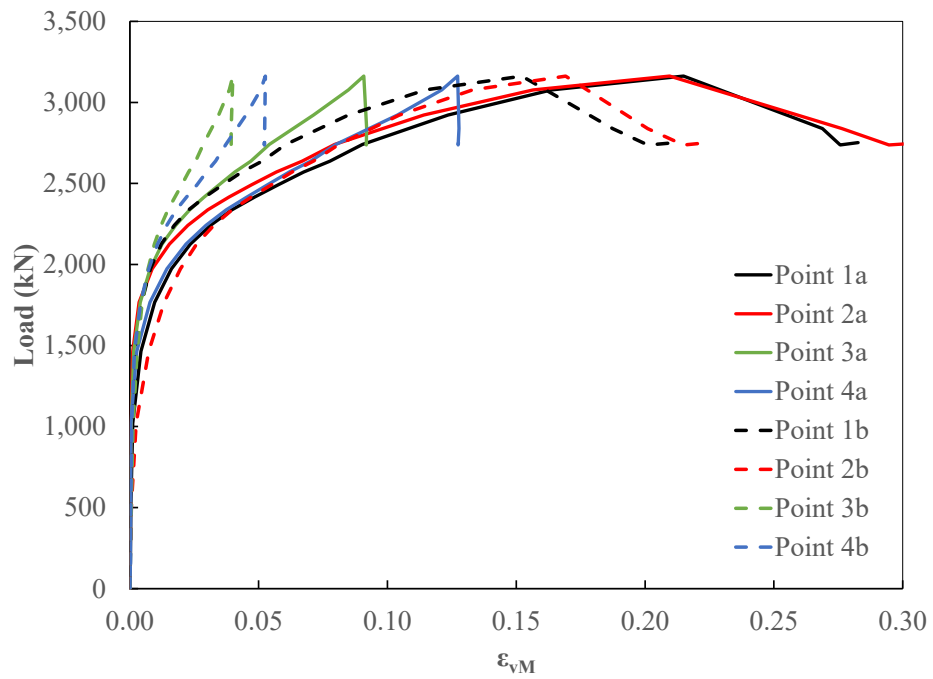
Figure 4 - 18. Load-von Mises Strain relationship of Specimen 3.

Table 4 - 4. Von Mises strain of each point in Specimen 1 under applied load

Load [kN]	ε_{vM}							
	1a	2a	3a	4a	1b	2b	3b	4b
3	0.0001	0.0002	0.0001	0.0002	0.0001	0.0001	0.0001	0.0001
30	0.0001	0.0001	0.0002	0.0001	0.0001	0.0001	0.0001	0.0001
96	0.0002	0.0001	0.0002	0.0001	0.0001	0.0002	0.0001	0.0001
245	0.0002	0.0002	0.0003	0.0001	0.0002	0.0003	0.0002	0.0001
459	0.0002	0.0001	0.0004	0.0003	0.0002	0.0003	0.0004	0.0003
718	0.0004	0.0003	0.0004	0.0002	0.0002	0.0003	0.0007	0.0004
964	0.0007	0.0004	0.0003	0.0007	0.0003	0.0005	0.0010	0.0007
1,184	0.0015	0.0008	0.0003	0.0014	0.0005	0.0011	0.0016	0.0015
1,373	0.0024	0.0012	0.0004	0.0027	0.0011	0.0028	0.0025	0.0027
1,534	0.0038	0.0022	0.0007	0.0043	0.0023	0.0052	0.0035	0.0047
1,667	0.0055	0.0035	0.0011	0.0062	0.0042	0.0082	0.0051	0.0073
1,780	0.0073	0.0055	0.0017	0.0082	0.0066	0.0114	0.0068	0.0101
1,874	0.0094	0.0074	0.0024	0.0103	0.0095	0.0150	0.0089	0.0134
1,939	0.0116	0.0097	0.0031	0.0125	0.0130	0.0189	0.0112	0.0168
2,016	0.0138	0.0122	0.0040	0.0149	0.0166	0.0229	0.0134	0.0202
2,073	0.0161	0.0146	0.0051	0.0172	0.0206	0.0270	0.0159	0.0237
2,122	0.0186	0.0172	0.0061	0.0196	0.0248	0.0314	0.0185	0.0274
2,163	0.0212	0.0198	0.0073	0.0223	0.0293	0.0357	0.0212	0.0309
2,211	0.0239	0.0227	0.0084	0.0245	0.0337	0.0402	0.0241	0.0344
2,245	0.0266	0.0255	0.0097	0.0267	0.0386	0.0449	0.0268	0.0380
2,280	0.0295	0.0284	0.0109	0.0292	0.0433	0.0495	0.0298	0.0418
2,309	0.0325	0.0312	0.0121	0.0319	0.0483	0.0543	0.0327	0.0455
2,339	0.0354	0.0342	0.0135	0.0343	0.0535	0.0591	0.0356	0.0492
2,414	0.0387	0.0372	0.0150	0.0369	0.0628	0.0680	0.0411	0.0562
2,477	0.0418	0.0403	0.0163	0.0398	0.0735	0.0782	0.0471	0.0637
2,537	0.0452	0.0435	0.0177	0.0425	0.0847	0.0896	0.0530	0.0720
2,606	0.0485	0.0466	0.0191	0.0456	0.0970	0.1006	0.0592	0.0796
2,683	**0.0520**	**0.0499**	**0.0207**	**0.0485**	**0.1099**	**0.1134**	**0.0657**	**0.0877**
2,631	0.0534	0.0512	0.0212	0.0497	0.1138	0.1171	0.0673	0.0889

Table 4 - 5. Von Mises strain of each point in Specimen 2 under applied load

Load [kN]	ε_{vM}							
	1a	2a	3a	4a	1b	2b	3b	4b
1	0.0000	0.0000	0.0000	0.0000	0.0000	0.0000	0.0000	0.0000
63	0.0001	0.0001	0.0001	0.0000	0.0001	0.0001	0.0000	0.0001
300	0.0002	0.0002	0.0004	0.0003	0.0002	0.0001	0.0001	0.0001
696	0.0002	0.0006	0.0011	0.0008	0.0003	0.0002	0.0003	0.0002
1,112	0.0006	0.0023	0.0020	0.0021	0.0011	0.0004	0.0004	0.0007
1,432	0.0017	0.0071	0.0035	0.0043	0.0033	0.0010	0.0007	0.0025
1,691	0.0043	0.0127	0.0056	0.0079	0.0067	0.0028	0.0014	0.0057
1,873	0.0086	0.0188	0.0079	0.0124	0.0108	0.0059	0.0027	0.0095
2,020	0.0139	0.0250	0.0107	0.0180	0.0152	0.0101	0.0044	0.0136
2,121	0.0196	0.0314	0.0132	0.0241	0.0198	0.0148	0.0064	0.0178
2,214	0.0259	0.0379	0.0162	0.0303	0.0248	0.0199	0.0086	0.0222
2,289	0.0325	0.0448	0.0189	0.0367	0.0301	0.0252	0.0110	0.0265
2,358	0.0394	0.0517	0.0216	0.0429	0.0356	0.0307	0.0134	0.0311
2,415	0.0463	0.0587	0.0242	0.0487	0.0415	0.0366	0.0160	0.0356
2,486	0.0534	0.0656	0.0268	0.0545	0.0477	0.0428	0.0186	0.0409
2,533	0.0606	0.0727	0.0293	0.0601	0.0542	0.0492	0.0213	0.0461
2,607	0.0677	0.0797	0.0319	0.0656	0.0609	0.0561	0.0241	0.0512
2,666	0.0745	0.0866	0.0343	0.0713	0.0684	0.0636	0.0270	0.0558
2,803	0.0866	0.0986	0.0388	0.0810	0.0827	0.0767	0.0322	0.0650
2,976	0.1059	0.1183	0.0461	0.0967	0.1079	0.1023	0.0403	0.0787
3,111	0.1276	0.1406	0.0529	0.1122	0.1377	0.1325	0.0471	0.0878
3,236	0.1542	0.1669	0.0591	0.1257	0.1760	0.1715	0.0499	0.0912
3,297	0.1826	0.1948	0.0658	0.1379	0.2154	0.2130	0.0499	0.0920
3,324	**0.2189**	**0.2298**	**0.0728**	**0.1494**	**0.2548**	**0.2499**	**0.0496**	**0.0921**

Table 4 - 6. Von Mises strain of each point in Specimen 3 under applied load

Load [kN]	ε_{vM}							
	1a	2a	3a	4a	1b	2b	3b	4b
0	0.0000	0.0000	0.0000	0.0000	0.0000	0.0000	0.0000	0.0000
5	0.0000	0.0000	0.0001	0.0001	0.0000	0.0000	0.0001	0.0001
9	0.0001	0.0001	0.0001	0.0001	0.0001	0.0001	0.0001	0.0001
165	0.0002	0.0001	0.0001	0.0002	0.0001	0.0001	0.0002	0.0002
526	0.0004	0.0001	0.0001	0.0003	0.0004	0.0007	0.0005	0.0004
1,020	0.0011	0.0004	0.0006	0.0004	0.0010	0.0025	0.0013	0.0008
1,464	0.0043	0.0011	0.0015	0.0027	0.0022	0.0073	0.0029	0.0018
1,767	0.0097	0.0036	0.0040	0.0078	0.0046	0.0134	0.0048	0.0042
1,973	0.0161	0.0087	0.0079	0.0144	0.0080	0.0196	0.0071	0.0073
2,126	0.0235	0.0154	0.0125	0.0218	0.0122	0.0259	0.0095	0.0108
2,242	0.0313	0.0226	0.0178	0.0296	0.0173	0.0327	0.0122	0.0144
2,338	0.0396	0.0303	0.0232	0.0374	0.0229	0.0397	0.0148	0.0181
2,415	0.0484	0.0385	0.0289	0.0454	0.0291	0.0471	0.0175	0.0220
2,492	0.0576	0.0473	0.0347	0.0535	0.0360	0.0550	0.0202	0.0261
2,571	0.0675	0.0569	0.0408	0.0619	0.0435	0.0630	0.0228	0.0298
2,638	0.0777	0.0669	0.0470	0.0702	0.0514	0.0713	0.0255	0.0333
2,741	0.0903	0.0795	0.0542	0.0800	0.0605	0.0811	0.0285	0.0373
2,922	0.1235	0.1141	0.0713	0.1039	0.0848	0.1046	0.0344	0.0450
3,077	0.1636	0.1565	0.0848	0.1211	0.1148	0.1330	0.0386	0.0508
3,162	**0.2149**	**0.2096**	**0.0908**	**0.1273**	**0.1522**	**0.1692**	**0.0400**	**0.0526**
2,838	0.2688	0.2764	0.0919	0.1277	0.1875	0.2010	0.0394	0.0523
2,737	0.2758	0.2946	0.0918	0.1274	0.2011	0.2150	0.0393	0.0523
2,752	0.2827	0.3086	0.0919	0.1276	0.2122	0.2247	0.0392	0.0523

The equivalent strain in specimen 1 is the lowest of all three tests since no data was captured after a load of 2700 kN. At this load, no cracks were observed in the lead pile nor in the external coupler. The ultimate fracture strain of 0.6353 was not reached (Fig. 4 - 16 and Table 4 - 3).

In specimens 2 and 3, the cracks were observed in the lead pile, but not in the external coupler. Hence, the strains in the external coupler did not reach the limiting strain of 0.6353. In specimen 2, the equivalent strain is very similar for points 1a, 1b, 2a, and 2b. The large deformation of the top hole shows higher values of strain than the ones for the bottom hole. Points 3a, 3b, 4a, and 4b show

varying strains, but they remain lower than those measured at the top hole. This indicates a tendency of the material below the top hole to crack first. The drop in the load at a strain of 0.22 mm/mm in specimen 2 occurred due to the crack of the lead pile.

In specimen 3, the same pattern as in specimen 2 was observed. The points at which the equivalent strain was retrieved, in the top holes (1a, 2a, 1b, 2b) had higher values than the ones retrieved at the bottom hole (3a, 3b, 4a, 4b). The difference between the holes from side "a" and holes from side "b" showed also the non-symmetric application of the load between the two sides of the assembly. The drop in the load is also noticeable in specimen 3 due to the failure of the material of the lead pile.

In the experiments, the cracks formed in the lead pile and they led to the failure of the assembly. However, the external coupler remained uncracked and the strains were lower than the ultimate fracture strain of 0.6353. The maximum equivalent strain reached by the external coupler did not exceed the ultimate fracture strain calculated previously, as expected.

CHAPTER 5.   FINITE ELEMENT ANALYSIS

5.1 Introduction

In this chapter, a finite-element analysis model of the mechanical connection in steel helical piles is discussed. The performance of the model is compared to the results obtained from experimental testing.

5.2 Finite-Element Model

The model was developed using finite element software Abaqus/CAE 6.14-2 (Simulia 2012). Measured material properties and dimensions were incorporated into the model. The model also accounted for the type of boundary conditions and loading regimes used during the test.

5.2.1 Geometry

The mechanical connection consists of a lead pile, an extension pile, an external coupler, a fillet weld, and two high-strength steel pins (Fig. 5 - 1). The pins are used to transfer the forces from the lead pile to the external coupler.

The assembly contains four plug welds used to help the fillet weld transferring the load from the extension pile to the external coupler. These plug welds were modelled as common-node constraints and will be discussed later in this section.

As explained in Chapter 4, the most convenient position for the Digital Image Correlation system to retrieve the deformation during the experiments was upside-down (Fig. 5 - 2 (a) and (b)). The finite-element model of the assembly was built to reproduce the testing conditions, with the extension pile at the bottom and the leading pile at the top
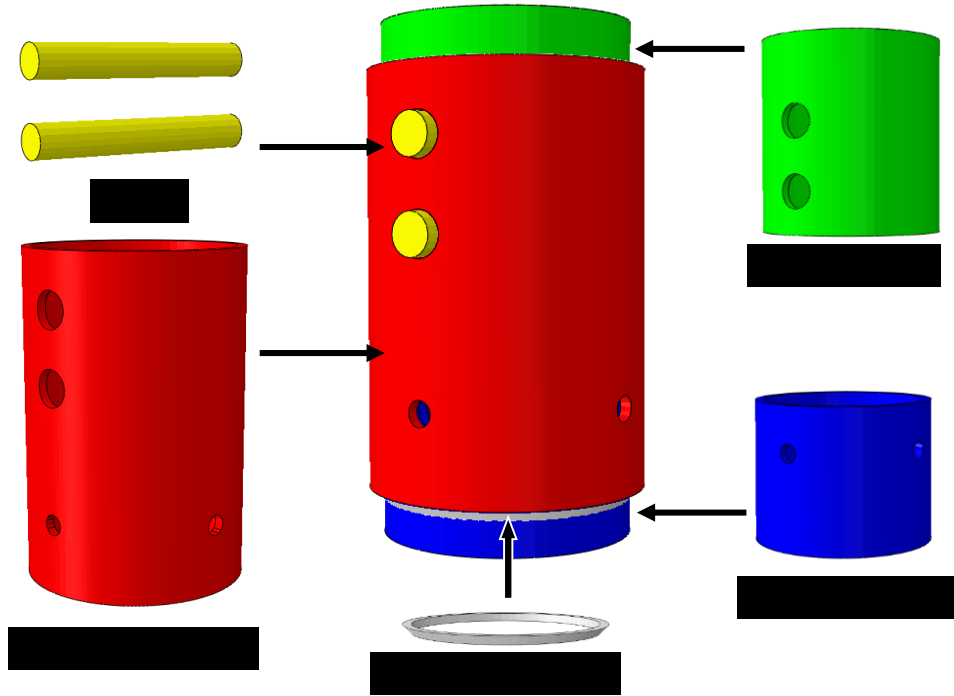
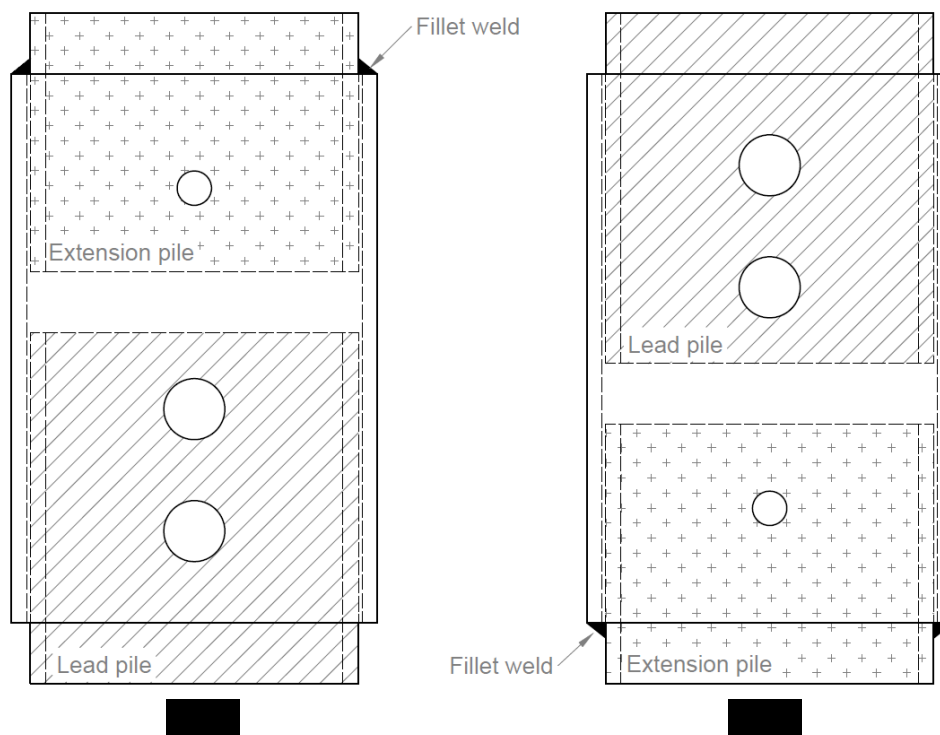Figure 5 - 1. Model of mechanical connection.

Figure 5 - 2. (a) Assembly position in field conditions. (b) Assembly position for tests.

In the interface of Abaqus, each one of the components is called a "part". All parts, with the exception of the fillet weld, were modelled as deformable bodies. The fillet weld was modelled as a discrete rigid part. A deformable part represents a body that can deform under mechanical, thermal, or electrical load, while a discreet deformable body can be shaped arbitrarily and cannot deform (Simulia 2012). The fillet weld was modelled as a rigid part because the investigation of the weld properties was out of the scope of this study, and it was assumed that the weld would not be the governing component in the strength of the assembly. This assumption was verified when the experimental works took place, as the weld did not exhibit significant deformations nor perceptible damage under the failure load.

The external coupler was extruded from a 2D sketch of a ring with an internal diameter of 279.4 mm [11"] and an external diameter of 304.8 mm [12"]. These dimensions represent the thickness of 12.7 mm [½"] of the external coupler. The holes for the pins had a diameter of 50.8 mm [2"], and the holes for the plug welds had a diameter of 28.575 mm [1 ⅛"]. The length of the external coupler was 457.2 mm [1' 6"].

The internal diameter of the lead pile and the extension pile was 247.65 mm [9 ¾"] and the external diameter was 273.05 mm [10 ¾"].

The lead and the extension pile extended 50.8 mm [2"] out of the external coupler. Therefore, the total length of the lead pile is 292.1 mm [11 ½"], and the total length of the extension pile is 215.9 mm [8 ½"].

The pins had a diameter of 47.625 mm [1 ⅞"] and a length of 330.2 mm [13"]. Since the holes for the pins had a diameter of 50.8 mm [2"], the initial gap of 3.175 mm between the pins and the holes was taken into account when the displacement of the assembly was retrieved.

The weld was a ½" fillet weld, with a triangular section with a height of 12.7 mm [½"] and base of 12.7 mm [½"] as well. As discussed before, the weld was defined as a rigid body. No perceptible damage nor deformation were observed at the weld during the application of the load.

Once all the components were modelled and added to the assembly, they were positioned in a way that no initial contact between the surfaces took place. The steel pins were located at the center of the holes under zero imposed load-deformation. The contact properties between surfaces are discussed next.

5.2.2 Contact Properties

The contact interaction was defined as "General Contact". When a "General Contact" interaction is defined in Abaqus, it is not necessary to explicitly indicate the surfaces that could be in contact during the analysis, with the model identifying those surfaces automatically. This type of interaction is convenient since it avoids any overlapping of the components in the assembly if any of the surfaces is neglected.

The interaction property defined for "General Contact" can be determined as "friction" or "frictionless". In this model, friction properties were used between the components of the connector.

The user can define the contact properties in the normal and tangential direction of the surfaces in contact. The normal behaviour property was defined as "hard" contact for pressure-overclosure. The "hard" contact relationship minimizes the penetration of the slave surface into the master surface at the constraint locations and does not allow the transfer of tensile stress across the interface (Simulia 2012). The constraint enforcement method was left as the default provided by Abaqus, which is the "direct" method. The direct method attempts to strictly enforce a given pressure-overclosure behaviour per constraint, without approximation or use of augmentation iterations (Simulia 2012).

For the definition of the tangential behaviour property, an "isotropic" directionality was defined under the "penalty" formulation. This means that a uniform friction coefficient was used for the surfaces in contact. A friction coefficient of 0.7, for steel-to-steel contact was implemented in the model (Sullivan 1998).

5.2.3 Mesh

5.2.3.1 Element Type Selection

There are different element types available in Abaqus to define the mesh of the model. The type of element should be selected following the geometry of the part to be meshed and the nature of the problem to be solved. The aim of the current study is to analyze the piles under a 3-dimensional scenario of loads and boundary conditions.

To model the deformable parts (pins, coupler, and piles), three different element types are available in Abaqus: hexahedral, tetrahedral, and wedge. Tetrahedral and wedge elements have a simple, constant-strain formulation that may make them stiffer than hexahedral elements of the same size (Simulia 2012). Thus, a very fine mesh is required to obtain an accurate solution when using tetrahedral elements. In general, hexahedral elements allow for more accurate solutions for the same element sizes. Since a very fine mesh is less convenient in terms of computation time, a coarser mesh with hexahedral elements was selected.

The 3D Stress element was used as the element type for the deformable bodies. The final mesh was formed by contains 8-node linear brick, reduced integration, hourglass control elements.

Since the weld was modelled as a rigid body, the element shapes do not include the wedge option. In terms of element type, Abaqus only allows to choose the family of Discrete Rigid Elements for meshing rigid bodies. As a result, 4-node 3-D bilinear rigid quadrilateral-shaped elements were assigned to the weld. The main difference between these elements and the elements used in the deformable parts, is that the elements used for a rigid body do not deform during the application of the load and the penetration of another mesh is not allowed (Simulia 2012).

5.2.3.2 Sensitivity Analysis

When meshing the areas near the holes, the size of the elements was reduced in an attempt to capture the stress concentration in these areas.

To determine the size of the elements around the holes, a sensitivity analysis was conducted. The chosen convergence criteria for the analyses was determined by the maximum displacement reached by one node under a certain applied load. The selected node was located in the center of the longitudinal axis of one pin. The load-displacement relationship of the 5 analyses conducted is presented in Fig. 5 - 3.

The legend in each of the models contains three numbers. The first is the size of the elements in the surface of the piles, followed by the size of the elements around the holes, and finally the size of the elements in the pins. Here, size is defined in Abaqus as length dimensions (millimeters in this case).

Convergence was reached for model 12_3_5. This model has an overall mesh size 12. The elements around the holes are size 3, and the mesh in the pins is size 5. This model showed a displacement of 10.92 mm, while the displacement in the model 12_1_3 was 10.68 mm, with the difference deemed to be negligible. Model 12_3_5 was selected because the computation time was three times lower than that of Model 12_1_3. The final meshed elements are shown in Fig. 5 - 4.
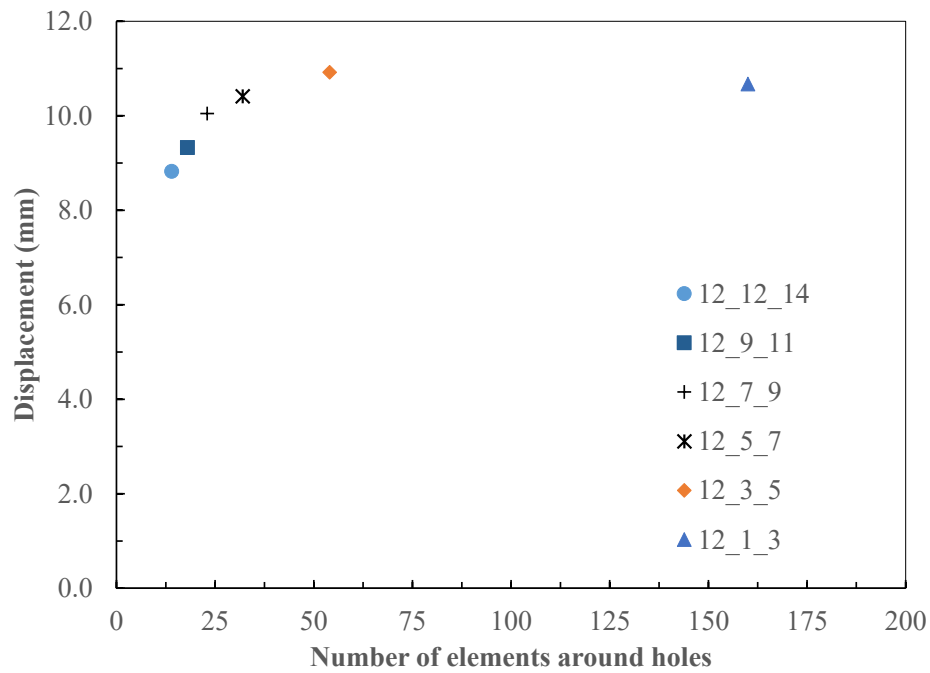
Figure 5 - 3. Displacement of the pins at a load of 2463 kN with different mesh size.
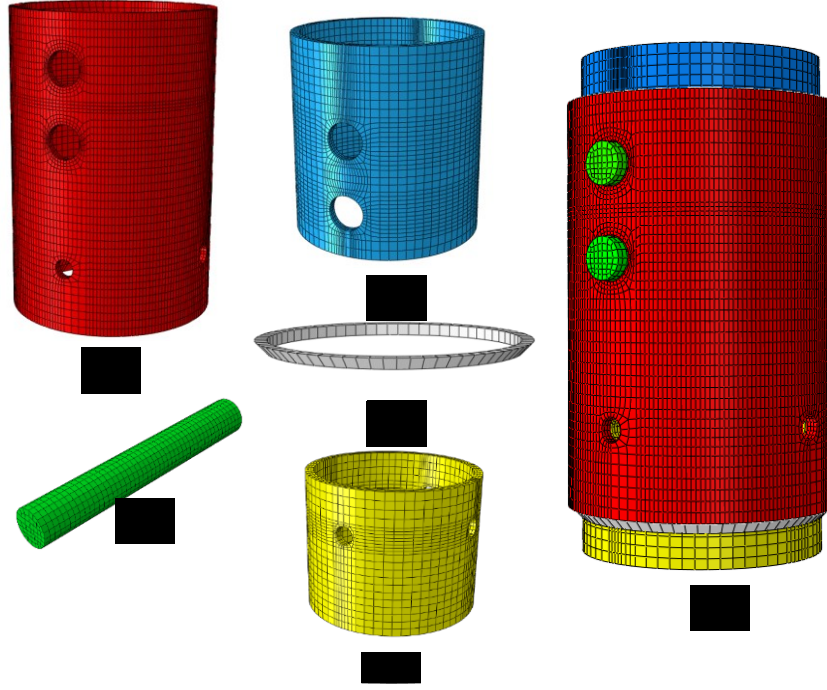
Figure 5 - 4. Meshed components of mechanical connection.
(a) External coupler, (b) steel pin, (c) lead pile, (d) fillet weld, (e) extension pile, (f) complete assembly.

5.2.4 Material properties

True stress-strain relationships were used to model the behaviour of the steel materials in the connector (Simulia 2012). The true strain is defined as the sum of all infinitesimal elongations dL of successive values of a specific gauge length L, divided by the original length. This is expressed as:

$$(5 - 1) \qquad \int_{L_0}^{L} \left(\frac{dL}{L}\right) = log_e\left(\frac{L}{L_0}\right) = log_e(1 + \varepsilon) = \varepsilon_{True}$$

where L_0 is the original gauge length and ε is the normal strain (Roark and Young 1976).

The true stress is defined by the following expression:

$$(5 - 2) \qquad \sigma_T = \sigma (1 + \varepsilon)$$

where σ_T is the true stress, and σ and ε are the static stress and strain obtained from the coupon tests.

The behaviour of the steel is generally divided into the elastic and the plastic ranges of the material. The elastic range can be defined by the Young's modulus (E) and the Poisson's ratio (υ). The transition point between the elastic and plastic ranges is defined as the yield strength of the material.

When assigning values for the elastic range, the Young's modulus and the Poisson's ratio were input into the model with values of 200,000 MPa and 0.3 respectively.

The plastic behaviour of the material was input in terms of the yielding and ultimate stress and plastic strain. The plastic strain was calculated at yielding and ultimate conditions as follows:

$$\varepsilon_P = \varepsilon_T - \varepsilon_E$$

(5 - 3)

where ε_P is the plastic strain, ε_T is the total strain obtained at the coupon tests, and ε_E is the elastic strain.

5.2.4.1 Piles and External Coupler

Stress-strain relationships for steel were obtained through coupons tests, discussed in Chapter 3. For convenience, the data is reproduced in Fig. 5 - 5.

Using the original length of the coupon and cross-section area measurements, a dynamic stress-strain relationship was obtained. Since the dynamic response shows the effects of the strain rate in the response of the material, it was converted into a static stress-strain curve.

Static points were taken during the tests to help to determine the static stress-strain curve. The static response minimizes the effect of the strain rate of the tests and allows the calculation of the true stress-strain relationship.

The static stress-strain response was converted into a true stress-strain relationship according to Eq. (5 - 1) and Eq. (5 - 2) and then input into the FE model. The three curves presented in this section are shown in Fig. 5 - 6.

86
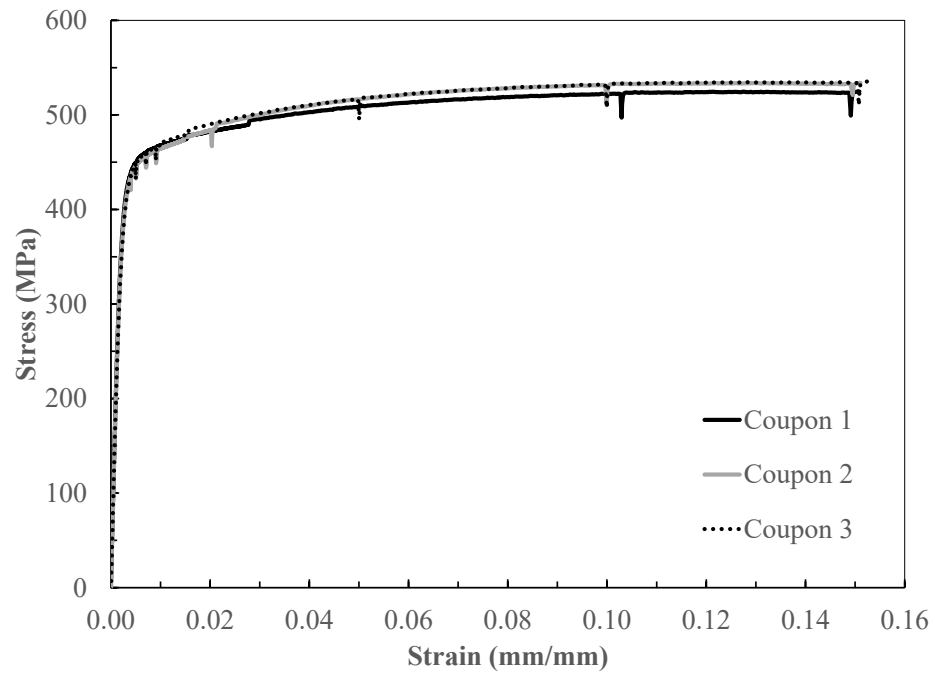
Figure 5 - 5. Dynamic stress-strain curves from tensile coupon tests.
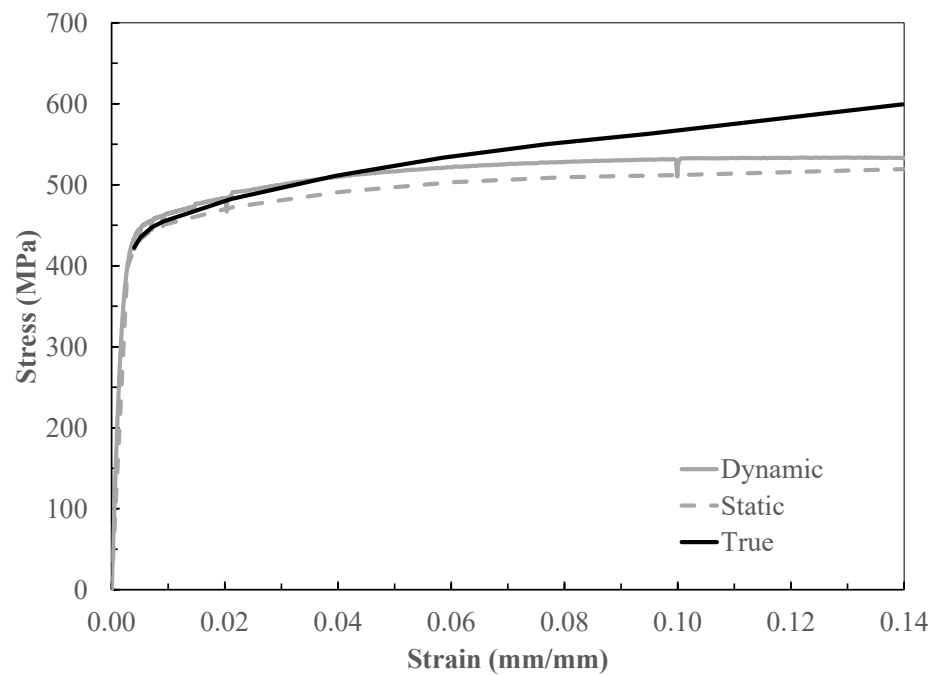
Figure 5 - 6. Dynamic, static and true tress-strain relationships.

The values for the true stress are shown in Table 5 - 1. The yielding and ultimate strength of the material are indicated. The yielding stress and strain values correspond to those obtained through the 0.2% offset yield strength method. The values for the plastic strain (ε_P) were obtained through Eq. (5 - 3).

Table 5 - 1. Stress and strain values used for input in FE model

	σ_T (MPa)	ε_E	ε_T (mm/mm)	ε_P
F_y	422	0.004	0.0040	0.0000
	435		0.0051	0.0011
	447		0.0071	0.0031
	454		0.0091	0.0051
	482		0.0212	0.0172
	511		0.0396	0.0356
	533		0.0585	0.0545
	550		0.0771	0.0731
	563		0.0947	0.0907
F_u	599		0.1397	0.1357

5.2.4.2. Steel pins

The properties for the steel pins were obtained from a stress-strain relationship obtained from the manufacturer. The true stress-strain bilinear curve was calculated from the results of the tensile tests reported in the Material Testing Report (MTR) provided by the steel fabricator. The bilinear stress-strain curve from the MTR and the calculated true stress-strain curve as per Eq. (5 - 1) to Eq. (5 - 3) are presented in Fig. 5 - 7. The stress and strain values are presented in Table 5 - 2 for both engineering and true stress-strain relationships.
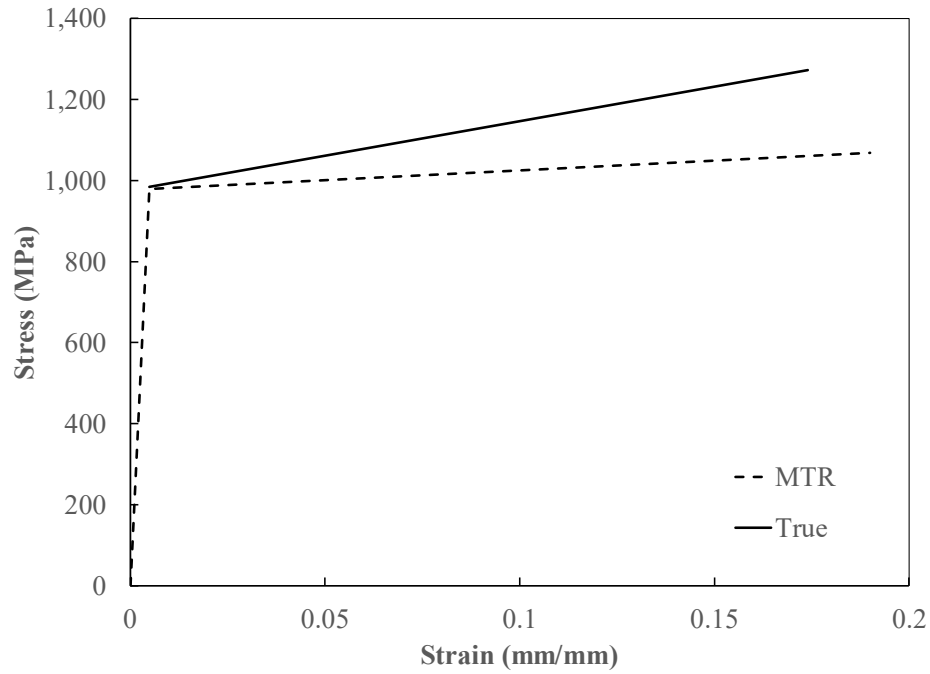
Figure 5 - 7. Stress Strain curves of the steel pins.

Table 5 - 2. Material properties for the pins

MTR				True			
σ (MPa)		ε_T (mm/mm)		σ_T (MPa)		ε_P (mm/mm)	
F_y	979	ε_y	0.0049	F_y	983	$\varepsilon_{y,P}$	0
F_u	1069	ε_u	0.1900	F_u	1272	$\varepsilon_{u,P}$	0.1691

5.2.4.3. Fillet Weld

The weld was assumed to behave rigidly. To verify the adequacy of this assumption, an analysis was conducted assuming an elastic behaviour (E = 200,000 MPa) for the weld. The results are shown in Fig. 5 - 8.

It is observed that if the weld is modelled as a perfectly elastic material, the difference with a weld modelled as rigid material is negligible. The advantage of using a rigid weld consisted on significant savings in computation time.
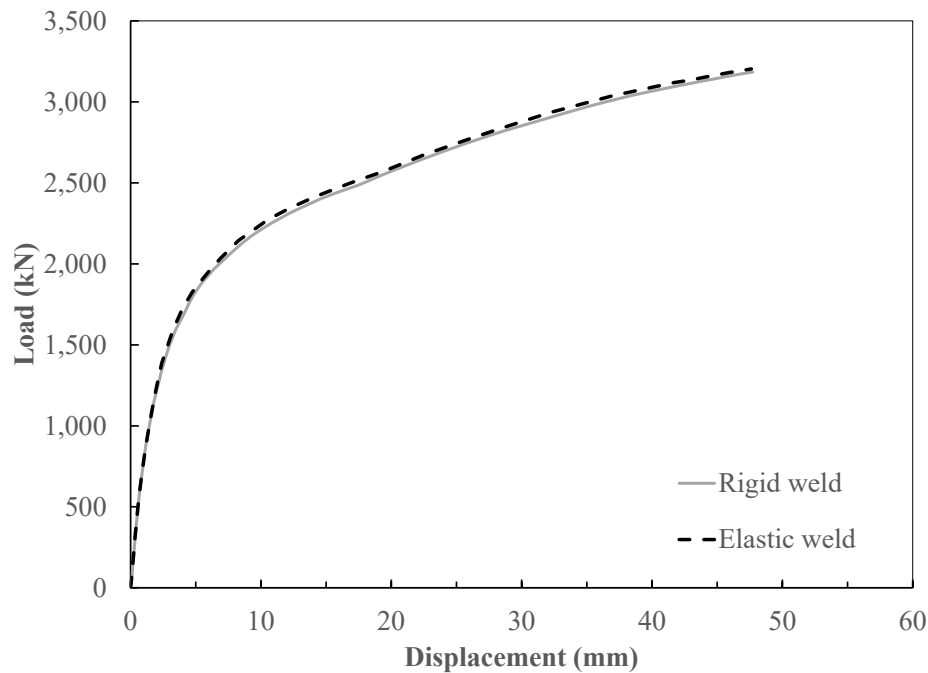
Figure 5 - 8. Load-displacement curves for model with elastic and rigid well.

5.2.4.4 Plug Welds

To enhance the strength of the connection between the mechanical coupler and the extension pile, the assemblage has four plug welds located as shown in Fig. 5 - 9.

Experimental evidence showed no perceptible deformations nor damage occurring at the plug welds. Therefore, the connection between the mechanical coupler and the extension pile at the location of the plug welds was defined using the "tie" constraint in Abaqus. By assigning this type of constraint, the two surfaces connected will not present relative displacement between them during the application of the load (Simulia 2012).
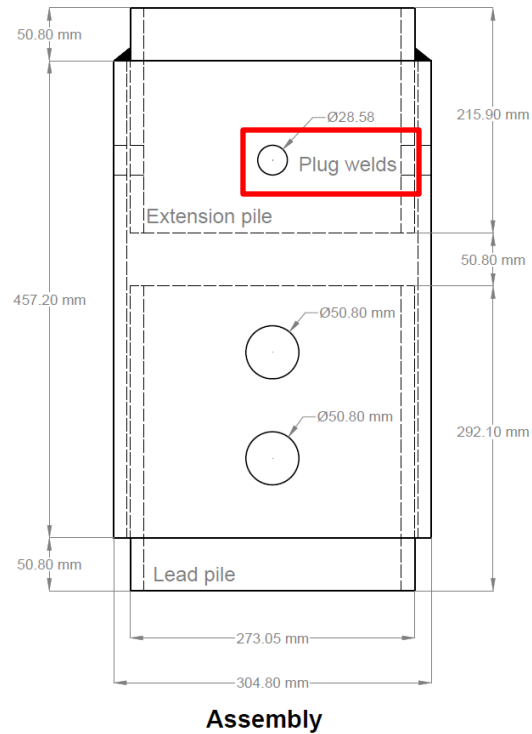
Figure 5 - 9. Location of the plug welds in the assembly.

5.2.5 Loading and Boundary Conditions

The boundary conditions applied to the model intended to reproduce the conditions in which the specimens were tested in the laboratory as close as possible. Ideally, the loading plates from the MTS 6000 machine should be explicitly included in the model, with a suitable value of friction to represent the lateral restraint provided by the plates. However, a preliminary analysis showed that the models that incorporated plates did not reach convergence for high loads. To investigate the influence of the plates on the overall results, an analysis with different boundary conditions was conducted.

To account for the presence of the plates in a simplified manner, two "coupling" constraints were added to the bottom of the extension pile and the top of the lead pile. These constraints were modelled between a reference point and the horizontal surfaces of the piles. The boundary conditions for the model between the top and bottom plates were assigned initially as pinned-pinned and then fixed-fixed.

The pinned-pinned boundary conditions allowed the cross-section of the piles in contact with the plates to experience unrestricted radial horizontal deformation under loading. The assumption is that the contact between the piles and the loading plates is frictionless.

The fixed-fixed boundary conditions did not allow any radial horizontal deformation of the pile cross-sections in contact with the plates. It is assumed that the friction between piles and plates was high, restraining the piles from expanding horizontally when the load was applied. The results in the load-displacement curves for each one of this models is presented in Fig. 5 - 10.

It is seen that there is no difference between the two different cases of boundary conditions. This shows that the effect of the friction between the plates in the MTS and the piles can be neglected to investigate the global axial load-displacement response. It is noted, however, that other response items (such as the radial deformation of the tubes near the ends) may be influenced by the boundary conditions. However, these parameters are out of the scope of this study.

For the derivation of results that follow, the model with pinned boundary conditions was selected for convenience.
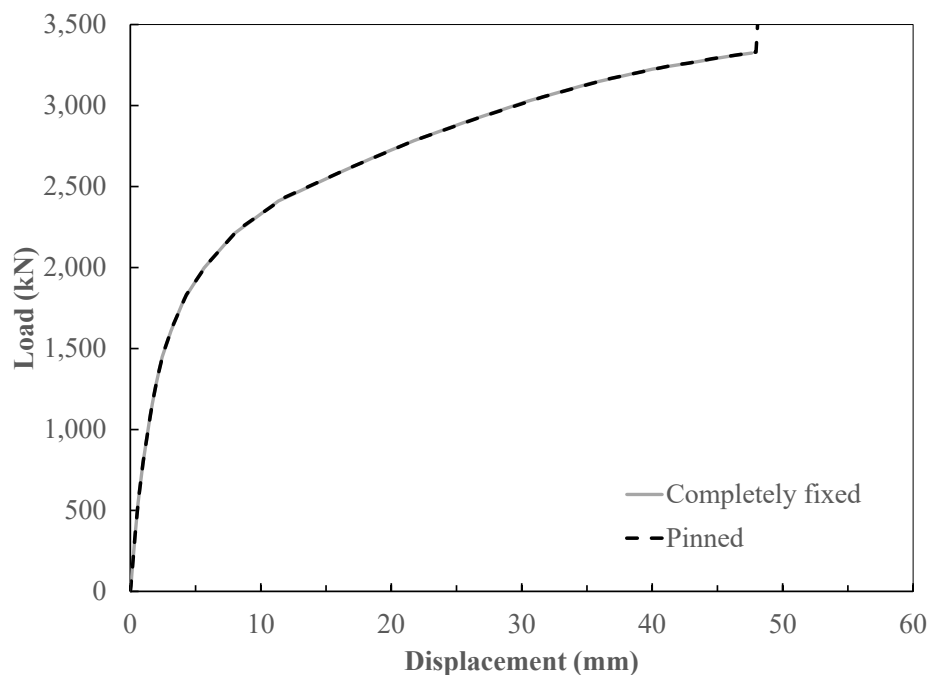
Figure 5 - 10. Load-displacement curves for pinned and completely fixed boundary conditions.

To apply the compression load, a two-step displacement-controlled analysis was performed. The first step was named "Contact". A vertical displacement equal to the gap between the pins and the holes was imposed until the pins engaged with the inner surface of the holes. No reaction force was calculated in the assembly during this load step.

Once the engagement of the pins was achieved, the second load step was initiated. It was named "Displacement" and represents a downward displacement of the lead pile (compression) until closure of the gap between the extension pile and the lead pile, which in the case of the tested assembly was 50.8 mm [2"], as shown in Fig. 5 - 11. An extra displacement of 2 mm was added to simulate the increment in the load when the internal piles establish contact.
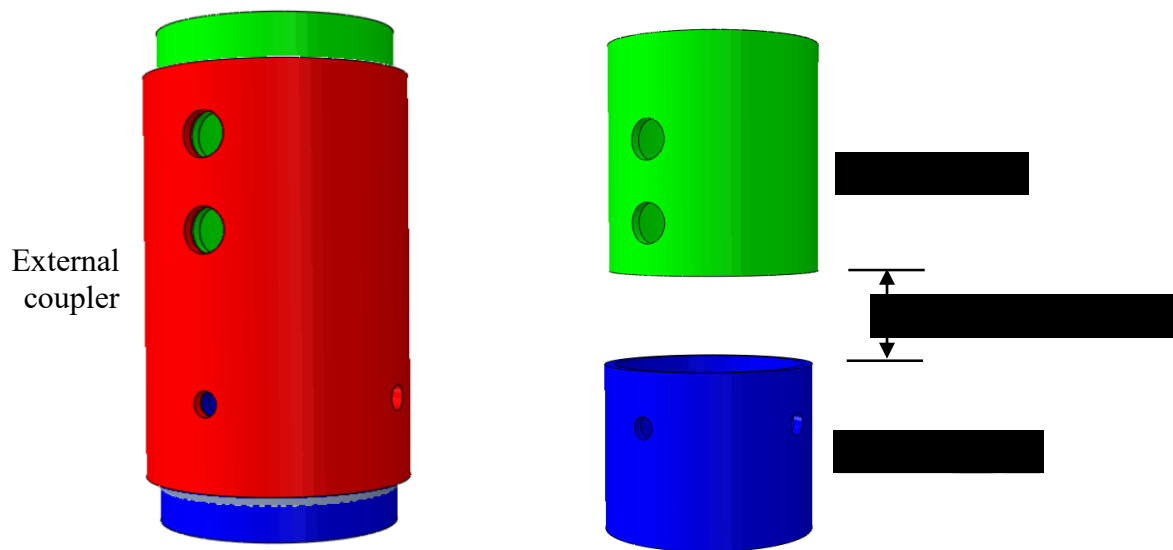
Figure 5 - 11. Gap between lead pile and extension pile.

5.2.6 Scope of FE Analysis Model

The main objective of the FE analysis was to predict with reasonable accuracy the maximum axial load that can be applied to the mechanical connection and the associated vertical displacement. In addition, the model was used to investigate important aspects of the connection behaviour, such as the deformation of the holes and stresses in the components.

Shear tear-out of the material between the holes was the observed mode governing the failure of the assembly during the tests. Due to the type of elements and material properties used, the FE model used in this study is unable to explicitly simulate cracking in the material. Therefore, is expected that the measured and calculated response are similar before the failure point.

5.3 Experimental vs. Analytical Results

As mentioned in Chapter 4, three identical specimens of the mechanical connection were tested under compressive axial load. The results from the experimental testing were compared to the results from the FE model. For simplicity, in all the calculated results that follow, the portion of the analytical results that precedes the engagement of the pins is not shown, since there is not a reaction force associated to that analysis.

5.3.1 Load-Deformation Response

To determine the analytical axial load-deformation curve of the assembly, the reaction load calculated at the bottom of the extension pile was plotted against the vertical displacement calculated at the top of the lead pile. The calculated load-deformation response is obtained after the point in which the pins engaged with the holes, as there was no reaction force before pin engagement. The comparison between measured and calculated load-deformation response is shown in (Fig. 5 - 12). While the initial, elastic portion of the measured response differs significantly from the calculated response, the plastic portion is well predicted. The differences noted in the initial elastic response can be attributed to several factors, discussed next.

First, a consideration must be made about the testing conditions. Prior to any load being applied to the coupler during the experiment, the pins are assumed to have settled onto the holes and theoretically, full contact is already established. However, if the calculated response is compared to the measured response, it is noted that the initial stiffness is significantly overestimated by the model.

While the calculated reaction force rises steeply once contact is established between the pins and the holes, the measured reaction force rises more gradually, meaning that full contact was not

achieved at the beginning of the experimental test. One possible reason for not having full contact could be a possible misalignment between the holes in the coupler.
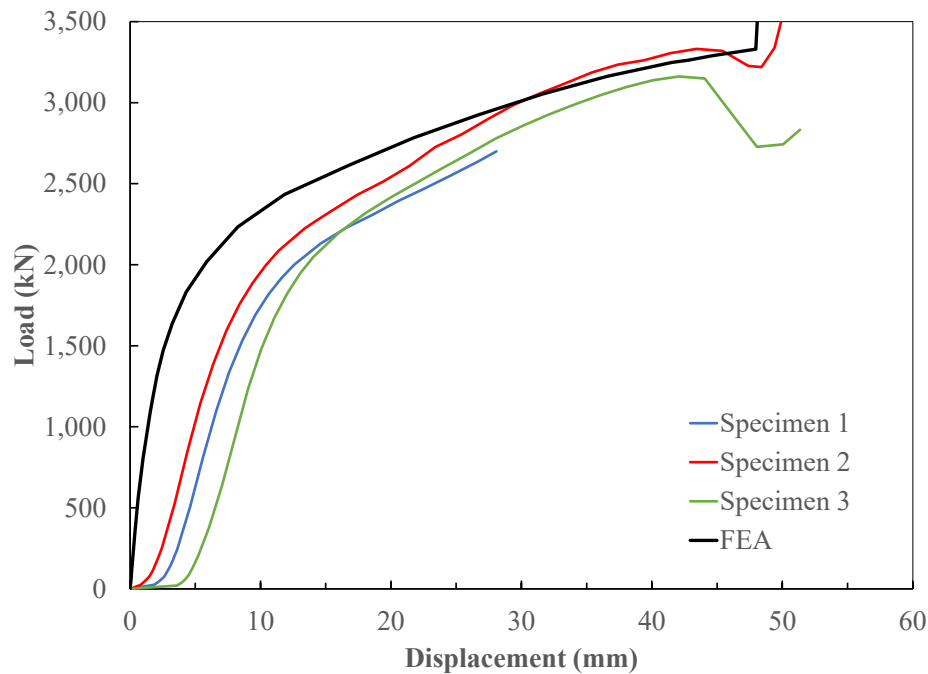
Figure 5 - 12. Load-displacement in FE analysis and tests.

A parametric analysis was conducted to investigate the influence of misalignments of the holes. This misalignment can be defined as horizontal misalignment (HM) or vertical misalignment (VM) of the holes in the lead pile. The current FE model was called "Symmetric" within this parametric analysis because there are no misalignments taken into account. Besides the Symmetric model, five more cases were studied:

Vertical misalignment of 1 mm.

Vertical misalignment of 2 mm.

Horizontal misalignment of 1 mm.

Horizontal misalignment of 2 mm.

Vertical and horizontal misalignments of 2 mm.

The misalignment distance was set with respect to the original location of the holes. For the horizontal misalignment, the four holes were moved one or two millimetres away of the central axis of the pile. For the vertical misalignment, the holes in one side of the pile were moved one or two millimeters in opposite directions to the holes on the other side (Fig. 5 - 13). The same loading and boundary conditions were applied to the new models. The load-displacement results corresponding to the vertical misalignment of the holes and the comparisons to the Symmetric model and specimen 2 are presented in Fig. 5 - 14.

Figure 5 - 13. Vertical and horizontals misalignment of the holes in the lead pile.
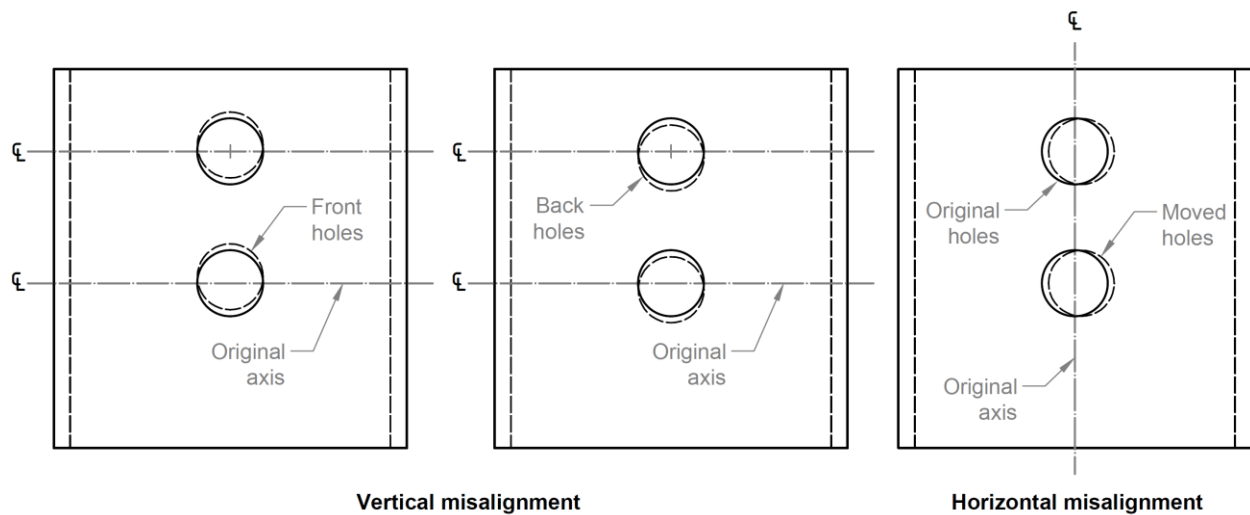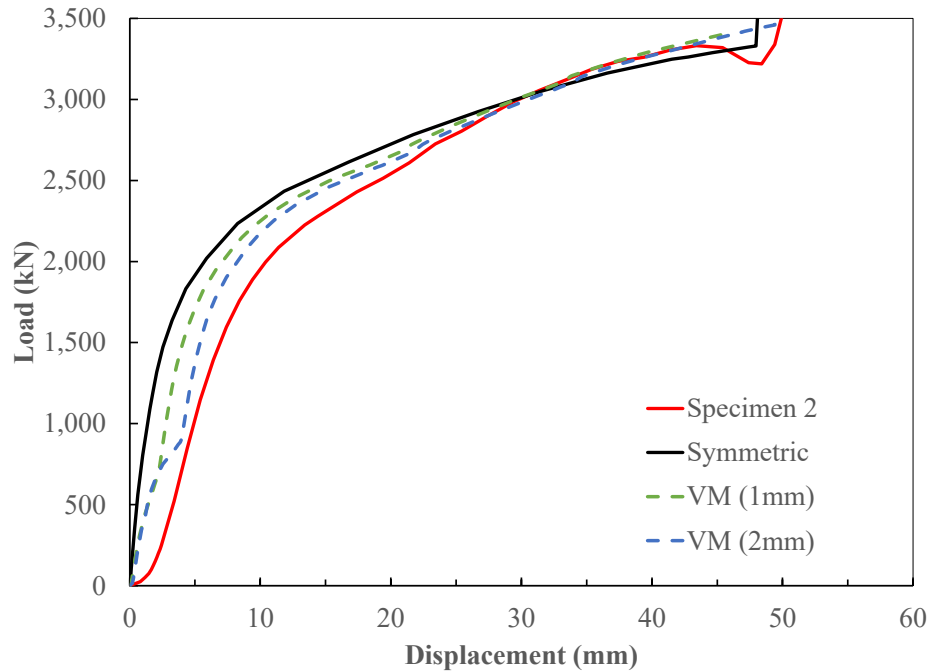
Figure 5 - 14. Load-displacement of models accounting for vertical misalignments.

It is seen that the stiffness in the initial stage reduces importantly when the misalignment takes place in the vertical direction. The larger the misalignment, the higher the reduction of the stiffness. This is because the vertical misalignment caused the pins to establish contact at different time on opposite sides of the assembly. The delay of the contact means that only one side of the connection was working, causing larger displacements than if the load was symmetric. The effects of the vertical misalignments are negligible once full contact is established and the nonlinear stage is reached.

The modifications in the horizontal direction caused a low impact on the reduction of the stiffness (Fig. 5 - 15). However, the effect of the misalignment is noticeable at the beginning of the analysis. The stabilization corresponds very accurately to the tests results from specimen 2 under loads below 100 kN. As the load increases, the stiffness of the FE model starts increasing at a higher rate than the stiffness in specimen 2, getting closer to the Symmetric model. Under loads above 2500 kN, the difference of stiffness of tests and FE model with misalignments are negligible.
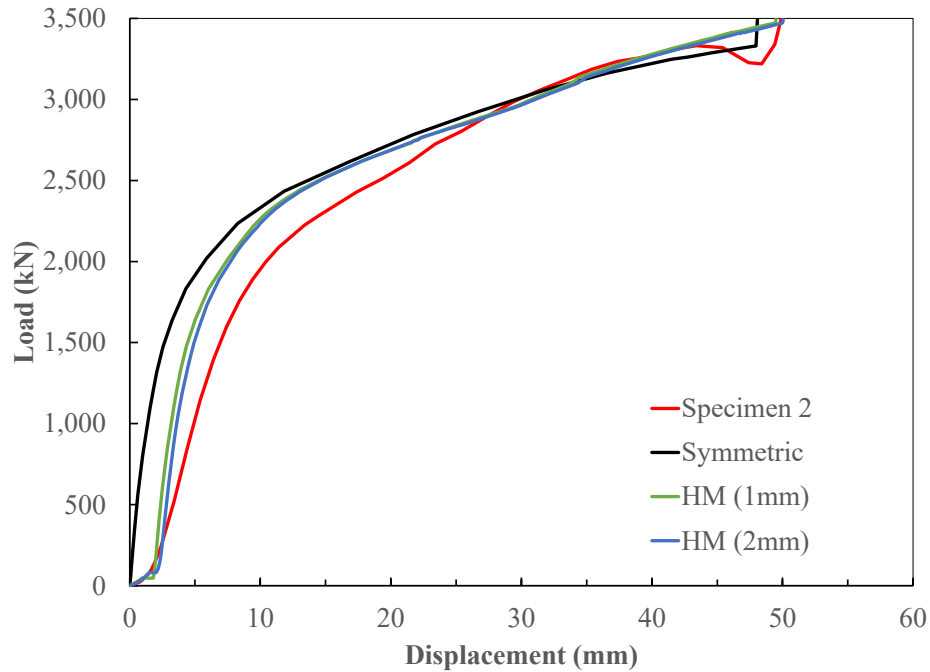
Figure 5 - 15. Load-displacement of models accounting for horizontal misalignments.

The last analysis conducted to investigate the effect of the deformations took into account the most critical vertical and horizontal misalignments, which were 2 mm of misalignment in each direction. The result of the model with both misalignments is presented in Fig. 5 - 16. The reduction of the stiffness due to the vertical misalignment occurred once again, getting closer to the results from specimen 2. The initial stabilization of the assembly due to horizontal misalignment under low loads was slightly reduced. However, the effect of the horizontal misalignment led to larger displacements when comparing against the symmetric model during the complete application of the load.
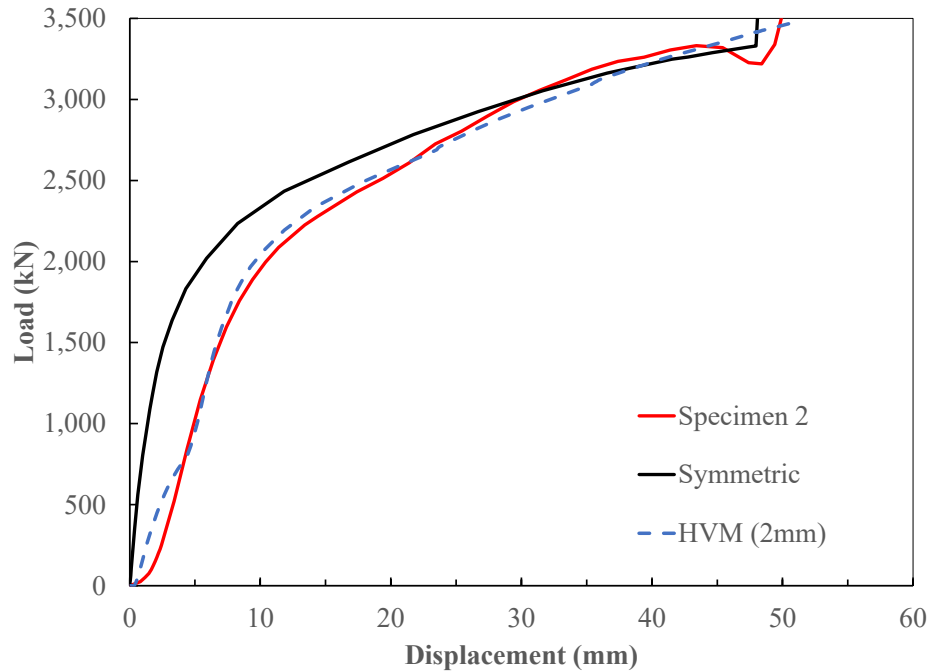
Figure 5 - 16. Load-displacement of models accounting for horizontal and vertical misalignments.

Based on the parametric analyses conducted, the cause of the differences between the model and the test can be attributed to vertical and horizontal misalignments happening simultaneously. The major effect in the initial stiffness of the assembly is due to vertical misalignments, but the horizontal misalignments cause larger displacements in the overall load-displacement response. Unfortunately, the existence of misalignment could not be verified experimentally post-mortem, because the holes suffered large deformations after the tests.

To quantify the effect of the misalignments in the stiffness of the assembly, two stages were considered in the load-displacement response:

1. Elastic stage.
2. Plastic stage.

The stiffness of the initial "elastic" stage was defined from the point in which the load increased at a constant rate in the three specimens ($\approx$200 kN) to the proportional limit of the curves ($\approx$1200 kN). The plastic stage was defined from 2200 kN to 3000 kN, which is the load level close

to the failure load of the assemblies. The load beyond 3000 kN was not considered because the inability of the FE model to predict the ultimate load. Each stage is depicted in Fig. 5 – 17.
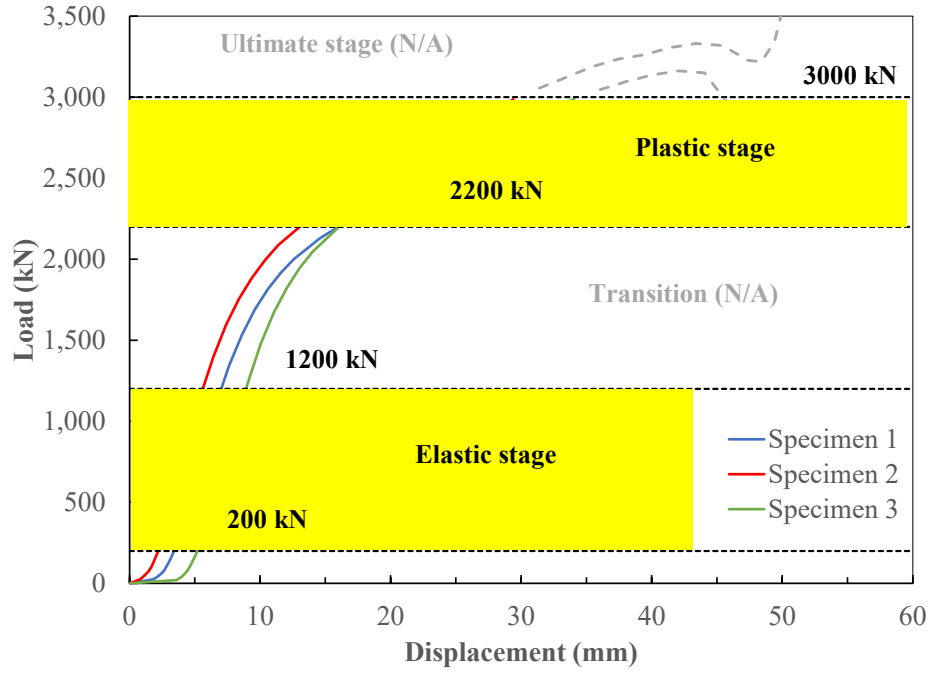
Figure 5 - 17. Stages for stiffness comparison between models and tests.

The comparison was made by calculating the Analytical/Experimental stiffness ratio in each stage of the load-displacement chart according to Eq. (5 - 4).

(5 - 4)
$$Stiffness\ ratio = \frac{k_{An}}{k_{Ex}}$$

where k_{An} is the stiffness obtained from the FE model and k_{Ex} is the averaged stiffness from the three specimens.

The results obtained from each stage for each model are summarized in Table 5 - 3. The Analytical/Experimental stiffness ratio indicates the accuracy of the model in predicting the capacity of the assembly. For the elastic stage, the symmetric model overestimates the capacity by 2.2 times. But this estimation is importantly reduced to 0.91 when vertical and horizontal misalignments are considered in the model.

100

The plastic stage is where the model presented higher accuracy at determining the stiffness of the assembly. Even though the capacity of the connection was underestimated by the assembly, the accuracy goes beyond 80% in all the cases. This indicates that the model can predict at an acceptable measure the plastic behaviour of the assembly once all the components are effectively engaged. The trend of the stiffness ratio for each model within the corresponding stage is shown in Fig. 5 - 18.

Table 5 - 3. Stiffness Ratio at each stage

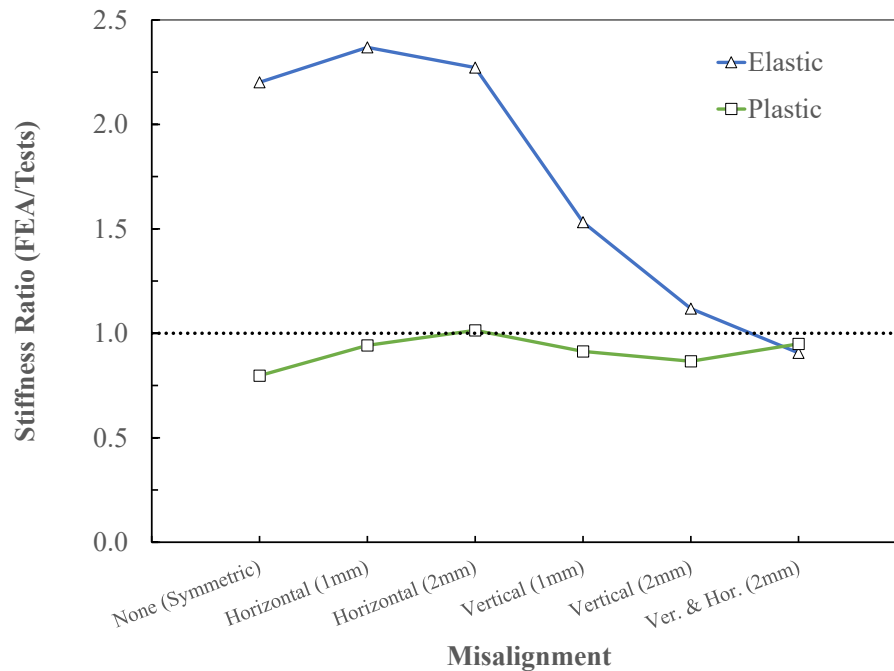| Misalignment Condition	Stiffness Ratio	
	Elastic	Plastic
None (Symmetric)	2.20	0.80
Horizontal (1mm)	2.37	0.94
Horizontal (2mm)	2.27	1.01
Vertical (1mm)	1.53	0.91
Vertical (2mm)	1.12	0.87
Ver. & Hor. (2mm)	0.91	0.95

Figure 5 - 18. Stiffnes ratio trend for different conditions of misalignment.

101

A second calculation was done in terms of load-carrying capacity when a displacement of 25.4 mm (serviceability conditions) was achieved. The FEA/Test load-capacity ratio was determined by comparing the load for each model against the averaged load of the three specimens. The comparison is presented in Table 5 - 4 and reflects the effectiveness of the symmetry when assuming that the holes in the piles where misaligned during the drilling process.

Table 5 - 4. Load-carrying capacity ratio under a displacement of 25.4 mm

Misalignment Condition	Load (kN)	Ratio (FEA/Test)
Tests (Avg.)	2,683	-
None (Symmetric)	2,887	1.076
Horizontal (1mm)	2,848	1.061
Horizontal (2mm)	2,842	1.059
Vertical (1mm)	2,861	1.066
Vertical (2mm)	2,831	1.055
Ver. & Hor. (2mm)	2,785	1.038

In summary, it can be postulated that the model is able to capture with reasonable accuracy the load-displacement response of the assembly if the possibility of misalignments is taken into account.

5.3.2 Prediction of Failure Load: Equivalent Plastic Strain

As presented in Section 4.4.4, plasticity is the ability of the material to accommodate high permanent strains until fracture appears (Kut 2010). The ultimate fracture strain was calculated and a value of 0.6353 obtained.

In Abaqus, the equivalent plastic strain is termed "PEEQ", and it represents the strain in the assembly during the application of the load. It is calculated by the software according to the von Mises criterion, i.e. the strain that takes into account the normal strains occurring in all directions (Noronha et al. 2010). The equivalent plastic strain is defined by the following expression:

$$(5\text{-}5) \qquad \varepsilon_{eq} = \frac{1}{1+\upsilon}\sqrt{\frac{1}{2}[(\varepsilon_1 - \varepsilon_2)^2 + (\varepsilon_2 - \varepsilon_3)^2 + (\varepsilon_3 - \varepsilon_1)^2]}$$

where υ is the Poisson's ratio, and ε_1, ε_2, and ε_3 are the principal components of the strain tensor.

The PEEQ was retrieved from the elements around the holes because it was at these locations where the cracks appeared in the tests. The PEEQ was tracked during the application of the load until the ultimate fracture strain value of 0.6353 was reached. The analyzed elements for the lead pile and external coupler are shown in Fig. 5 - 19.

The PEEQ obtained from the lead pile and the external coupler are plotted against the applied compressive load is shown in Fig. 5 - 20. The values for strain and load associated to this graph are presented in Table 5 - 5. The load at the ultimate fracture strain is the one determining the ultimate strength of the assembly provided by the FE model. This ultimate strength was compared to the ultimate strength reached by the tests.
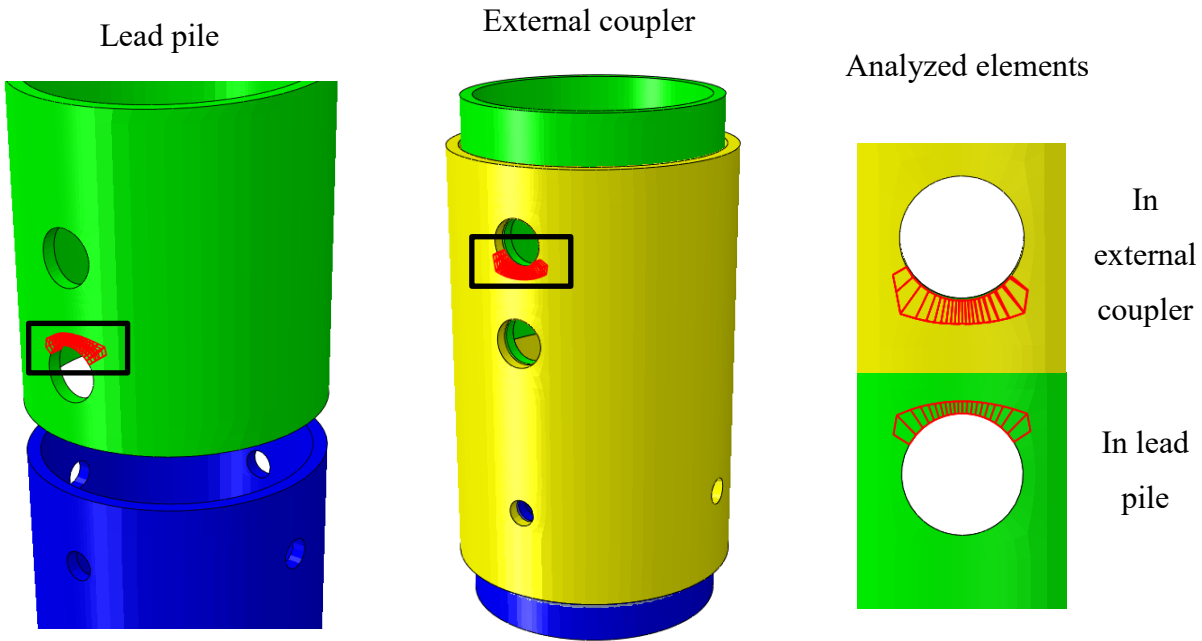

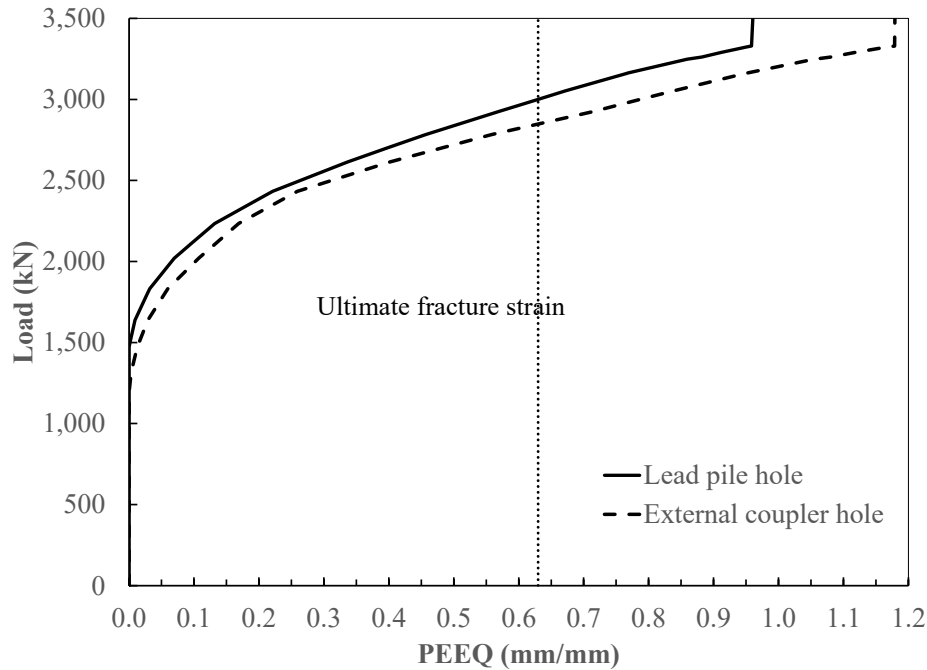Figure 5 - 19. Location of elements where PEEQ was retrieved.

Figure 5 - 20. PEEQ developed in holes of lead pile and external coupler.

It is seen that the holes in the external coupler were the first ones to reach the ultimate fracture strain at a load of 2853 kN. The holes in the lead pile reached it at a load of 3007 kN. This small difference (about 5%) is due to the fact that both pile and coupler have the same thickness and the onset of their plastic stage occurs almost simultaneously if the load is assumed to be evenly distributed in both of them.

The average ultimate load reached by specimens 2 and 3 was 3246 kN. The ultimate strength of the assembly defined by the PEEQ in the external coupler presents an accuracy of 88% when comparing to the average of the values from the tests, which is considered to be reasonable.

Figure 5 - 21 to Fig. 5 - 24 show the development of the equivalent plastic strain at four loads: when the holes in the external coupler reached ultimate fracture strain (2853 kN), when the holes in the lead pile reached ultimate fracture strain (3007 kN), and at the ultimate loads reached by specimen 3 (3161 kN) and specimen 2 (3331 kN).

The development of PEEQ started where the contact between the pins and the holes occurred. As the load increased, the strain started increasing rapidly in the elements located at the sides of the holes rather than in the surfaces in contact. These elements at the sides of the holes are the starting

location of the cracks and they are the ones developing the highest strain values through the range of the applied load in this study.

Table 5 - 5. PEEQ developed in holes due to applied compressive load

| Applied load (kN) | Equivalent plastic strain (PEEQ) | |
| | Holes | |
	Lead pile	External coupler
300	0.0000	0.0000
600	0.0000	0.0000
900	0.0000	0.0000
1,200	0.0000	0.0003
1,500	0.0015	0.0154
1,800	0.0280	0.0547
2,100	0.0928	0.1303
2,400	0.2064	0.2440
2,700	0.3975	0.4812
2,853	0.5120	**0.6353**
3,000	0.6295	**0.7869**
3,007	**0.6351**	**0.7937**
3,161	**0.7664**	**0.9492**
3,331	**0.9585**	**1.1789**
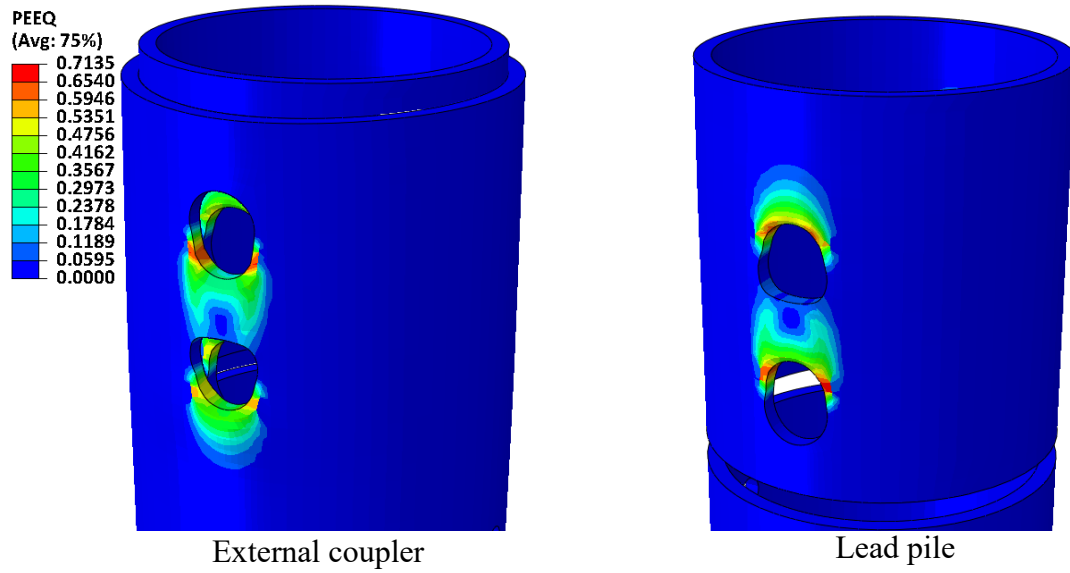
Figure 5 - 21. Equivalent plastic strain at 2853kN of applied compressive load.
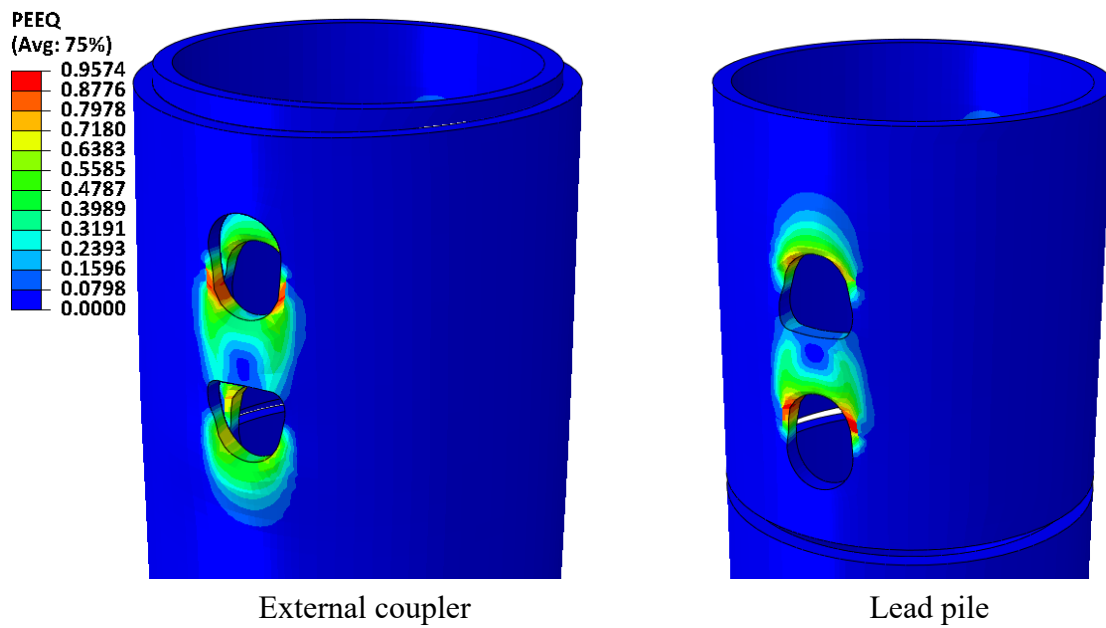
Figure 5 - 22. Equivalent plastic strain at 3007 kN of applied compressive load.

PEEQ
(Avg: 75%)
1.0619
0.9734
0.8849
0.7964
0.7079
0.6194
0.5309
0.4424
0.3540
0.2655
0.1770
0.0885
0.0000

External coupler

Lead pile
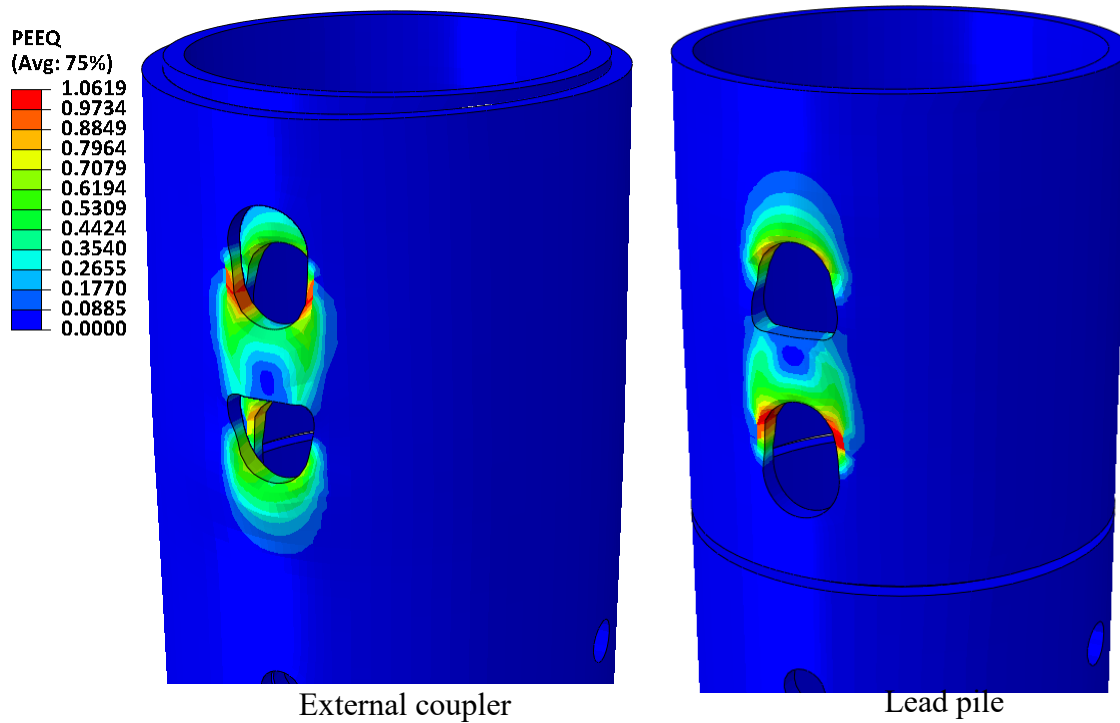
Figure 5 - 23. Equivalent plastic strain at 3161 kN of applied compressive load.

PEEQ
(Avg: 75%)
1.1795
1.0813
0.9830
0.8847
0.7864
0.6881
0.5898
0.4915
0.3932
0.2949
0.1966
0.0983
0.0000

External coupler

Lead pile

Figure 5 - 24. Equivalent plastic strain at 3331 kN of applied compressive load.

107

5.3.3 Hole Deformation (Ovalization)

The deformation of the holes, also termed "ovalization", of both the lead pile and external coupler is an important response parameter since in some cases the pile needs to be removed or replaced, with the mechanical connection in need to be reused. Therefore, the holes need to preserve as much of their original geometry during installation or service loads. The ovalization is different for the top and bottom holes of the piles. These differences are illustrated in Fig. 5 - 25, which s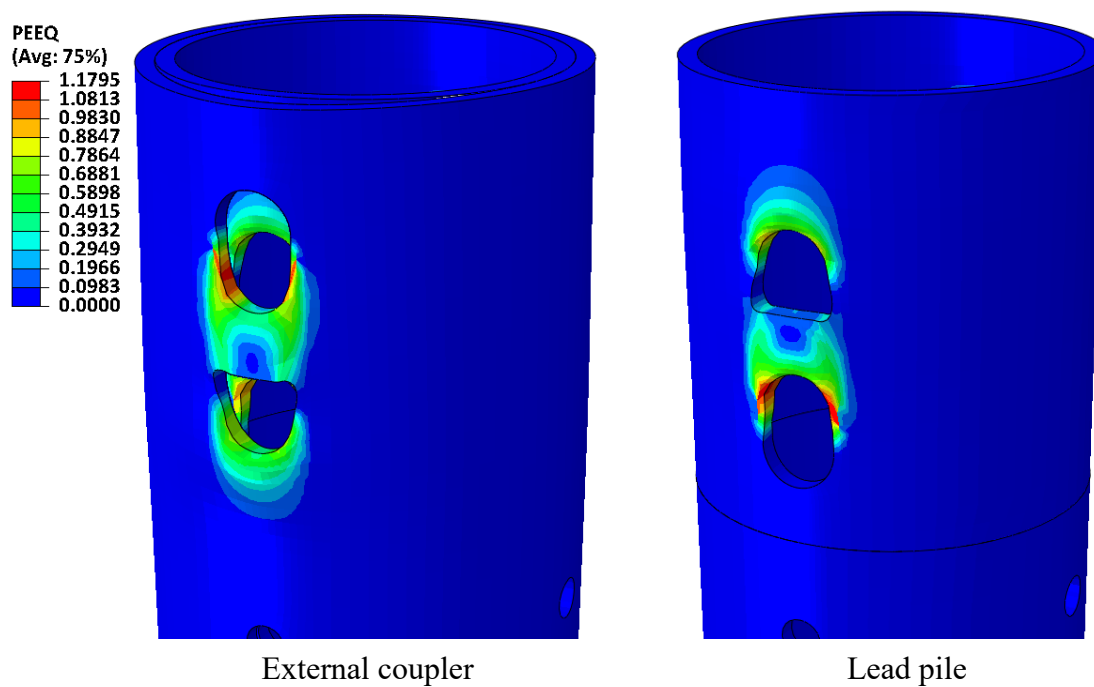hows the measured and calculated vertical displacements in the external coupler under the ultimate load of 3331 kN, in specimen 2.

The ovalization was measured using the digital imaging system automatically in all three specimens as mentioned in Chapter 4. The ovalization in the FE model for a given hole was calculated by the following expression:

(5 - 6)
$$Ovalization = U2_b - U2_t$$

where $U2_b$ is the vertical displacement of the node located at the center bottom of the hole and $U2_t$ is the vertical displacement of the node located at the center top of the hole as shown in Fig. 5 - 26. The relative displacement of the bottom node relative to the top node in each hole was calculated as per Eq. (5 - 6).

Calculated

Measured
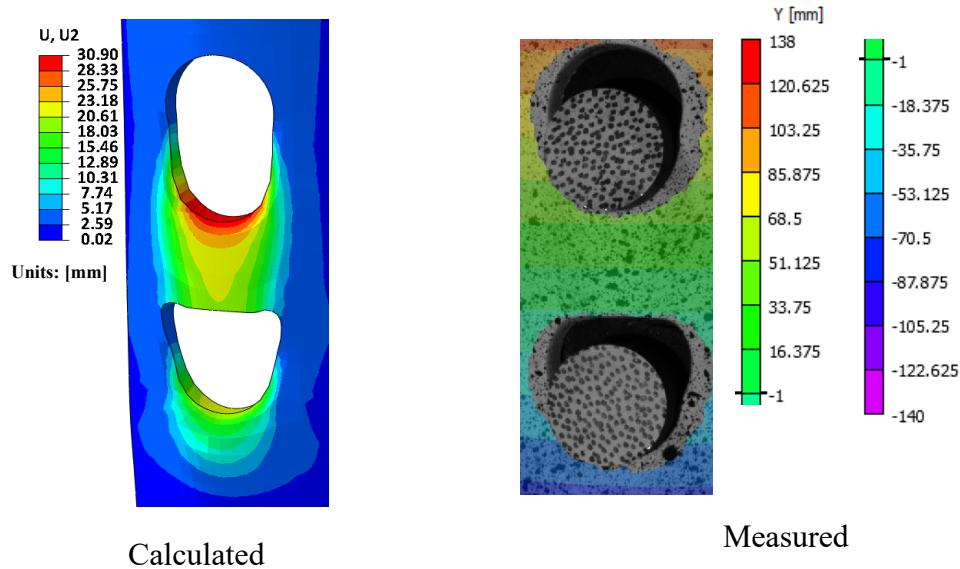
Figure 5 - 25. Vertical displacements of the external coupler of specimen 2 under a load of 3331 kN.
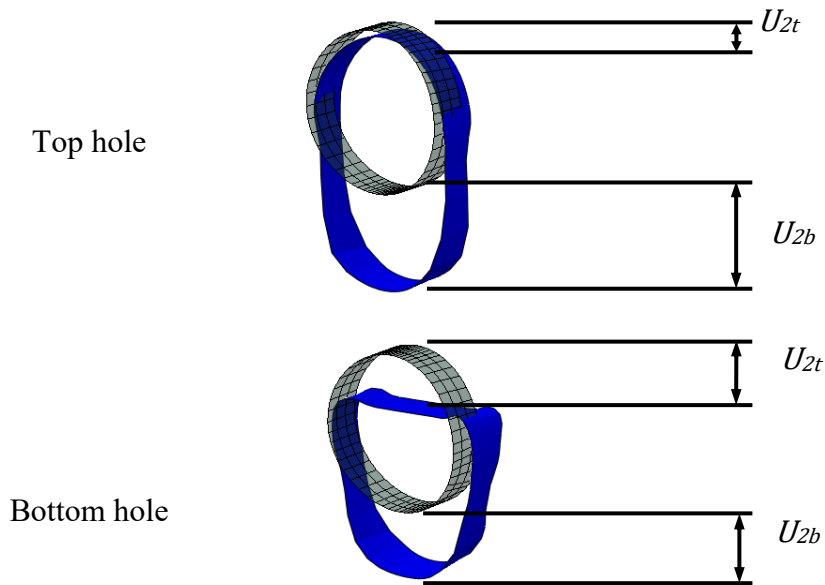
Figure 5 - 26. Relative deformations in the holes used to calculate the ovalization.

Numbers 1 and 2 were assigned to the top holes located on opposite sides of the coupler. Numbers 3 and 4 were assigned to the bottom holes (see Fig. 5 - 27 for details). The load-ovalization relationship for the FE model and for each test is shown in Fig. 5 - 28 to Fig. 5 - 30.

The ovalization of all four holes from each test are plotted because they did not exhibit equal deformations. On the other hand, only one top hole and one bottom hole from the FE model is presented under the assumption that the application of the load was perfectly symmetrical.
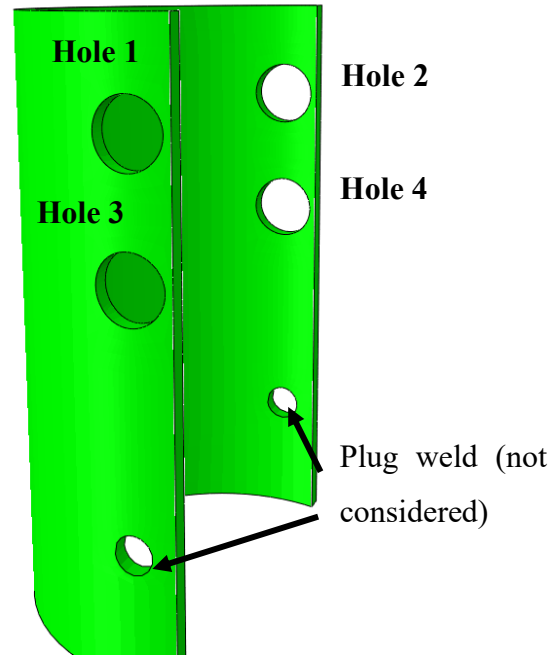
Figure 5 - 27. Numbering of holes in external coupler.
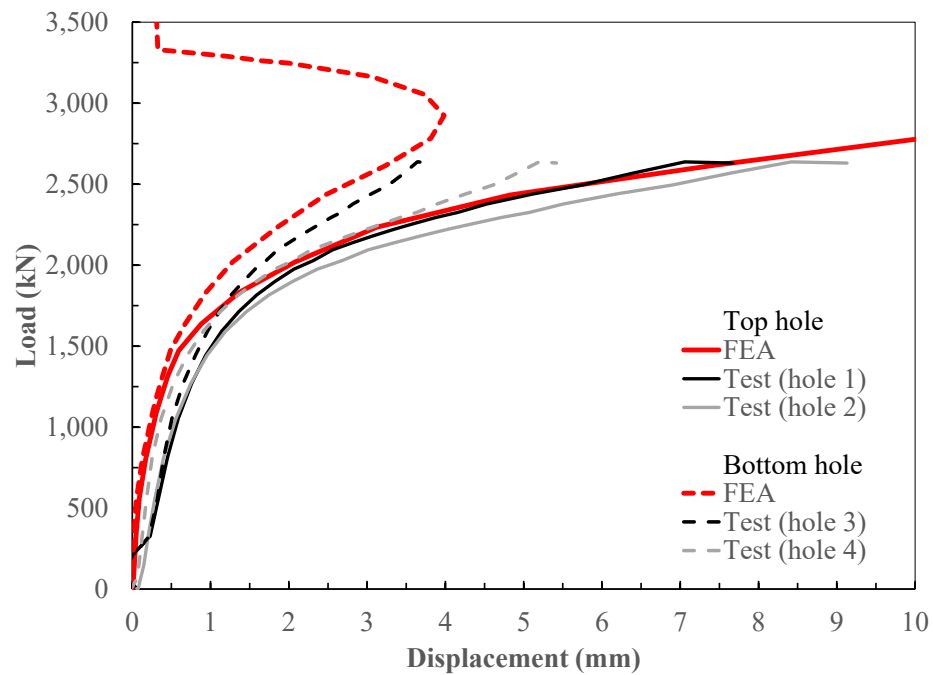
Figure 5 - 28. Load-ovalization relationship in FE model and in specimen 1.
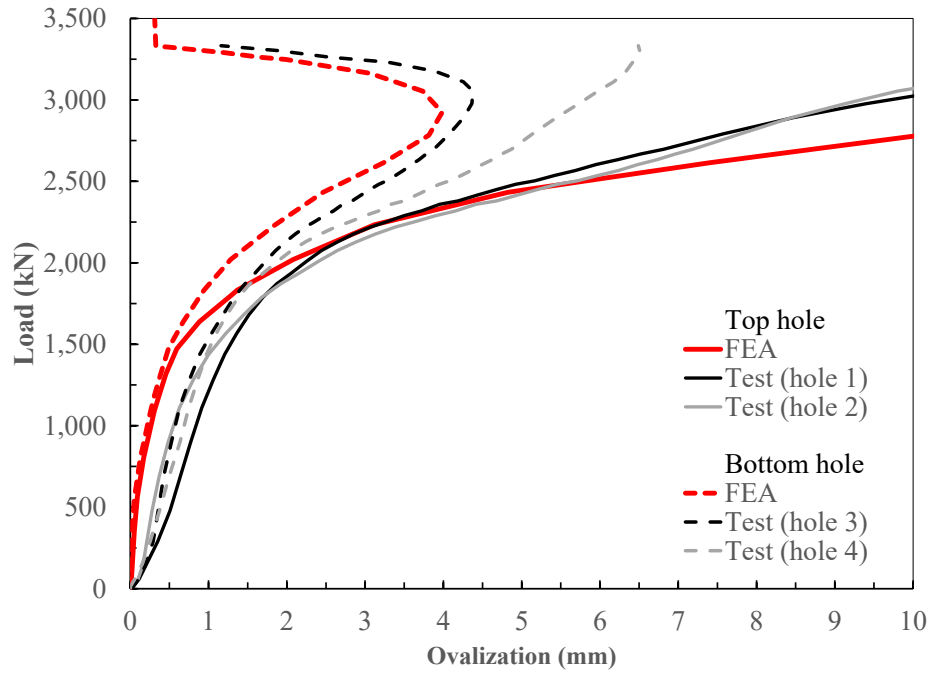
Figure 5 - 29. Load-ovalization relationship in FE model and in specimen 2.
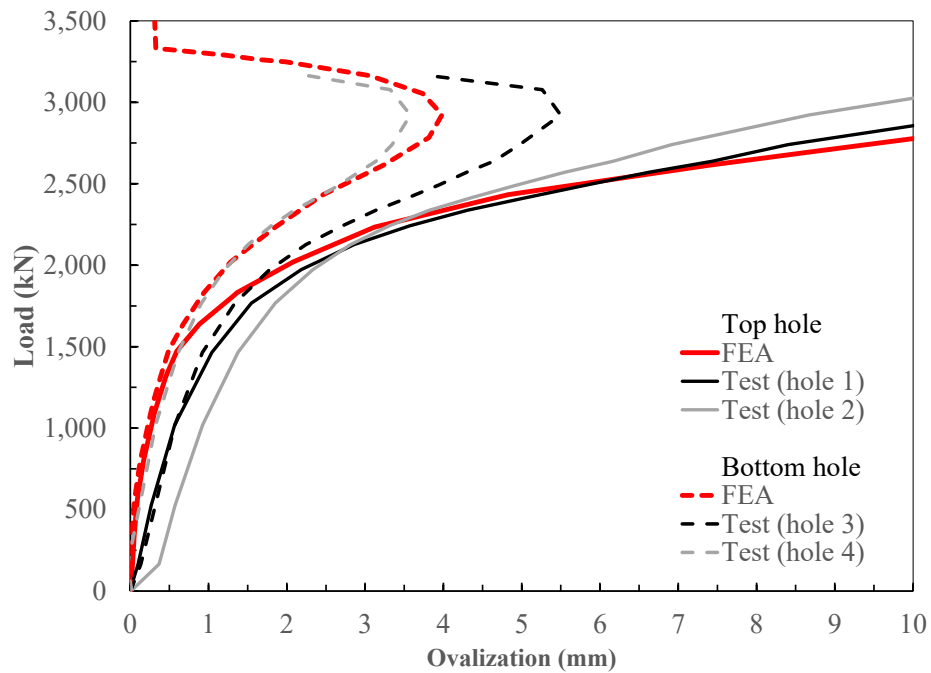
Figure 5 - 30. Load-ovalization relationship in FE model and in specimen 3.

111

It is seen that he FE model predicted accurately enough the ovalization observed in the experimental tests. However, a small difference can be perceived at the initial stage of the application of the load. This difference is due to the uneven settlement of the pins in opposite sides of the connection. As the application of the load continues, the engagement of the pins in the holes becomes symmetric and allows the effective transmission of the load in both the experiments and FE model, predicting more similar results as plasticity is developed.

The limitation of the FE model to predict the occurrence of the cracks leads to some differences after the ultimate load was reached by the experiments. Though, the general behaviour of the mechanical connection was effectively reproduced. The ovalization of the holes is presented in Table 5 - 6.

Table 5 - 6. Ovalization results in tests, FE model, and Ovalization Ratio

Load (kN)	Specimen 1				Specimen 2				Specimen 3				Averaged tests		FE model	
	TH		BH		TH		BH		TH		BH		TH	BH	TH	BH
300	0.19	0.19	0.21	0.13	0.36	0.22	0.29	0.26	0.17	0.46	0.21	0.03	0.26	0.19	0.05	0.02
600	0.35	0.31	0.34	0.19	0.59	0.33	0.40	0.46	0.31	0.62	0.36	0.15	0.42	0.32	0.10	0.07
900	0.49	0.45	0.43	0.29	0.77	0.49	0.53	0.64	0.49	0.84	0.51	0.27	0.59	0.44	0.22	0.17
1,200	0.70	0.68	0.60	0.48	0.99	0.72	0.70	0.81	0.70	1.08	0.68	0.43	0.81	0.62	0.38	0.32
1,500	1.01	1.04	0.86	0.77	1.29	1.12	0.97	1.04	1.12	1.45	0.97	0.65	1.17	0.88	0.64	0.52
1,800	1.53	1.67	1.22	1.29	1.72	1.73	1.36	1.41	1.66	1.92	1.40	0.95	1.71	1.27	1.29	0.90
2,100	2.61	3.08	1.89	2.34	2.54	2.77	1.92	2.15	2.75	2.74	2.18	1.46	2.75	1.99	2.47	1.50
2,400	4.77	5.77	2.92	4.04	4.33	4.83	2.90	3.59	4.98	4.31	3.51	2.36	4.83	3.22	4.54	2.36
2,700	-	-	-	-	6.83	7.20	3.88	4.87	8.13	6.71	4.90	3.31	7.22	4.24	8.77	3.53
3,000	-	-	-	-	9.75	9.37	4.38	5.82	12.27	9.65	5.50	3.51	10.26	4.81	14.87	3.84
3,161	-	-	-	-	12.28	11.12	4.01	6.30	16.75	12.95	3.84	2.28	13.28	4.11	19.22	3.08
3,331	-	-	-	-	16.99	14.62	1.16	6.49	-	-	-	-	15.80	3.82	26.98	0.33

CHAPTER 6. PARAMETRIC STUDY

6.1 Introduction

A parametric study was conducted to investigate the effect of several design parameters on the performance of the connector. Since the pile company sponsoring this study has been using a modified version of the connector described in this study in a few pilot projects, it was decided to conduct the parametric analysis on the new connector. It is assumed that the FE analysis model will have a similar performance in predicting the response of the newer connector, based on the results obtained for the original one.

6.2 Design Details of the Connection

The components in this modified connector are similar to those used in the original one (lead pile, extension pile, external coupler, pins). The modified connector possess slightly larger diameters for both the piles and coupler, and three pins instead of two (1 pin is installed perpendicular to the other 2). The details of the mechanical connection used in this section are presented in Table 6-1 and the design is shown in Fig. 6-1.

The parametric analysis consisted on investigating the effects of three design variables: (1) different thicknesses of the external coupler, (2) different diameters of the pins, and (3) different locations of the connection in a full-length piles system. The details of each variable and the results of each analysis are presented in the following sections.

Table 6 - 1. Geometric properties of the mechanical connection used in parametric study

Component	Coupler	Lead Pile	Extension Pile	Pins	Weld
External diameter (mm)	355.60	323.85	323.85		-
Internal diameter (mm)	325.85	298.45	298.45		-
Thickness (mm)	14.88	12.70	12.70		-
Length (mm)	609.60	431.80	238.12	374.65	-
Number of holes/pins	3	3	-	3	-
Diameter of holes/pins (mm)	47.62	47.62	-	44.45	-
Details of weld	-	-	-	-	1/2" fillet weld
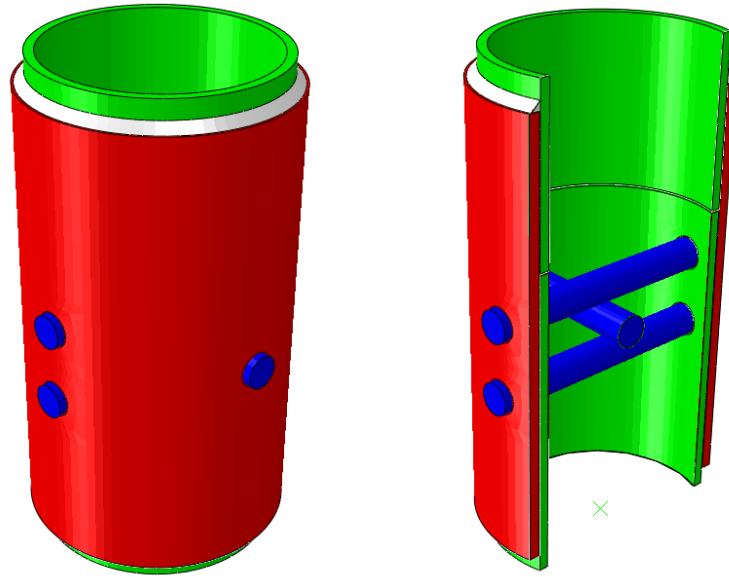
Figure 6 - 1. Final design of mechanical connection used in parametric study.

6.3 Thickness of the External Coupler

Four different thicknesses of the external coupler were investigated as shown in Table 6-2. Note that the existing gap between the piles and the external coupler changed accordingly. The geometry of the rest of the components in the mechanical connection was not changed.

Table 6 - 2. Variations of dimensions in the external coupler

Feature	Analysis 1	Analysis 2	Analysis 3	Analysis 4
External diameter (in)	14.0000	14.0000	14.0000	14.0000
Internal diameter (in)	13.2500	13.0000	12.8300	12.7900
Coupler thickness (in)	0.3750	0.5000	0.5856	0.6050
Gap between coupler and piles (in)	0.2500	0.1250	0.0390	0.0200

6.3.1 Results

6.3.1.1 Load-Displacement Response

The load-displacement relationship for axial compression shows the tendency of a connection with a thick coupler to be stiffer than that with a thinner one (Fig. 6 - 2) as expected. The thickness of the coupler provides an increased stiffness to the assembly when applying axial compressive load.

Figure 6 - 2. Load-displacement of the mechanical connections under axial compressive load.

6.3.1.2 Ovalization

As per the design specification of this connection provided by the piling company, the compressive load during its life service is expected to be 800 kN. The deformations of the holes under this load are 2.3 times higher when using a coupler with a thickness of 0.605" than the ones where the coupler has a thickness of 0.375" as shown in Table 6 - 3. The ovalization under the service compressive load is higher when thinner tubes are used, as expected.

Table 6 - 3. Ovalization of holes under compressive load of 800 kN

	Analysis 1	Analysis 2	Analysis 3	Analysis 4
Coupler thickness (in)	0.375	0.5	0.5856	0.605
Gap (in)	0.25	0.125	0.039	0.02
Zones	Max ovalization of holes (mm)			
External coupler holes	0.56	0.33	0.26	0.24
Lead pile holes	0.28	0.29	0.28	0.28

6.4 Variation of the Diameter of the Pins

The tested connection and the FE analysis made previously showed that the von Mises stress in the pins is lower than those obtained at other locations. This suggests that the pins size can be optimized (reduced). A parametric analysis was conducted for the pin diameters of 1.00, 1.25, 1.50 and 1.75 inches. The original size of the pins used by the piling company is 1.75 inches. The diameter of the holes was reduced accordingly to have approximately a gap of 1 mm around the pin in all cases. The geometry of the rest of the components remained unchanged. Table 6 - 4 shows the diameter of pins and holes used for the four analyses.

Table 6 - 4. Variations of diameters of pins and holes

Feature	Analysis 1	Analysis 2	Analysis 3	Analysis 4
Pin diameter (in)	1.000	1.250	1.500	1.750
Hole diameter (in)	1.125	1.375	1.625	1.875

6.4.1 Results

6.4.1.1 Load-Displacement Response

For the load-displacement relationship of the four analyses shown in Fig. 6 - 3, in can be seen that the larger the diameter of the pin used, the stiffer the mechanical connection behaviour. As stated before, a load of 800 kN is the service load that is imposed to a mechanical connector of these dimensions. This service load can be well sustained by reducing the diameter of the pins to 1.50 inches or 1.25 inches, since the displacement remained below 1 mm as in the original model.

However, deformations of 2 mm are seen when reducing the diameter to 1 inch, indicating that this might not be a suitable alternative for the assembly.
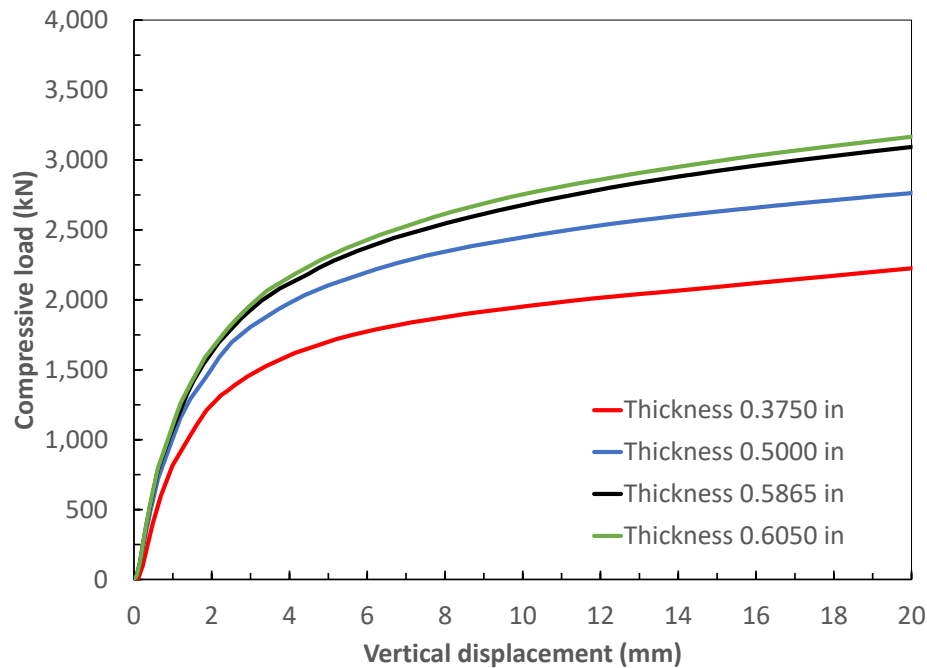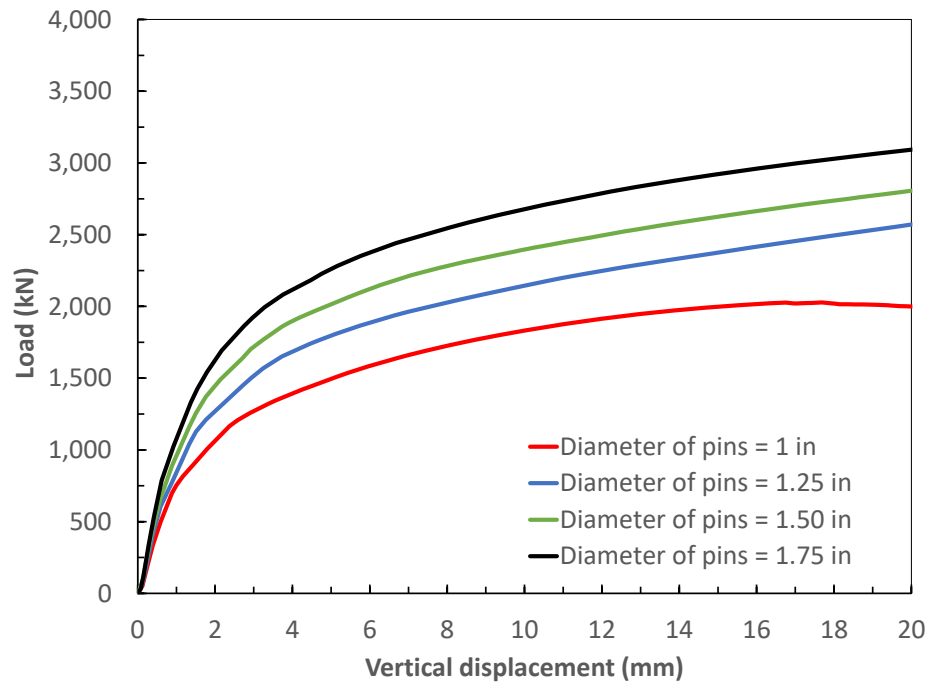

Figure 6 - 3. Load-displacement of the mechanical connections under axial compressive load.

6.4.1.2 Ovalization

When analyzing the deformations of the holes in Table 6 - 5, it is observed the large deformations occurring when having pins with small diameters. The reduced area in contact increases the stress at the holes, causing higher strains and these large deformations. The discrepancies in the deformations for Analysis 3 can be assumed as stabilization of the model and neglected, since the design load occurs at a very early stage of the analysis.

Table 6 - 5. Ovalization of holes under compressive load of 800 kN

	Analysis 1	Analysis 2	Analysis 3	Analysis 4
Diameter of pins (in)	1.00	1.25	1.50	1.75
Zones	Max ovalization of holes (mm)			
External coupler holes	0.57	0.37	0.40	0.26
Lead pile holes	0.65	0.52	0.36	0.28

6.5 Analysis In-Air of Full-Length Piles

The analysis in-air for the full-length piles aimed to investigate the performance of the piles under axial compressive load and lateral load applied separately. Table 6 - 6 shows the four different locations of the mechanical coupler that were analyzed. These four different systems were compared with a continuous pile shaft with a length of 30 ft. (9.14 m) without coupler.

Table 6 - 6. Lengths for lead and extension pile in full-length system

Model	Lead pile length	Extension pile length
Model A	5 ft.	25 ft.
Model B	10 ft.	20 ft.
Model C	15 ft.	15 ft.
Model D	20 ft.	10 ft.

Figure 6 - 4 shows the representation of "Model A" in Abaqus extracted from the sketch provided by the fabricator. The geometry of the components besides the length of the piles can be revised in Section 6.2. The gaps, diameters and length of the external coupler and pins did not change from among the models.
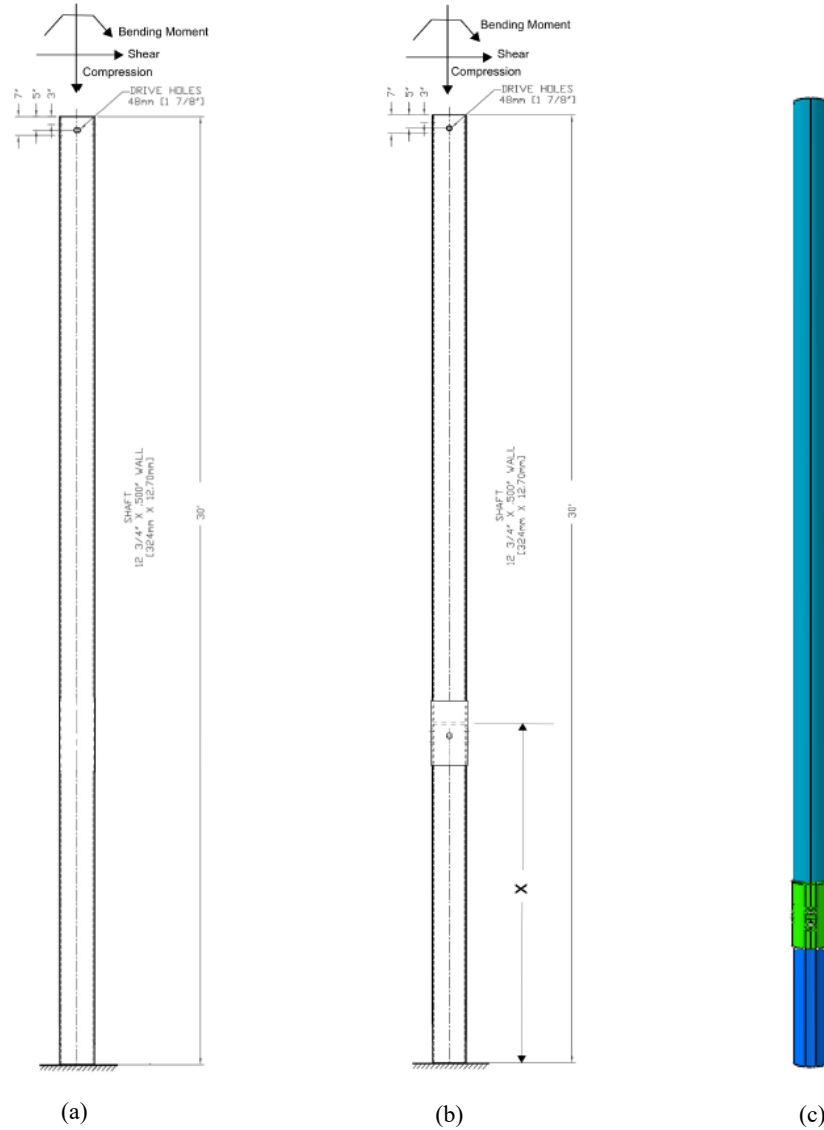
Figure 6 - 4. (a) Continuous shaft, (b) piles with coupler, (c) model with coupler in Abaqus.

6.5.1 Actions Applied to the Model

The boundary conditions of the system were assumed to be fixed at the bottom face of the lead pile and pinned vertically or horizontally at the top face of the extension pile depending on which displacement is being applied. The load scenarios were: (1) compression and (2) lateral displacement. Both scenarios consisted of an applied load at the top face of the extension pile.

Since the analysis was intended to be done in 2 dimensions, all displacements and rotations out-of-plane were constrained. For the top face of the lead pile under compression, the horizontal displacement and in-plane rotation were also constrained. When the system was under lateral displacement, the vertical displacement and in-plane rotation were constrained. For both loading scenarios, the boundary conditions of the pins were only constrained for out-of-plane displacements and rotations. Figure 6 - 5 depicts the locations of displacements and boundary conditions.
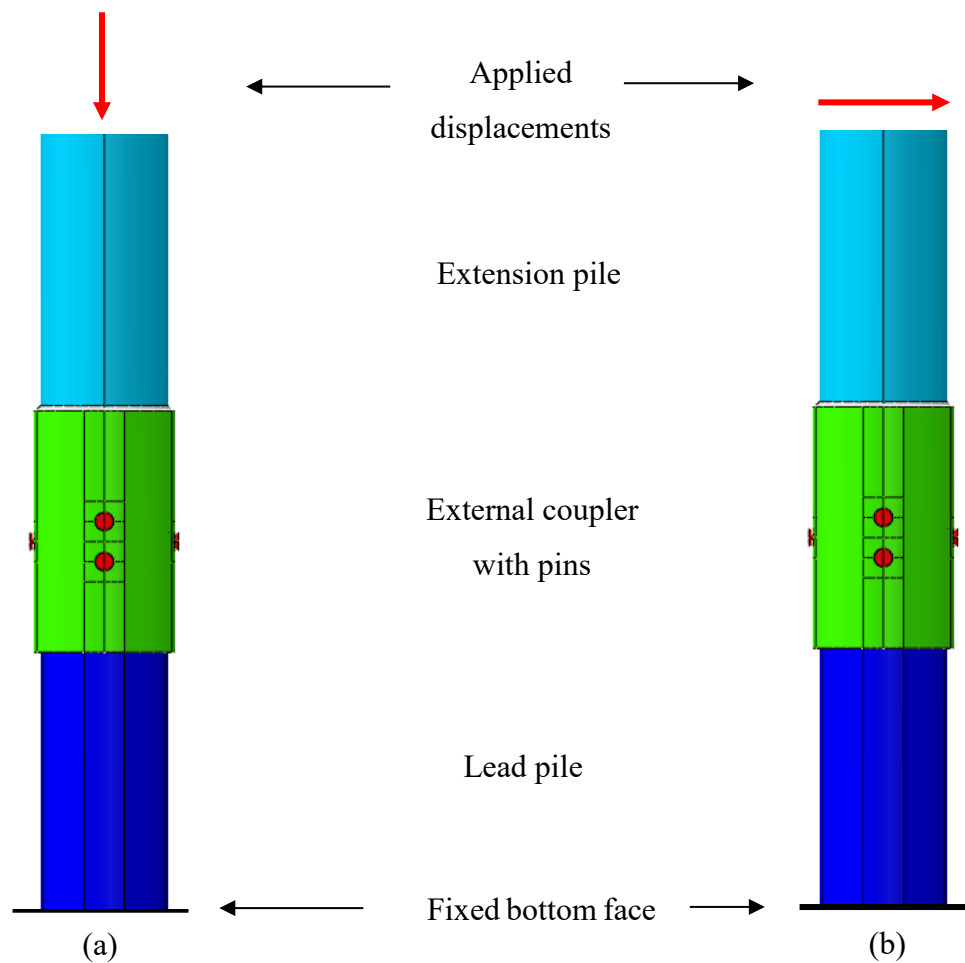

Figure 6 - 5. Locations of applied displacements.
(a) Compression and (b) lateral displacement.

6.4.2 Results

6.5.1.1 Results of the Compression Analysis

The applied displacement at the top face of the extension pile was retrieved as reaction force in the bottom face of the lead pile. The load-displacement relationship for the four models and the pile shaft without mechanical coupler is shown in Fig. 6 - 6.
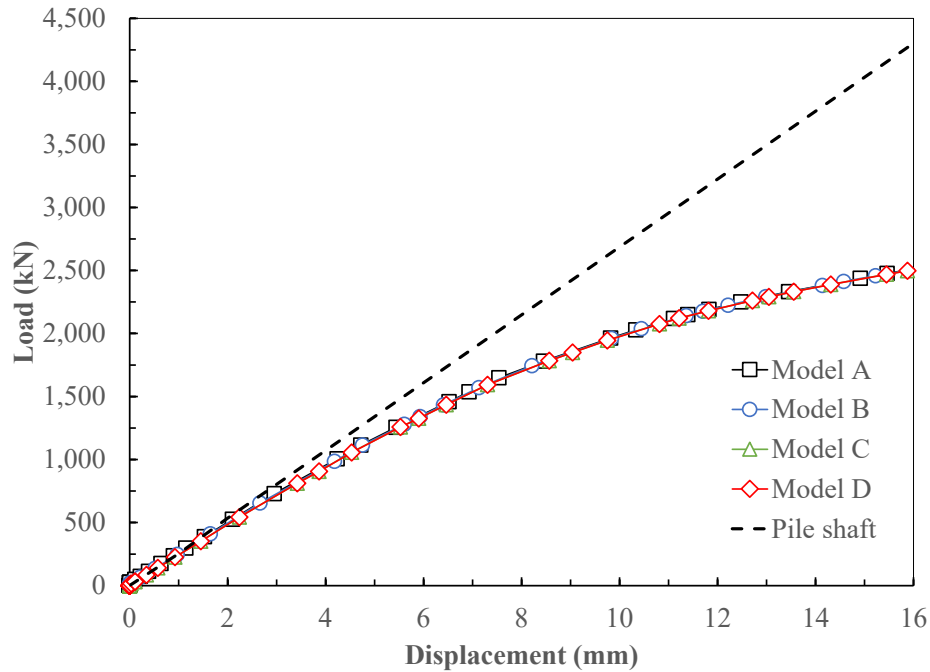

Figure 6 - 6. Load-displacement relationship for the four models without taking displacement before contact into account.

The results show the exact same behaviour of the four models under compressive load. This indicates that the location of the mechanical connection does not have an influence in the response of the system under compression. The small gap that was considered (1 mm) between the piles and the external coupler can be taken as the principal factor causing these similarities in the models.

When comparing against the pile shaft, the reduced stiffness is obvious. When a displacement of 16 mm is achieved, the piles with mechanical connector reached plastic deformations in some areas, while the pile shaft with no mechanical coupler is still increasing its compressive capacity.

6.5.2 Results of the Lateral Displacement Analysis

When applying a lateral load to the system, it was seen that the location of the mechanical coupler has a large influence in the stiffness and the deformed shape of the system. The results for the four analyses and the pile shaft are plotted in Fig. 6 - 7. This chart presents the bending moment of a system fixed in both ends with an applied displacement on the top. The bending moment was calculated as the following expression:

(6 - 1)
$$M = V \ x \ \frac{l}{2}$$

where M is the bending moment at the bottom of the pile, V is the shear force and l is the length.
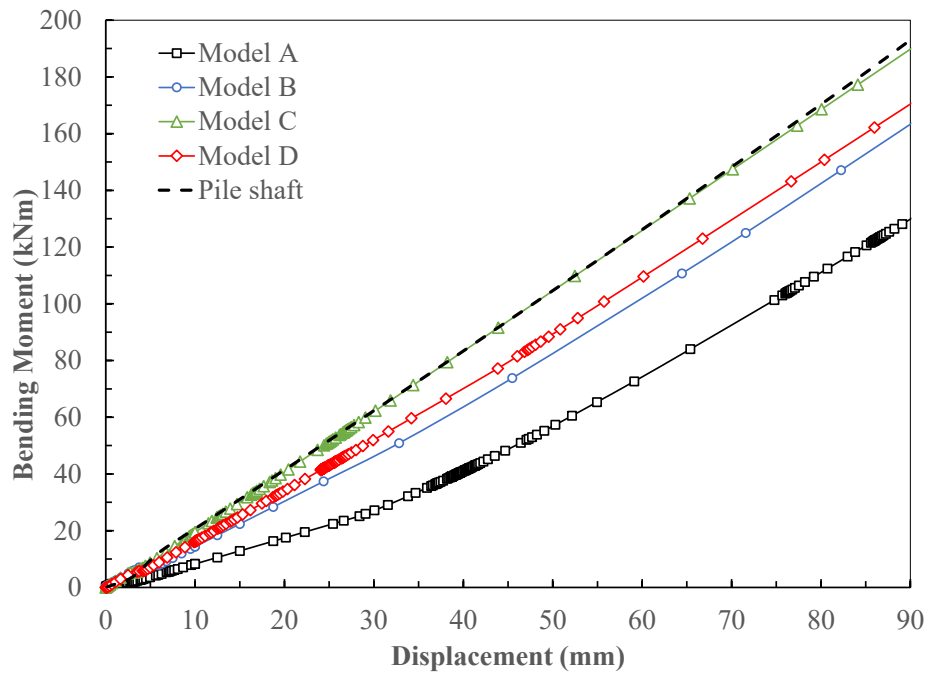

Figure 6 - 7. Load-displacement relationship of the four models and the pile shaft.

It is seen that all the four analyses presented elastic deformations up to a displacement of 90 mm. This displacement is considered already large, since is almost 30% of the diameter of the lead pile. The lateral load capacity tends to decrease as the mechanical coupler is closer to the ground (Model A), i.e. it has a shorter lead pile. This occurs due to the presence of higher moments and shear forces at this location. The shear and moment diagrams for an in-air pile shaft under lateral displacement at the top are presented in Fig. 6 - 8, where the different locations of the coupler can

123

be seen side by side to where the highest moments will occur in a fixed-fixed system. The shear reaction is constant through all the length of the pile and the moment is maximum at the top and bottom, and minimum at the midpoint.
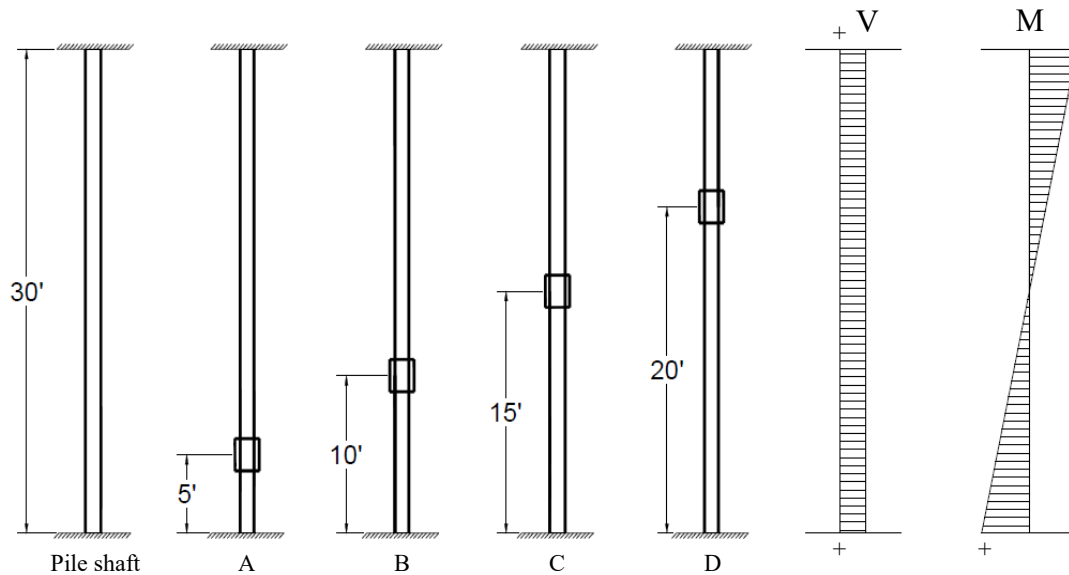

Figure 6 - 8. Location of coupler and shear and moment diagrams of a pile.

If the results of Model B and Model D are compared, it can be seen that they are very similar because the location of the mechanical coupler is where the same bending moments occur. Model C has a response very similar to the continuous pile shaft because the bending moment at the midpoint of the pile is minimum, and here is where the connector is located. This allows Model C to be almost as stiff as a simple shaft without coupler.

The shear force obtained from the bending moment of a continuous shaft at a displacement of 90 mm is close to 40 kN. This lateral load was used to retrieve the horizontal displacement at every 2.5 ft. from each different model and compare the differences. Figure 6 - 9 shows that all models are presenting a deformed shape very similar to the continuous pile shaft. However, the difference is noted in the discontinuity of the deformed shape where the coupler is located in each one of the models. Figure 6 - 10 shows the deformed shape of the four FE models under a load of 40 kN.
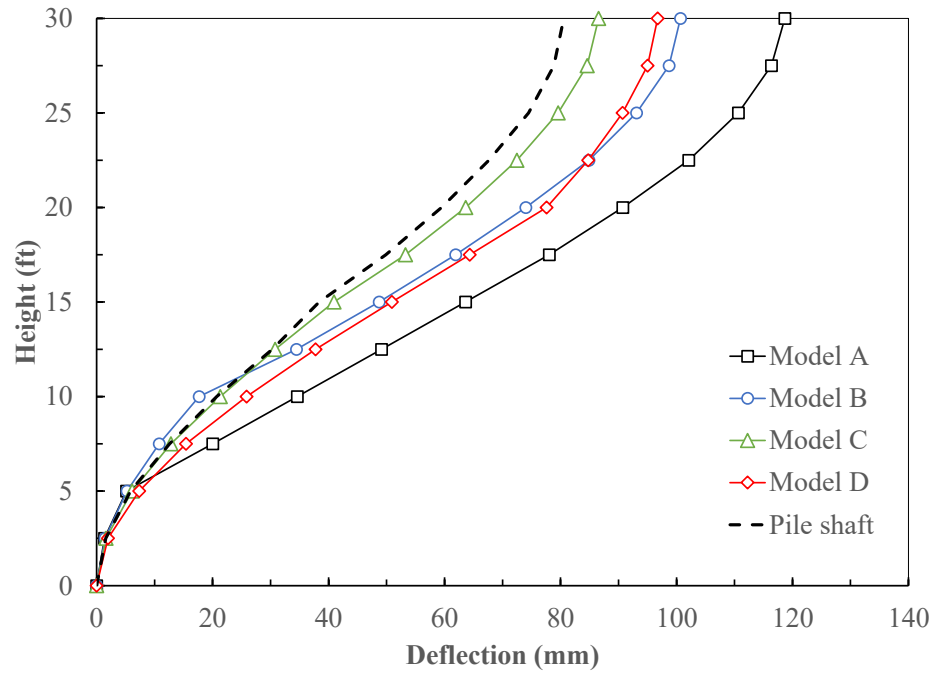
Figure 6 - 9. Lateral displacement of shafts under an applied load of 40 kN.
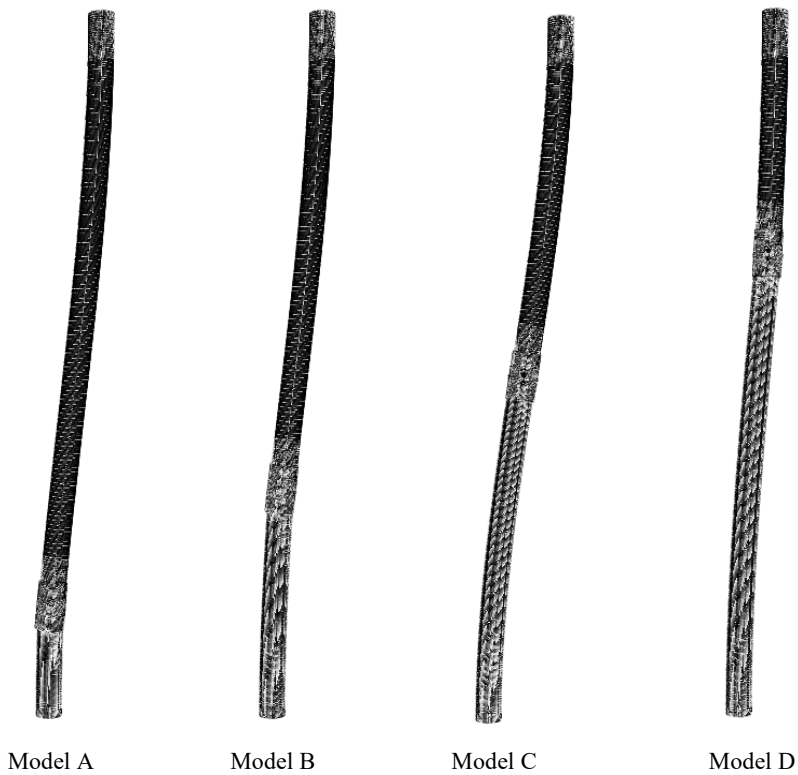
Figure 6 - 10. Deformed shapes of each one of the models with mechanical coupler.

125

The displacement at the top of the extension pile under the lateral load of 40 kN is presented in Table 6 - 7. As expected, the largest displacement is occurring in Model A, where the connector is under highest moment and shear. Models D and B are very similar and Model C has almost the same displacement as the pile shaft.

Table 6 - 7. Displacement of each model under 40 kN of lateral load

Model	Displacement (mm)
Model A	116.25
Model B	98.27
Model C	84.12
Model D	94.33
Pile shaft	82.32

CHAPTER 7.   SUMMARY AND CONCLUSIONS

7.1 Summary

A pile-to-pile mechanical connection was designed in this study, and its experimental performance under axial compressive loads was conducted. A finite-element analysis model was developed to capture the response of the different components of the connection.

The design was performed based in the limit states design as per several references. Six failure modes were evaluated to predict the maximum strength of the assembly: global compressive resistance, bearing resistance of the holes, *block shear*, *end tear-out*, shear resistance of bolts, and strength of the weld. The failure mode predicted by the design equations was *end tear-out* in the lead pile obtained as per CSA S16 expression.

In the experimental program, three specimens of the connection were fabricated as per the proposed design and were subject to compressive axial load. The observed failure mode corresponded to the mode predicted, being this the *end tear-out* between the holes in the lead pile. An initial settlement of the pins was observed at the initial stage of the tests and up to a load of approximately 100 kN. The three specimens exhibited elastic behaviour up to a load of 1200 kN and developed plastic strength up to an averaged load of 3264 kN, where failure occurred. The pins and the weld did not present considerable deformations.

A finite element model was developed incorporating the actual geometry of the components, the material properties, and the loading and boundary conditions. The initial settlement of the pins was reproduced by the model by assuming horizontal and vertical misalignments of the holes in the lead pile. The strength of the connection was determined as per the von Mises stress, the plastic equivalent strain, and the shear stress. The results given by the plastic equivalent strain were the most accurate compared to the tests results. The deformation of the holes in the lead pile and coupler were also tracked during the analysis.

A parametric study was conducted in a finite-element model of a mechanical connection issued by the sponsored company in pilot projects. The thickness of the coupler and the diameter of the pins where the two parameters studied to investigate their influence in the strength of the connection.

The location of the connection was a third analysis developed to study its influence in the compressive and lateral loading conditions in a system of full-length piles.

7.2 Conclusions

The following conclusions were obtained from this study:

- The proposed connector designed in this study had a satisfactory performance in terms of stiffness (for the serviceability stage) and a ductile behaviour in the plastic stage up to failure (the ultimate limit state).
- The failure mode predicted to occur in the test under axial compressive load was *end tear-out* of the material between the holes of both the lead pile and the external coupler. Even though the failure mode was accurately predicted, the strength as per the CSA S16 standard (2614 kN) approximated the failure load only by 80% because this expression was developed assuming that the failure will arise when yielding strength of the material is reached. However, the method to calculate *end tear-out* proposed by Kulak and Grondin (3162 kN) was able to predict the failure load with an accuracy of 96% because the average of the yielding and ultimate strength of the material was considered in the formula, rising the predicted capacity of the connection closer to the test results.
- The model was able to accurately capture the stiffness of the connection at the elastic and inelastic response. However, a combination of vertical and horizontal misalignments increased the accuracy of the model from an overestimation of 2.2 times to an approximation of 0.91 the compressive capacity of the assembly.
- When a load-carrying capacity was FEA/Test ratio was calculated, the misalignment of the holes improve the accuracy to the results of the specimens from a difference of 7.6% to 3.8%.
- The method proposed by Kut (2010) was found to be an accurate method to determine the ultimate load of the mechanical connection. The method used to by tracking the equivalent plastic strain (PEEQ) in the model up to the ultimate fracture strain presented an accuracy of 88%.

- In the parametric analyses, it was observed that reducing the thickness of the coupler by 50% will reduce the strength of the assembly up to 2.3 times within the range of thicknesses studied. While changing the diameter of the pins will lead to the reduction of strength as well.

- In the full-length piles system, the compression capacity did not change when varying the location of the coupler. However, the presence of the mechanical coupler in the pile caused an important reduction of the stiffness of the system when comparing with a pile without coupler. For the lateral resistance, it was found that the most convenient location of the coupler will be where minimum bending moment acts simultaneously with the constant shear in the full-length piles system.

7.3 Recommendations for Future Work

Some aspects should be considered for future work:

- The strain value in the zones where the cracks occurred in the lead pile was not known because the lead pile was obstructed by the external coupler. Strain tracking instrumentation is advised to be installed in the lead pile to determine the strains and deformations occurring in all components as the load is applied.

- Strain gauges located in the areas near the holes are advised to validate the results obtained from the digital Image Correlation System.

- A limitation of the FE model in the current study is the inability to reproduce the failure mode observed in the tests. The *end tear-out* found to occur in the experimental test was not captured by the model. Further improvements to the model are suggested to investigate crack propagation in the critical areas of the system.

- Other loads and their combinations of loads should be addressed in future experimental and analytical work: compression, shear, and bending during service and ultimate conditions, torsion and compression during installation (in helical piles), and tension during pulling out (when removing the piles).

- The boundary conditions assumed in the parametric analysis when lateral loads were applied could be underestimating the moment demands when compared to a fixed-pinned conditions. Fixed-fixed conditions should be compared to a new analysis that is conducted assuming pinned conditions at the top pf the pile.

REFERENCES

Adeeb, Samer. 2017. *Introduction to Solid Mechanics & Finite Element Analysis*. Retrieved from: http://sameradeeb.srv.ualberta.ca.

ASTM Standard. 2002. "Standard Specification for Welded and Seamless Steel Pipe Piles." West Conshohocken, PA, USA. doi:10.1520/A0252-10.2.

———. 2009. "Standard Test Methods for Tension Testing of Metallic Materials." West Conshohocken, PA, USA. doi:10.1520/E0008.

———. 2012. "A193-16: Standard Specification for Alloy-Steel and Stainless Steel Bolting for High Temperature or High Pressure Service and Other Special Purpose Applications." West Conshohocken, PA, USA. doi:10.1520/A0193.

Bullivant, A. Roger. 1998. Apparatus for Use in Forming Piles. US 5,833,399 A, issued 1998.

CSA Standard S16-01. 2007. "Design of Steel Structures." *Canadian Standards Association*. 9th Edition.

CSA Standard S16-09. 2010. "Design of Steel Structures." *Canadian Standards Association*. 10th Edition.

Duan, Lian, and W.F. Chen. 1999. "Effective Length Factors of Compression Members." In *Structural Engineering Handbook*, edited by Chen Wai-Fah. CRC Press LLC. doi:10.1201/b15616-19.

Hettinger, F.L.; Vetcor Offshore Inc. 1979. "A New Mechanical Pile Connector Speeds Offshore Construction Projects." Dallas, Texas, USA.

Jones, Robert L. 2006. Modular Tubular Helical Piering System. US 7,037,045, B2, issued 2006.

Kulak, G.L., and G.Y. Grondin. 2011. *Limit States Design in Structural Steel*. 9th ed. Canada: Canadian Institute of Steel Construction.

Kut, S. 2010. "A Simple Method To Determine Ductile Fracture Strain in a Tensile Test of Plane Specimens." *Metalurgija* 49 (4): 295–99.

Montanari, Paolo, and Oneglio Sala. 1988. Quick-Coupling Connector Group for Pipes, Piles, or

the Like. US 4,790,571, issued 1988.

Nilsson, Jan Ake, and Sten Börje. 1967. Jointing Devices for Concrete Piles. US 3,356,398, issued 1967.

Noronha, Dauro Braga, Ricardo Rodrigues Martins, Breno Pinheiro Jacob, and Eduardo de Souza. 2010. "Procedures for the Strain Based Assessment of Pipeline Dents." *International Journal of Pressure Vessels and Piping* 87 (5). Elsevier Ltd: 254–65. doi:10.1016/j.ijpvp.2010.03.001.

Roark, R. J., and W. C. Young. 1976. *Formulas for Stress and Strain*. *Journal of Applied Mechanics*. 7th ed. Vol. 43. McGraw-Hill. doi:10.1115/1.3423917.

Rogers, Colin A, and Gregory J. Hancock. 2000. "Failure Modes of Bolted-Sheet-Steel Connections Loaded in Shear." *Journal of Structural Engineering ASCE* 126 (2).

Rupiper, Stan. 2003. Helices Pier Coupling System Used for Soil Stabilization. US 6,615,554 B2, issued 2003. doi:10.1016/j.(73).

Simulia. 2012. "Abaqus 6.12 Documentation." Providence, Rhode Island, USA.

Sullivan, James F. 1998. *Technical Physics*. Edited by Wiley. USA.

Tomlinson, Michael, and John Woodward. 1995. *Pile Design and Construction Practice*. 5th ed. Vol. 22. New York, NY, USA: Taylor & Francis. doi:10.1139/l95-101.

Vesic, Aleksandar S. 1977. *Design of Pile Foundations*. Washington D.C., USA: Transportaion Research Board.